

The Physical Basis of Extreme Animal Coloration

by

Alexander Lee Davis

Department of Biology
Duke University

Date: _____

Approved:

Sönke Johnsen, Supervisor

H. Frederik Nijhout

Stephen Nowicki

V. Louise Roth

Tracey Sutton

Dissertation submitted in partial fulfillment of
the requirements for the degree of Doctor
of Philosophy in the Department of
Biology in the Graduate School
of Duke University

2022

ABSTRACT

The Physical Basis of Extreme Animal Coloration

by

Alexander Lee Davis

Department of Biology
Duke University

Date: _____

Approved:

Sönke Johnsen, Supervisor

H. Frederik Nijhout

Stephen Nowicki

V. Louise Roth

Tracey Sutton

An abstract of a dissertation submitted in partial
fulfillment of the requirements for the degree
of Doctor of Philosophy in the Department of
Biology in the Graduate School of
Duke University

2022

Copyright by
Alexander Lee Davis
2022

Abstract

Animals use color to hide from predators, signal to mates, and communicate, among other functions. Some animals, such as birds, butterflies, and spiders, have evolved extreme forms of coloration that push the limits of absorption and reflectance. In these animals, pigments and structural elements are combined to produce high absorption or high reflectance. Compared to more typical pigmentary or structural colors, relatively little work has been done to examine the physical basis of extreme coloration across taxa. In this dissertation, I use butterflies, deep-sea fishes, and cleaner shrimp to further explore the presence of extreme coloration in different taxa and the underlying color production mechanisms.

In Chapter 2 I began my investigation of extreme coloration with butterflies. First, I identified several species of butterflies from four subfamilies that all have a reflectance $< 0.5\%$. After identifying a set of particularly black butterflies, I used scanning electron microscopy (SEM) to visualize the morphology of the black scales for each species. I found that hole shape and size varied dramatically across species, with no correlation to reflectance. However, two structural features were consistently found in all species - steep ridges and expanded trabeculae compared to dark brown butterflies. Using finite-difference time-domain (FDTD) modeling, I discovered that those two conserved features reduce reflectance from the scales by up to 16-fold. Furthermore,

additional modeling demonstrated that the ridges and trabeculae create more scattering, leading to more absorption by melanin embedded within the scales. Given that ultra-black scales in butterflies are often found adjacent to bright, colored scales, ultra-black may be used to increase the contrast of color signals.

After analyzing the underlying basis of ultra-black coloration in butterflies, I turned to deep-sea fishes. Many deep-sea fishes exist in a world where the primary source of light is bioluminescence. Predators with sensitive eyes can detect even dim reflections from potential prey. I hypothesized that deep-sea fishes have evolved structural features or pigments to minimize reflectance from the skin. Similar to my approach in Chapter 1, I began by identifying 16 species of fishes with exceptionally low reflectance. I found that in all 16 species there was a continuous layer of melanosomes in the skin. My FDTD modeling showed that the melanosomes in the skin had the optimal size and shape to minimize reflectance. Furthermore, the melanosomes in deep-sea fishes are larger and more elongated for a given size than what is typical in other ectothermic vertebrates. In this case, unlike other ultra-black animals, where scattering is created by a keratin or chitin matrix, fish melanosomes provide both scattering and absorption. Ultra-black skin reduces sighting distance by predators by more than 6-fold compared to typical black fishes, making it a highly effective form of camouflage in the deep-sea.

Between birds, butterflies, fishes, and spiders, the mechanisms underlying ultra-black coloration are relatively well understood. However, less attention has been paid to bright white coloration. In Chapter 4, I used similar methods to Chapters 2 and 3 to explore the physical basis of bright white coloration in cleaner shrimp antennae. Cleaner shrimp engage in a mutualistic relationship with client fishes. Some species of cleaner shrimp use long white body parts to signal to these client fish and advertise their services. Two such species are *Ancylomenes pedersoni* and *Lysmata amboinensis*, which signal to client fish using their white antennae. Using SEM, I found that the antennae in both species contain a 1-3 μ m thick layer of non-pigmented nanospheres. With FDTD modeling, I showed that these nanospheres are the optimal size to maximize reflectance and that they can increase reflectance by up to 19-fold compared to antennae without these nanospheres. Similar to what I found in deep-sea fishes, the nanoparticles create a highly scattering structure that, in the absence of absorption from melanin, forms a bright white color instead of ultra-black. Collectively, the three chapters presented here build upon a small, but growing, body of research into the physical basis of extreme animal coloration. This work provides a foundation for new investigations into the functional effects and the evolution of extreme coloration and has the potential to inspire novel man-made materials.

Dedication

This work is dedicated to the memory of my grandmother, Mary Davis, who wanted to attend Duke in the late 1950's but could not afford to. For 25 years she supported me, encouraged me no matter what I was working on, and made sure everyone in the family felt special during the big moments of their lives. Although she could not be here for this moment, her memory remains, now, and for every other important moment of my life. I love you, Grandma.

Contents

Abstract	iv
Dedication	vii
List of Tables	xii
List of Figures	xiii
Acknowledgements	xv
1. Introduction	1
1.1 Functions of color in nature	1
1.2 Producing color.....	4
1.2.1 Pigments	5
1.2.2 Structural Colors.....	9
1.3 Pushing the limits of color	12
1.4 Summary of the work presented here	15
2. Diverse nanostructures underlie thin ultra-black scales in butterflies.....	20
2.1 Introduction.....	20
2.2 Methods	23
2.2.1 Specimen Acquisition	23
2.2.2 Reflectance measurements	24
2.2.3 Characterization of wing scales.....	24
2.2.4 Finite-difference time-domain modeling	25
2.3 Results	28

2.3.1 Wing reflectance spectra.....	28
2.3.2 Scale nanostructure	29
2.3.3 Finite-difference time-domain modeling	31
2.4 Discussion.....	36
3. Ultra-black camouflage in deep-sea fishes	40
3.1 Introduction.....	40
3.2 Methods	41
3.2.1 Sample collection.....	41
3.2.2 Reflectance measurements	42
3.2.3 Histological analysis	43
3.2.4 Comparing melanosome geometry to published values.....	46
3.2.5 Optical Modeling.....	47
3.2.6 Sighting distance calculation	49
3.2.7 Quantification and statistical analysis.....	50
3.2.7.1 Reflectance spectra.....	50
3.2.7.2 Melanosome geometry	51
3.2.7.3 FDTD simulations.....	51
3.3 Results	52
3.3.1 Reflectance of ultra-black fishes	52
3.3.2 Close-packed melanosome layers mediate extremely low reflectance.....	54
3.3.3 Size and aspect ratio of melanosomes combine to produce low reflectance	58
3.3.4 Effect of melanosome layer thickness.....	61

3.3.5 Effect of reflectance on underwater sighting distance	63
3.3 Discussion.....	65
4. Nanosphere layers increase visual signal conspicuousness in the cleaner shrimps <i>Ancylomenes pedersoni</i> and <i>Lysmata amboinensis</i>	67
4.1 Introduction.....	67
4.2 Methods	69
4.2.1 Specimen acquisition	69
4.2.2 Spectroradiometry	69
4.2.3 Morphological analysis.....	70
4.2.4 Optical modeling.....	71
4.3 Methods	73
4.3.1 Spectroradiometry.....	73
4.3.2 Are there structures in the antennae that may increase reflectance?	75
4.3.3 Are the nanosphere layers optimized to maximize reflectance?	78
4.4 Discussion.....	81
5. Conclusions and Future Directions	84
5.1 Future Directions	86
5.1.1 Empirical Tests of the Effects of Increasing Contrast on Signal Effectiveness .	86
5.1.2 Effects of pigment granule geometry on chromatophore reflectance.....	88
5.1.3 Comparative studies of optical adaptations in cleaning and non-cleaning shrimps	90
Appendix A. Supplemental information for Chapter 2.....	92
Appendix B. Supplemental information for Chapter 3	98

References	102
Biography.....	123

List of Tables

Table 1: Black butterfly specimen list for reflectance measurements.....	92
Table 2: Butterfly scale simulation model parameters.....	93
Table 3: Species list for spectral measurements and histology.....	98

List of Figures

Figure 1: Reflectance of ultra-black and control butterflies.	29
Figure 2: Ultra-black butterfly scales are widespread and morphologically diverse.	31
Figure 3: Removing conserved structural elements increases reflectance three- to sixteen-fold.	33
Figure 4: Decoupling the effects of structure and absorption on scale reflectance.	34
Figure 5: Reflectance is primarily driven by the imaginary part of the refractive index..	36
Figure 6: Phylogenetic distribution and reflectance of ultra-black, deep-sea fishes.	54
Figure 7: Skin ultrastructure and melanosome geometry.....	57
Figure 8: Finite-difference time-domain modeling of close-packed melanosomes.....	61
Figure 9: Effect of layer thickness and camouflage benefit of ultra-black skin.....	64
Figure 10: Reflectance from cleaner shrimp antennae.....	75
Figure 11: Cross section of cleaner shrimp antennae.....	77
Figure 12: Nanosphere diameter in cleaner shrimp antennae.....	78
Figure 13: Finite-difference time-domain modeling of nanosphere layers.....	81
Figure 14: Diversity of butterfly scale hole shapes and sizes.	94
Figure 15: Scale trabeculae from ultra-black male and dark brown female butterflies. ...	95
Figure 16: Section of ultra-black butterfly wing sputter coated with gold.....	96
Figure 17: Butterfly scale unit cell diagram.....	96
Figure 18: Simulated reflectance of butterfly scales and blocks consisting of an equal volume of absorbing material.	97
Figure 19: Deep-sea fish reflectance spectra.....	99

Figure 20: Histology of ultra-black fishes.....	100
Figure 21: Simulated melanosome refractive index profile.	101

Acknowledgements

There is no one who deserves an acknowledgement and a tremendous thank you more than my mentor, Sönke Johnsen. Well before I joined his lab, Sönke took time out of his day to get coffee and give me impartial advice about graduate school and how to choose a mentor. That advice led me, thankfully, to his lab where his support, friendship, creativity, and sense of humor kept me sane and allowed me to grow as a person while I progressed through my early 20's. From our time at sea to me popping into your office to ask you a question that sounded silly as soon as it left my mouth, your guidance has been incredibly influential to how I view science, mentorship, and my own career. I am not exaggerating when I say that I would have left graduate school years ago, had it not been for your constant support and flexibility. Finally, and perhaps most relevant to this dissertation, thank you for your scientific insights. Our conversations about strange optical phenomena inspired, either directly or indirectly, many, if not all, of the ideas in this dissertation.

Similarly, I am grateful to current and past members of the Johnsen lab – Jesse Granger, Sarah Solie, Eleanor Caves, Carlos Taboada, Lori Schweikert, Kate Thomas, Jay Wheeler, Bob Fitak, Laura Bagge, and Julia Notar – for reading countless drafts, giving feedback on presentations, making me laugh, and generally being a fantastic group of people to work with. Jesse Granger and Sarah Solie deserve a particular thank you. Our

weekly meetings through much of my time at Duke provided a necessary balance of science, humor, and accountability that helped make every week just a little brighter.

I also thank my friends and collaborators outside of the Johnsen lab. I thank my committee – Fred Nijhout, Steve Nowicki, Louise Roth, and Tracey Sutton – for their mentorship and support. Further, I thank all of the staff, particularly Anne Lacey, Randy Smith, Jim Tunney, and Amy Clayton, who keep our department running smoothly. A different kind of thanks is also due to Steve Nowicki and Susan Peters for inviting me into their home, welcoming me into their lab when I became curious about a new question, and performing an immense amount of work to make the experiments related to that question possible. Journal clubs at your house will always be a particularly fond memory from my time at Duke.

I would be remiss if I did not thank my mentors at UNC, without whom I would not have considered a PhD, let alone have been able to complete one. I thank Laura Miller for taking a chance on an inexperienced, 19-year-old version of myself and showing me the power of interdisciplinary science. I thank Chris Martin for his friendship and guidance through writing my first manuscript. Finally, a very special thank you is due to Bill Kier. Although it took until graduate school for us to finally become collaborators, the classes you taught, our conversations about science and applying to graduate school, and your patience with me had an immeasurable impact on my life personally and professionally.

Lastly, I must thank my parents, Allison and Terry Davis, and my fiancée, Meredith Richards. A PhD can be a stressful and profoundly individual endeavor. All three of you have supported me, calmed me down when I was stressed about my career or a particular mistake, made me laugh, and have kept me smiling through the last four years. Without the three of you, I can truly say that none of this would have been possible. I am overjoyed and proud to have such an incredible, loving family. I love all three of you, dearly.

1. Introduction

1.1 Functions of color in nature

Color is part physics, part perception. The ambient illumination, such as sunlight or the fluorescent lights of an office building, combines with the physical and chemical properties of objects to reflect certain wavelengths of light. For example, when broadband sunlight hits a red picnic chair much of the short wavelength light is absorbed, leaving only longer visible wavelengths. This is not the entire picture, however. Perceiving the color “red” from this chair depends on photoreceptors in our eyes absorbing the wavelengths of light they are tuned to and also on our brain properly processing that neuronal signal (Cronin et al. 2014). Although the physical part of color is invariant with species, the receptors and post-receptor processing of visual information making up the other half of the equation are incredibly diverse (Hart 2001; Kelber et al. 2003; Peichl 2005; Stavenga and Arikawa 2006; Schweikert et al. 2018a). This diversity reflects the ways in which color vision and coloration mediate evolutionarily important processes that have implications for survival, reproduction, communication, and more (Cuthill et al. 2017).

A common function of color in organisms is camouflage. For organisms, surviving long enough to reproduce and pass on their genes is essential. To this end, animals and plants have evolved an astonishing number of color patterns and optical tricks to remain hidden. The most straightforward form of camouflage is background

matching (Cott 1940; Stevens and Merilaita 2011). Background matching is an attempt to mimic the surrounding environment and it can take many forms. For example, animals such as North American moths (Endler 1984), desert rodents (Nokelainen et al. 2020), and four-eyed turtles (Xiao et al. 2016) have a color pattern matching that of their environment. Often these color patterns are static, but there are phylogenetically widespread examples of dynamic color patterns that can be adjusted to match a range of backgrounds (Ramachandran et al. 1996; Allen et al. 2010; Schweiker et al. 2018b; Cuthill et al. 2019). Furthermore, though background matching is likely the most common form of terrestrial camouflage, there are other important ways animals use color to hide such as disruptive coloration (Merilaita 1998; Schaefer and Stobbe 2006; Stevens and Merilaita 2009; McElroy 2016), mirroring (similar to background matching – Denton and Nicol 1966), and mimicry (Garrouste et al. 2016; Barnett et al. 2021). On the opposite end of the conspicuousness spectrum from background matching and other forms of camouflage are aposematism and other forms of warning coloration. Warning colors are typically conspicuous, high contrast colors or patterns that alert a predator that an animal may be toxic or unpalatable, and thus not worth eating (Mappes et al. 2005). Regardless of the strategy, color is a key component of avoiding predators and staying alive.

Camouflage and warning coloration help keep an organism alive, but organisms also use color to communicate between one another. This communication often relies on signals. Generally, animal and plant signals are structures or behaviors that have

evolved to modify the behavior of receivers (Smith and Harper 2003) and should reliably convey information that both senders and receivers benefit from, on average (Grafen and Johnstone 1993; Searcy and Nowicki 2010). Color signals can have many functions, but one crucial function is attracting mates. For example, female zebra finches (*Taeniopygia guttata*) choose mates, in part, based on the color of their orange-red beaks that act as an honest signal of condition (Burley and Coopersmith 1987; Simons et al. 2011). Similarly, ultraviolet (UV) patterns are used in mate choice in some species of fiddler crabs and birds (Pearn et al. 2001; Detto and Backwell 2009). These examples, along with countless others (Kemp and Rutowski 2011; Svensson and Wong 2011; Bell et al. 2012), underscore the importance of color in attracting mates.

Communication through color extends beyond sexual signals. Color signals underlie several ecologically important mutualistic relationships. Plant pollinator interactions, such as the relationship between bees and flowering plants, have resulted in the evolution of an innumerable variety of flower colors and patterns (Spaethe et al. 2001; De Ibarra and Vorobyev 2009; Muchhala et al. 2014). Bees, and other pollinators, use these flower color patterns to detect flowers, identify flower species, and find nectar (in the case of nectar guides) (Leonard and Papaj 2011; Hansen et al. 2012). A second example of the importance of color signals to mutualisms is the cleaner-client interactions on coral reefs. Organisms providing cleaning services remove dead skin and ectoparasites from clients, yielding food for the cleaner and reducing parasite load on

clients. Cleaner wrasse and gobies display a yellow and blue pattern to help advertise their services, where the yellow color has high contrast against open blue water and the blue color has high contrast against the more colorful and complex reef background (Cheney et al. 2009). Other cleaners, such as the cleaner shrimp *Ancylomenes pedersoni*, use their white antennae to signal to clients, much in the same way fishes use yellow and blue (Caves et al. 2018).

From camouflage to cleaning (and a myriad of other functions – Cuthill et al. 2017), color is critical to organisms. Color keeps organisms alive, allows them to find mates and reproduce, and helps them find food. But, to connect the functions of observed color patterns in animals and plants to their physiology, genes, and evolution, we must understand how those colors are created.

1.2 Producing color

Colors are produced by pigments, micro- or nanoscale structures, or some combination of the two. Studying the physical and chemical basis of coloration in animals creates a foundation that can be used to explore the links between color production and the functions of color in animals. Similarly, a well-developed understanding of the function of color can be used to generate hypotheses about the specific color production mechanisms that underlie those functions.

1.2.1 Pigments

Pigments are compounds that selectively absorb certain wavelengths of light depending on the chemical structure of the compound (Hashimoto et al. 2021). For example, the red picnic chair from Section 1.1 has pigments that selectively absorb shorter wavelength light and reflect the longer wavelengths, giving us the perception that the chair is red. Pigment-based coloration has been extensively studied across multiple levels of organization, from biochemistry to macroevolution (Mallet 1993; Insausti and Casas 2008; Eliason and Clarke 2018; Weaver et al. 2018). Although there are many classes of animal pigments, the most studied are melanins, carotenoids, and pterins (Andrade and Carneiro 2021). Together, these three classes of pigments play a major role in coloration, among other functions such as immunity (McGraw and Ardia 2003; Jacquin et al. 2011), heavy metal sequestration (Sarna and Plonka 2005; Chatelain et al. 2014), and structural support (Bonser 1995; Moses et al. 2006).

Melanin is made up of two primary subclasses, pheomelanin and eumelanin (all melanin subclasses reviewed in Cao et al. 2021). Pheomelanin is associated with light-brown and reddish-brown colors such as red hair in humans or the orange-brown cheek patches of zebra finches (Ozeki et al. 1996; Micillo et al. 2017). Eumelanin, however, is associated with darker brown or black coloration such as dark mammalian fur or a raven's feather (Galvan and Solano 2016; Caro and Mallarino 2021). One example of the relationship between the functions of color and its production is Gloger's rule. There are

several formulations of the rule, however, generally, animals that live in warmer and more humid climates display darker coloration than those in cooler, drier climates (Delhey 2019). Warmer climates tend to have higher UV radiation that can damage DNA (Delhey 2017), prompting the need for photoprotection. Similarly, humid climates tend to have richer, darker soil and more bacteria that can degrade integumentary tissues, requiring animals to evolve darker coloration for camouflage and tissues that are more resistant to bacterial degradation (Bonser 1995; Burt and Ichida 2004; Goldstein et al. 2004; Gunderson 2008; Delhey 2019). Melanin's dark color, photoprotective capabilities, and resistance against bacterial degradation make it a well-suited pigment for animals in hot, humid environments. Another example of environment and function dictating mechanisms of color production is coloration in increasingly common urban environments. As a result of heavy use of asphalt, concrete, and other common building materials, urban environments are often darkly colored and more monochromatic than natural environments. Furthermore, there are often more pollutants, including metal ions that can negatively affect fitness (Snoeijs et al. 2004; Scheifler et al. 2006; Roux and Marra 2007; Chatelain 2014). Urban environments necessitate both darker coloration in light-colored animals and a mechanism of sequestering toxic metal ions (Chatelain et al. 2014). Similar to the example of Gloger's rule, we again see that melanin is well suited for these functions. Melanin is used in black and grey coloration that is good match for urban backgrounds, and melanin has the ability to bind metal ions and sequester them

in tissues such as feathers (Chatelain et al. 2014). Indeed, we see that urban populations of several species, such as the pigeon *Columba livia*, have increased melanic coloration (Jacquin et al. 2011; Smith et al. 2021). Both Gloger's rule and increasingly dark coloration in urban environments highlight the way constraints placed on animals by their environment and the necessary functions of color patterns dictate how color is produced.

Carotenoids, like melanins, are well studied and they play a key role in behavior. Carotenoids are responsible for producing yellow, orange, and red coloration across taxa, particularly in birds and fishes (Hofreiter and Schoneberg 2010; Sefc et al. 2014; Zhou et al. 2014; Weaver et al. 2018). It is hypothesized that carotenoid ornamentation is an honest signal of quality in many species, such as blue-footed boobys and cichlid fishes (Velando et al. 2006; Sefc et al. 2014; Weaver et al. 2018). Generally, honest signals must reliably signal some aspect of the signaler's quality such as health status, foraging capabilities, etc. Vertebrates are unable to synthesize carotenoids, so they must be ingested and sequestered in tissues to produce a visible color (Bhosale and Bernstein 2007). Carotenoid availability in the body is also linked to immune function in addition to coloration (McGraw and Ardia 2003). Because the availability of carotenoids is linked to foraging success through the need to ingest them, and linked to immune function, carotenoids are an excellent pigment to underlie honest color signals in taxa that are unable to synthesize them. (Olson and Owens 1998; Candolin 2000; Hill and Farmer

2005). Again, we see that the pigments underlying animal coloration are well tuned to higher-level functions and constraints.

Pterin pigments have not received as much attention as carotenoids or melanins, despite being found in almost all major vertebrate groups and many large invertebrate groups, such as Teleosts, Anurans, Squamates, Lepidopterans, and Dipterans (Andrade and Carneiro 2021). Pterins span the color gamut and can be white, yellow, orange, bright red, or a dark brown/red. Serving many functions, pterins act as the foundation for aposematic color patterns in Hymenopterans, Hemipterans, and Squamates (Exnerova et al. 2006; Plotkin et al. 2009; Kikuchi et al. 2014), sexual signals in *Anolis* lizards and Lepidopterans (Ortiz et al. 1963; Rutowski et al. 2005), and screening pigments in the eyes of Dipterans (Stavenga 1989). One of the more interesting insights into the connection between higher-level functions of color and pterins pigments is the use of pterorhodin in several species of Phyllomedusan frogs. During the daytime, Phyllomedusan frogs rest on leaves. These leaves are green, but also reflect near-infrared light. Because there are some predators that may be able to sense infrared light (Goris 2011), frogs must also reflect infrared light to camouflage themselves while they sleep. This poses an issue for the frogs, however, as melanin in the melanosomes of frog chromatophores strongly absorbs infrared light (Bagnara et al. 1968; Stavenga et al. 2015). Blending in with their surroundings requires maintaining their green coloration, while reflecting more infrared light than typical frogs. To achieve this, as

Phyllomedusan frogs develop, melanin in their melanosomes is replaced by dark red/brown pterorhodin pigments (Bagnara 2003). Pterorhodin absorbs less infrared light than melanin, thus switching the pigment through development causes the frogs to reflect more infrared light, allowing them to mimic the chromatic properties of the leaves they rest on (Schwalm 1977).

Even from this brief and incomplete review of animal pigments, it is clear that environmental constraints and functional necessities dictate the physical and chemical building blocks used in animal color patterns. In the next section, I discuss a second category of colors, structural colors.

1.2.2 Structural Colors

Structural colors, unlike pigments, do not rely on selective absorption to produce color. Instead, alternating higher and lower refractive index materials create selective reflection of light that produces the color we observe (Johnsen 2012). Structural colors are particularly diverse and common in birds, insects, mollusks, and fishes (Kinoshita 2008; Cronin et al. 2014). As a result of this diversity, structural colors are found in sexual signals (Kemp and Rutkowski 2007; Pryke 2007; Griggio et al. 2010), warning coloration (Fabricant et al. 2014; Fukuda and Konuma 2019), and mirror-based camouflage (Denton and Land 1971; Johnsen 2014; Rosenthal et al. 2017), among other functional color patterns.

The production of structural colors is well studied, particularly by engineers, physicists, and materials scientists, however, there have been fewer attempts to link the function of structural colors to specific production mechanisms compared to pigments. One example of such a link pertains to animals inhabiting areas with dynamic light environments such as forests (Cronin et al. 2014). Forests have both sunny and shaded areas that change location depending on the position of the sun. Sunny areas receive sunlight unfiltered, but shaded areas are illuminated by light that has been filtered by the canopy. This presents an issue for animals signaling with pigment-based colors because the appearance of pigment-based colors depends on absorption from the pigment and the illumination spectrum. That is, the reflectance of pigment-based colors, which is a product of the illumination spectrum and absorption of the pigment, changes with the illumination spectrum. Unlike pigment-based colors, however, structural colors reflect a very narrow wavelength range, so their appearance is less dependent on the illuminant (Cronin et al. 2014). For example, the apparent color of the red chair is different when viewed in direct sunlight versus light filtered by the canopy. The color of structurally colored butterfly wing, however, may change intensity depending on the availability of the wavelengths it is tuned to reflect, but the resulting hue is relatively unchanged. Here, where consistent signals are needed in complex light environments, structural colors are more effective than pigmentary colors.

A second example where function drives the preferential use of structural colors is the creation of dynamic signaling displays (Pirih et al. 2011). Pigmentary colors are the same hue regardless of the viewing angle. Structural colors, on the other hand, are often orientation dependent. This means the angle of the viewer and the light source affect the apparent color. In situations where dynamic color signals are evolutionary advantageous, one expects to find structural colors underlying those signals.

Finally, similar to carotenoid-based coloration, structural colors may offer a signal of some aspect of individual quality. When animals are using color patterns to signal immune function or foraging success, carotenoids are a fitting pigment. Honest signals, however, may signal other aspects of quality such as developmental stress. Because structural colors rely on a specific geometry to produce color, developmental stress and degradation from parasites or age may reduce or change the properties of the resulting color, offering a signal of individual quality that is different than what carotenoid ornamentation offers (Keyser and Hill 1999; Kemp and Rutkowski 2007; Shawkey et al. 2007; Galvan 2010).

As with pigment-based coloration, we see that the needs of organisms as dictated by their environment or biology can be used to explain the color production mechanisms used. Many of the examples I have presented, so far, apply to many taxa and explain ordinary color patterns such as carotenoid ornamentation and melanin-based coloration. What if, however, environmental constraints or a color pattern's

function require animals to push the limits of what colors are possible to produce? What are the color production mechanisms underlying these extreme colors, and what can they tell us about color's underlying basis?

1.3 Pushing the limits of color

So far, I have described some of the functions of color, how color is produced, and a few of the ways in which color production and color's functions are linked. It is clear that an animal's environment and the specific function of coloration in a particular animal drive the usage of different pigments or structural colors. In this section, I explore cases where animals have evolved colors that push the limits of color, from the dark blacks to bright whites.

As discussed above, melanin is responsible for most light brown to black coloration in animals, but some animals have combined melanin with elements of structural colors discussed above to produce some of the blackest materials in the world. Take, for example, birds of paradise (Paradisaeidae). Contrast between a signal and its background is an important aspect of color signal effectiveness (Endler and Thery 1996; Endler and Day 2006; Arenas et al. 2014). Higher contrast between a color signal and the background makes it more detectable by receivers, and, indeed, we see that many animals display dark coloration surrounding brighter color signals (Marshall 2000; Doucet et al. 2007; Doucet and Meadows 2009; McClean et al. 2014). Several taxa that undergo strong sexual selection for mating displays (Irestedt et al. 2009; Girard and

Engler 2014) have taken this system a step further and evolved color signals surrounded by “super black” feathers or scales. For example, at least five species of birds of paradise have feathers that reflect $< 0.5\%$ of light (McCoy et al. 2018), approaching man-made carbon nanotube forests (Mizuno et al. 2009). This incredible absorption is produced by embedding melanosomes inside of highly scattering, expanded feather barbules that increase the path length of light, and thus increases the number of scattering events (McCoy et al. 2018). Similarly, later work found that species of birds from an additional 15 families display low reflectance, and all achieve it by integrating melanin into a highly scattering modified barbule (McCoy et al. 2019a). Birds are not alone in producing extremely low reflectance, however. Male peacock spiders (*Maratus*), use a microlens array and embedded melanin granules to create small, super black patches on their abdomen (McCoy et al. 2019b). In both birds and spiders, pigments and structural elements combine to produce super black patches adjacent to bright color signals. The relationship between bright color patches and super black coloration suggests that sexual selection may have driven the evolution of extreme coloration and color production mechanisms in birds and jumping spiders.

On the opposite end of the spectrum from super black birds and spiders pushing the limits of absorption, other animals have evolved to maximize reflectance. Animals often need to stand out from the background for sexual signaling or warding off predators (Endler and Thery 1996; Endler and Day 2006; Arenas et al. 2014). In some

taxa, this pressure to contrast against the background has led to evolution of high reflectance color patterns that can reflect > 80% of light. White Pierid butterflies (*Pieris rapae*) have wings that reflect ~ 80% of light across the visible range, approximately 20% more than the white patches of comparable butterflies (Stavenga et al. 2004). Pierids achieve such high reflectance by incorporating high refractive index, ellipsoidal beads of pteridine pigment into the scale structure (Stavenga et al. 2004; Wilts et al. 2017). Additional scattering created by the high refractive index scale beads reduces transmission and increases reflectance. Similarly, colorful Pierid butterflies create exceptionally bright orange and red scales using high refractive index scale beads containing pteridines that absorb short wavelength light (Wilts et al. 2017).

As we saw with more typical pigmentary and structural colors, the physical and chemical bases of extreme animal colors are driven by environmental factors and functional needs. These extreme colors, however, beget the need for more complex and specific color production mechanisms, often employing a combination of pigments and structural color to maximize or minimize reflectance. Interactions between pigments and structural elements are relatively understudied. Extreme animal colors offer an excellent system to explore these interactions and better understand the diversity of color production mechanisms in animals.

1.4 Summary of the work presented here

In this dissertation, I explore the pigmentary and structural basis of extreme coloration in animals from across the tree of life. I begin this exploration by examining the distribution and production of ultra-black coloration in butterflies (Chapter 2). Many species of butterflies have brightly colored patches on their wings that are hypothesized to be used for sexual signaling, similar to birds of paradise and jumping spiders (Kemp 2007; Kemp and Rutowski 2011; Medina et al. 2020). Sexual signaling with brightly colored patches is benefited by increasing contrast between the colored patches and their immediate background. The benefit of increased contrast may be especially important when signaling in bright habitats such as sunlight gaps in forests and open fields, where several species of butterflies are known to inhabit. Given the presumed benefits of increased contrast to butterfly color signals, I predicted that some butterflies may have evolved exceptionally black scales surrounding these signals, like we see in other colorful taxa (McCoy et al. 2018; McCoy et al. 2019). To investigate this hypothesis, I first quantified reflectance from four species of dark brown butterflies and twelve species of ultra-black butterflies from four subfamilies: Papilioninae, Biblidinae, Heliconinae, and Danainae. Then, I used scanning electron microscopy (SEM) to compare the scale structure in dark brown and ultra-black butterflies to identify any differences that may explain the increased absorption found in ultra-black species. After identifying the potential structures involved in reducing reflectance, I used finite-

difference time-domain (FDTD) modeling to model the contribution of different scale features on reflectance, as well as determine the effect of varying the refractive index or strength of absorption of the scales. I found that, although the size and shape of the scale holes vary greatly across species, robust trabeculae and steep ridges are found in all ultra-black species. My modeling shows that the larger trabeculae and ridges combined to create a highly scattering structure with an embedded pigment that, in turn, produces very low reflectance. Here, we see a similar combination of pigment combined with a structural component to what was found in birds and spiders.

After investigating the basis of ultra-black coloration that increases the contrast of butterfly color patches, I turned to a different system - deep-sea fishes (Chapter 3). Many deep-sea fishes exist in a world where the primary source of light is bioluminescence and there are no structures to hide behind. In a deep-sea environment, reflecting just a small fraction of the bioluminescent light available can reveal a fish to predators (Johnsen 2003). I predicted that, to overcome this environmental obstacle, deep-sea fishes may have evolved ultra-black skin or scales to camouflage themselves against the surrounding black abyss. To test this hypothesis, I collected sixteen species of deep-sea fish from seven orders and measured their reflectance. Then, I used SEM and transmission electron microscopy (TEM) to identify the structure responsible for producing low reflectance. Finally, I used FDTD modeling, similar to the work in Chapter 2, to test whether the structures found in deep-sea fish skin were optimized to

minimize reflectance. I found a continuous layer of ellipsoidal melanosomes in the skin of all 16 species of fish that had a reflectance $< 0.5\%$. FDTD modeling demonstrated that the melanosomes were the optimal size and shape to scatter light within the melanosome layer, preventing reflection or transmission and increasing the chance of any particular photon being absorbed. As we have seen in butterflies, combining multiple scattering with melanin is the primary principle underlying extremely low reflectance regardless of taxa or function. What is unique about the structure observed in deep-sea fishes, though, is that they are the only group of ultra-black animals where melanin itself is both the pigment and structural element.

To extend the work from Chapters 2 and 3 to compare the underlying principles of ultra-black coloration to those of other extreme colors, I investigated the brilliantly white antennae of the cleaner shrimp *Ancylomenes pedersoni* and *Lysmata amboinensis*. Cleaner shrimp engage in a mutualistic relationship with reef fishes, where cleaner shrimp remove dead skin and ectoparasites from the fish, that they then eat. As a part of this interaction, several species of cleaner shrimp signal to client fish by whipping their white antennae back and forth (Caves et al. 2018). White is one of the few colors that has a constant appearance regardless of water type or depth, making it an effective signaling color in aquatic habitats. The challenge for cleaner shrimp is that they are small animals signaling in a complex environment (coral reefs). I predicted that, in order to be more detectable to client fish cleaner shrimp may have evolved structures in their antennae to

increase reflectance. To test this prediction, I began by measuring the reflectance of cleaner shrimp antennae. Then, I used SEM to identify a continuous layer of nano-scale spherical particles in the antennae, similar to what I observed in the skin of deep-sea fishes. Finally, I again used FDTD methods to model layers of spherical nanoparticles with a range of refractive indices and sizes. I found the nanospheres in the antennae of *A. pedersoni* and *L. amboinensis* are the optimal size to maximize reflectance, and that they can increase reflectance by as much as 19-fold. Despite being bright white instead of black, cleaner shrimp antennae have a very similar nanostructure to what was found in deep-sea fishes. Here, instead of a highly scattering aggregation of pigmented nanoparticles that create low reflectance, the same nanostructure composed of non-absorbing nanoparticles creates high reflectance.

As I have illustrated throughout this section, an animal's environment and functional considerations determine the mechanisms through which animals create color patterns. When the environment or function of color necessitate the production of patterns with very low or very high reflectance, we find those colors are most often created through a combination of a pigment and a complex structure. Indeed, the work I present in this dissertation supports this notion. Furthermore, in the following sections I also outline a new variation of this mechanism where pigments alone produce a highly scattering nanostructure. Continuing to study the physical basis of extreme coloration

will further our understanding of color production in animals and potentially reveal novel combinations of pigments and structural elements.

2. Diverse nanostructures underlie thin ultra-black scales in butterflies

This chapter has been published in full as:

AL Davis, HF Nijhout, and S Johnsen. (2020) Diverse nanostructures underlie thin ultra-black scales in butterflies. *Nature Communications* 11, 1294.

2.1 Introduction

Ultra-black materials, those with both exceptionally low reflectance and high absorbance, have the potential to increase photovoltaic cell efficiency, improve stray light capture in telescopes, and inform the design of infrared or radar camouflage, among other applications (Liu et al. 2014; Yan et al. 2016; Jiang et al. 2018; Luo et al. 2018). Currently, most synthetic ultra-black materials are made from nano-patterned metals or carbon nanotubes (Brown et al. 2002; Mizuno et al. 2009). In both materials specular reflection is reduced by nano-scale surface roughness caused by either acid etching in the case of nickel-phosphorous alloys or nanotube deposition in carbon arrays. Light that is not reflected from the surface is scattered within the material until it is absorbed. The blackest of these synthetic ultra-black materials (Vantablack) is made from a sparse array of vertically aligned carbon nanotubes (Mizuno et al. 2009). The nanotubes, however, must be fabricated at high temperatures and are extremely susceptible to abrasion and other forms of damage, making them unsuitable for many uses. Naturally occurring ultra-black materials may offer insight into more robust absorbers for future replication.

Recently, it has been shown that several animals have evolved micro- or nanostructures that reflect as little as 0.05% of visible light, even at normal incidence (Vukusic et al. 2004; Han et al. 2015; Siddique et al. 2017; McCoy et al. 2018; McCoy et al. 2019). Several species of birds of paradise have evolved complex barbule microstructures that increase light scattering and, consequently, the number of opportunities for light absorption by melanin embedded within the feather (McCoy et al. 2018). Similarly, certain peacock jumping spiders have evolved a cuticular micro-lens array that limits surface reflection with multiple scattering between adjacent lenses and allows the light to pass further into the cuticle where it is absorbed (McCoy et al. 2019). Lastly, certain papilionid butterflies produce ultra-black wing patches with two layers of thin ($\sim 2.5 \mu\text{m}$), overlapping scales that have an upper lamina patterned with a quasi-honeycomb structure made of crossribs connecting ridges (Vukusic et al. 2004; Siddique et al. 2017). Butterflies, in particular, offer a versatile study system for investigating natural ultra-black surfaces because: (i) their scales have evolved a number of optical specializations including multilayer reflectors and thin films (Ingram and Parker 2008), (ii) the scales are several times thinner than other naturally occurring ultra-black materials or synthetic alternatives, and (iii) butterfly scales are under constraint to be both light and robust for use in flight.

Previous studies have demonstrated the nano-holes in the upper lamina of papilionid butterfly scales allow light to enter the interior of the scale where it is

absorbed by melanin that is bound to chitin in the cuticle (Vukusic et al. 2004; Zhou et al. 2011; Siddique et al. 2017). Additionally, slabs patterned with holes approximating the size of those in the butterflies (240 nm) have been shown to increase light absorption when compared to an un-patterned slab (Siddique et al. 2017). The role of the steep periodic ridges that border these nano-holes is less certain. One modeling effort supports an important role for the ridges in increasing absorption by channeling light into the holes (Zhou et al. 2011), while another found they have an insignificant effect on broadband absorption - particularly in the visible range (Siddique et al. 2017). These studies provide a foundation for evaluating how the structure of butterfly scales enhances light absorption, however, they are restricted to the family Papilionidae, they do not examine the differences between regular and ultra-black scales, and they consider absorption instead of reflectance (the latter of which is more relevant in biological contexts such as signaling or camouflage).

Here we use spectrophotometry, scanning electron microscopy, and finite-difference time-domain modeling to investigate the nanostructure underlying ultra-black wing patches in butterflies from four subfamilies to derive general design principles of natural ultra-black materials. We find that, despite considerable variation in the size and shape of the nano-holes, all ultra-black scales have steep ridges and trabeculae that are substantially deeper and wider than those found in regular black or brown scales. We confirmed with optical modeling that these two structural elements

are the key components in producing low reflectance, and that removing either of them drastically increases the reflectance by over an order of magnitude. Given that these structural changes increase the surface area for absorption, we conclude that butterflies operate under the same design principles as synthetic ultra-black materials – high surface roughness and a large area for absorption. We also hypothesize that because the ultra-black patches always border colored, white, or bright iridescent patches (i.e., there are no known butterflies that are entirely ultra-black) that they are used to increase the perceived brightness and saturation of colors used in aposematic or intraspecific displays.

2.2 Methods

2.2.1 Specimen Acquisition

Five species of ultra-black papilionid butterflies (*Trogonoptera brookiana* male, *Papilio bangui*, *P. iphidamus*, *P. oribaeus*, and *Troides helenia*), one regular black papilionid specimen (*Trogonoptera brookiana* female) and seven species of nymphalid butterflies (*Euploea dufresne*, *Euploea klugi*, *Euploea midamus*, *Heliconius doris*, *Heliconius wallacei*, *Catonephele antiope*, and *Eunica chlorocroa*) were obtained from Fred Nijhout's collection at Duke University. The remaining specimens (*C. numilia* male and female, *Heliconius ismenius*) were acquired from the North Carolina Museum of Life and Science (Durham, NC, USA). All specimens were kept mounted in wooden insect boxes with naphthalene to prevent decay between spectrophotometer measurements and electron microscopy.

Every specimen was chosen for minimal wear, as missing scales create small reflective spots on the wing. Because we were interested in the structural components underlying low reflectance, and not variation within a particular species, we chose one specimen per species.

2.2.2 Reflectance measurements

Spectral reflectance from the butterfly wings was measured using a multi-channel spectroradiometer (R400-7 Ocean Optics Inc., Dunedin, FL, USA) coupled with a Xenon UV-VIS light source (PX-2 Ocean Optics) and fiber-optic back-reflectance probe (USB2000). All measurements were taken at 90° relative to the plane of the wing to capture the maximum specular reflectance and thus provide a conservative estimate of how black a material is. The measurements from 3-5 locations on the wing were averaged for each species. During measurements, the wings were placed on a Spectralon™ block with 2% diffuse reflectance (Labsphere, North Sutton, NH, USA). Reflectance measurements were calibrated with the same 2% reflectance standard instead of a typical 99% reflectance standard. We used the black standard as opposed to a typical white standard because the reflectance of the wings was so low that the signal to noise ratio was small when calibrating with a white standard.

2.2.3 Characterization of wing scales

Small sections from the wings of the ultra-black butterflies *Trogonoptera brookiana* (male), *Catonephele antinoe*, *Catonephele numilia* (male), *Heliconius doris*, *Napeocles jucunda*,

Eunica chlorocroa, and *Euploea dufresne*, *Euploea klugi*, were mounted on aluminum SEM stubs with copper tape and sputter coated with ~7.5nm of gold (Denton Desk V; Denton Vacuum LLC, Moorestown, NJ, USA). Sections from regular black and dark brown butterflies *Trogonoptera brookiana* (female), *C. numilia* (female), *H. ismenius*, and *Euploea midamus* were mounted and coated using a similar protocol. We imaged the scales using an Apreo S scanning electron microscope (ThermoFisher Scientific, Waltham, MA, USA) at accelerating voltages of 1-5kV and magnifications of 512x – 100,000x.

2.2.4 Finite-difference time-domain modeling

Three-dimensional simulations of the reflectance and transmittance of ultra-black butterfly scales were performed with a Python implementation of the freely available software package MIT Electromagnetic Equation Propagation (MEEP) (Oskooi et al. 2010). MEEP implements the finite-difference time-domain (FDTD) modeling in which differential forms of Maxwell's equations are solved on a discrete grid and electromagnetic fields are evolved in time, step-by-step. We first verified our model by simulating the reflectance of a clear and an absorbing slab. All simulations were performed with a unit cell geometry and periodic boundary conditions in the z- and y- directions with perfectly matched layer (PML) absorbers in the x-direction (schematic of the unit cell: Appendix A – Figure 17). The source was a Gaussian pulsed plane wave traveling in the x-direction with a central frequency corresponding to a wavelength of 360nm and covering the range 200-2000nm. The linear resolution was set to 20nm to

allow for at least 10 sampling points per wavelength. All calculations were performed in the far field (> 4 wavelengths from the scale).

We created a custom geometry that consisted of one hole through the upper lamina, the crossribs, half of each scale ridge, and a lower lamina, that represented the unit cell of an ultra-black butterfly scale. We considered the standard unit cell to have a $500 \times 300 \text{ nm}$ hole, 600 nm ridges, and 1200 nm spacing between the upper and lower lamina (values derived from *C. antinoe*, the blackest butterfly considered here). The standard cell was simulated with a complex refractive index of $1.56n \pm 0.06i$, the reported value for a black *Morpho* ground scale (Vukusic et al. 1999). We used a fixed value for the refractive index because the exact dispersion of ultra-black scales is currently unknown, and the models are intended to identify important geometric features, not to exactly recreate the reflectance of a butterfly scale. Melanin was assumed to be evenly distributed throughout the structure as it appears to be in other ultra-black butterflies (Vukusic et al. 2004).

To determine the effects of specific structural features on the blackness of the scale, we systematically removed parts of the structure and repeated the simulation performed for the standard cell. Because some modifications reduce reflectance (R) but greatly increase transmission (T), which ultimately will be reflected back by the wing substrate or another scale, we compared the reflectance from two scales backed by a perfect reflector. This can be approximated by the expression $R + R(T^2) + T^4$ (this

expression was also used to calculate the values seen in Figs. 3 and 4). The structural modifications with the greatest effect on reflectance: removing the robust trabeculae, removing the scale ridges, and removing the lower lamina, are included here. All results reported in Fig. 3 are the result of averaging five simulations where the unit cell size is varied from 95% of the size of the original model to 105% of the size of the original model. This was done to eliminate any wavelength-specific resonant effects that may occur from having a perfectly periodic structure that does not reflect a real biological material.

As a means of decoupling the effect of the structure's effect on absorption from the direct absorption of the material making up the ridges or trabeculae, we simulated two additional sets of scales with either transparent ridges or transparent trabeculae. We did this by keeping the real part of the refractive index the same as the rest of the scale and setting the imaginary part to zero just for the component of interest.

To investigate whether the specific optical properties of melanin – high real and imaginary parts of the refractive index – are necessary to make this structure function, we decoupled the real and imaginary parts of the refractive index. We simulated the reflectance of scales with 99 unique combinations of real (n) and imaginary (k) parts at 550nm (a relevant wavelength of light in forest light that has been filtered by a canopy). We simulated $n = 1.33, 1.38, 1.44, 1.50, 1.56, 1.62, 1.68, 1.74, 1.80$ each with the following values for imaginary part of the refractive index: $k = 0.0, 0.015, 0.03, 0.045, 0.06, 0.075$,

0.09, 0.12, 0.15, 0.18, 0.20. The reflection from two wings backed by a reflector was plotted as a contour plot in Matlab using linear interpolation (Figure 4).

2.3 Results

2.3.1 Wing reflectance spectra

To explore the potential diversity of nanostructures underlying ultra-black color in butterflies, we first selected ten butterfly species visually assessed to be exceptionally black that represent four subfamilies: Papilioninae, Biblidinae, Danainae, and Heliconinae ($n = 10$ species; Appendix A - Table 1). We also chose brown or less black butterflies from four genera that contain ultra-black species to serve as controls ($n = 4$; Appendix A - Table 1). All of the ultra-black butterflies measured here had reflectances between 0.06% and 0.4% at 500 nm under perpendicular incident illumination (Figure 1) (approximately the wavelength of minimum reflectance for all species), approaching those of synthetic ultra-black materials like Vantablack (Surrey Nanosystems, New Haven, UK) and surpassing the darkest naturally occurring materials (ultra-black plumage of birds of paradise) when measured under the same geometry (Unpublished data). Control butterflies had reflectance values between 1% and 3%.

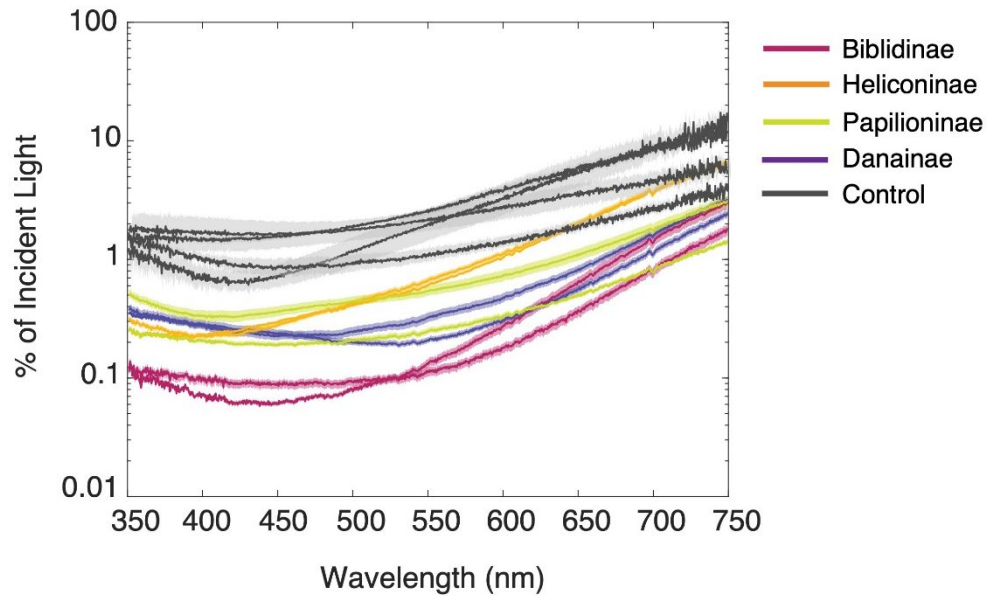


Figure 1: Reflectance of ultra-black and control butterflies. Reflectance (± 1 SE; $n = 3-5$) from 11 ultra-black butterflies from five subfamilies. Note the logarithmic scale for reflectance (y-axis).

2.3.2 Scale nanostructure

Ultra-black materials depend ultimately on an absorbing pigment embedded in a complex ultrastructure. We first characterized the scale structure of 11 butterflies (seven ultra-black, four control) using scanning-electron microscopy (SEM). All of the butterflies possessed scales with an upper lamina perforated by quasi-periodic holes (Fig. 2). There was considerable variation in the shape and size of the holes, with chevron-shaped holes in *Eunica chlorocroa*, 500 x 330 nm rectangular holes in *Catonephele antiope*, *Catonephele numilia*, and *Heliconius doris*, and 750 x 500 nm rectangular holes in *Euploea dufresne* and *Euploea klugi* (Fig. 2, Appendix A – Figure 14). Notably, none of the

nymphalid butterflies (those in the subfamilies Biblidinae, Danainae, and Heliconinae) had a honeycomb structure analogous to the one found in papilionids. The lack of a honeycomb structure, coupled with the variation in the size and shape of the holes, suggest that ultra-blackness in butterflies is not dependent on a particular hole shape or size, although some of the intra-individual variation in hole shape likely helps increase absorption at non-normal incidence angles (Zhao et al. 2011; Wang et al. 2014).

Two structural features, steep longitudinal ridges and robust trabeculae connecting the upper and lower laminae, were consistently found in all of the ultra-black specimens. Control butterflies had larger holes and either lacked or showed significantly reduced trabeculae (Appendix A – Figures 14 and 15). The presence of the ridges and large trabeculae in evolutionarily distant ultra-black butterflies, and the lack of robust trabeculae in control butterflies, suggests both of these features are important for producing low reflectance. Remarkably, all of the butterflies that possessed these features retained their black color when coated with gold for SEM while those that did not became reflective (Appendix A – Figure 16).

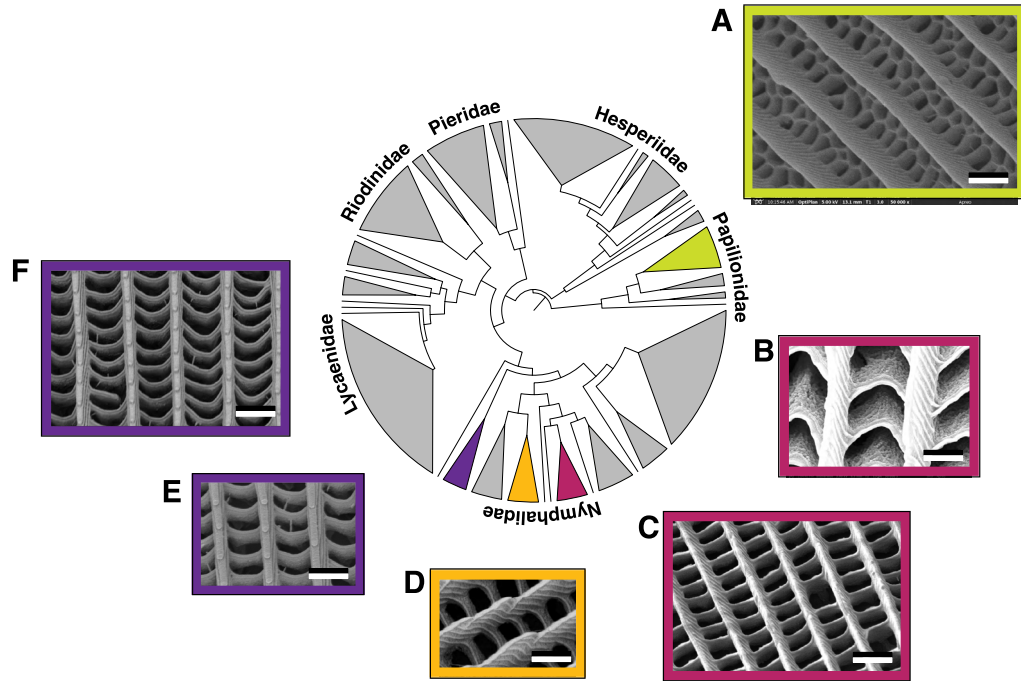


Figure 2: Ultra-black butterfly scales are widespread and morphologically diverse. A sub-family level phylogeny of butterflies adapted from (Espeland et al. 2018) showing the distribution of ultra-black coloration and SEMs of the underlying nanostructures. Note the variation in hole shape including honeycombs (A), large and small rectangles (C-F), and chevron-shaped holes (B).

2.3.3 Finite-difference time-domain modeling

After identifying the geometrical components common to all ultra-black butterflies among our sampled species, we determined their relative contribution to reflectance reduction. Because a scale could have low reflectance and be transparent (e.g., moth-eye structure) instead of black like the butterfly wings, we calculated the reflectance of two overlapping scales backed by 100% white surface to determine a

measure of blackness. We used the finite-difference time-domain (FDTD)¹⁶ method to simulate the reflectance of a structure with rectangular 500 x 330 nm holes, the dimensions of the blackest butterfly we measured, *C. antinoe* (model parameters Appendix A - Table 2; for schematic see Appendix A – Figure 17). We then ran the same simulation with the ridges, trabeculae, or basal lamina removed. The full butterfly scale model had a reflectance between 0.4 – 1.0% across the visible part of the spectrum (Fig. 3). This was 14 – 40 times lower than the simulated reflectance of two flat overlapping slabs on a 100% white background made from the same volume of absorbing material. Removing either the ridges or inner structure resulted in a three- to sixteen-fold increase in reflectance and removing both increases reflectance by seven- to twenty-eight-fold. In contrast, removing the same volume of the absorbing material from a flat block only increases the reflectance by at most two-fold (Fig. S5). Changes in reflectance after removing the basal lamina were marginal. The increase in reflectance when removing the trabeculae or ridges is consistent with the hypothesis that these are key structural components for making an ultra-black structure.

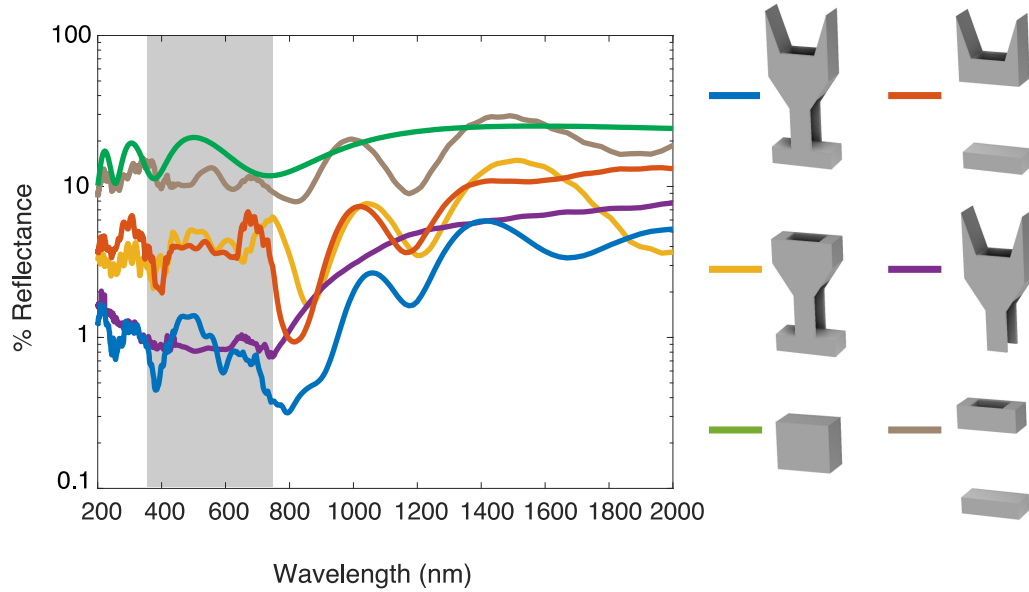


Figure 3: Removing conserved structural elements increases reflectance three- to sixteen-fold. Reflectance of two overlapping scales backed by a 100% reflecting white surface simulated with the finite-difference time-domain method (unit cell for each simulation is shown). Included is the full-scale model (blue), scales with trabeculae removed (red), with the ridges removed (yellow), with the basal lamina removed (purple), both ridges and trabeculae remove (brown), and a rectangular block made of the same volume of absorbing material as the full scale (green). Full scales reflect 2.5% - 10% of the light reflected from a rectangular block of absorbing material. Removing the robust trabeculae or ridges increases reflectance 3- to 16-fold, while the lamina has little effect on reflectance. Curves are made by averaging five simulation runs with unit cell sizes spanning $\pm 5\%$ of the standard cell.

To decouple the relative contributions of the structure to reflectance from the absorbing properties of the scale material, we simulated butterfly scales with either transparent ridges or transparent trabeculae while holding the real part of the refractive index constant. We found that the structure of the ridges alone decreases reflectance between 14 and 58% compared to a scale that has no ridges at all, and the structure of

the trabeculae decreases reflectance between 5% and 70% compared to a scale that lacks them (Fig. 4). That is to say, these structural features alone significantly reduce reflectance, even when they do not directly contribute to absorption. It should also be noted that the reduction in reflection is more prominent in the visible range, indicating specialization for absorbing visible light.

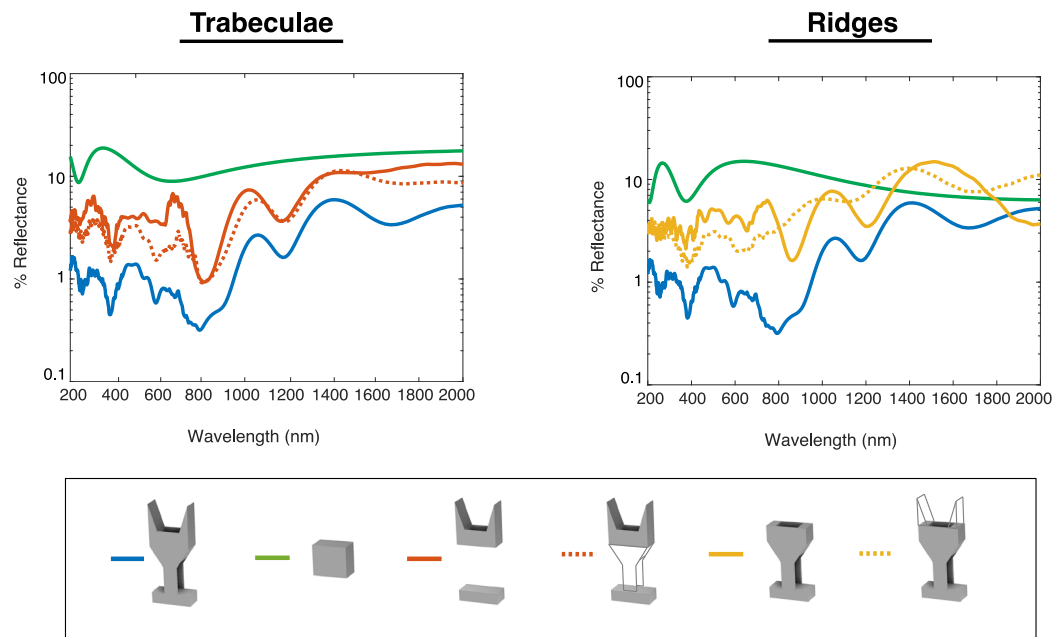


Figure 4: Decoupling the effects of structure and absorption on scale reflectance.(Left) Comparing simulations of scales with the trabeculae removed versus scales with non-absorbing trabeculae. Adding non-absorbing trabeculae to a scale that has none decreased reflectance between 5-70% in the visible range (350-700nm). (Right) Comparing simulations of scales with the ridges removed versus scales with non-absorbing ridges. Non-absorbing ridges contribute a reduction in reflectance between 14-58% in the visible range. For both the ridges and trabeculae, the structure contributes more to reduced reflectance in the visible range.

After characterizing the underlying structure, we next examined the absorbing pigment, melanin, to test whether its specific optical properties are critical in creating an ultra-black scale. Melanin has an unusually high real (n) and imaginary (k) refractive index for a biological material (Stavenga et al. 2015). Using the morphological parameters and configuration as described above, we simulated the reflectance at 550 nm using 99 unique combinations of real and imaginary parts of the refractive index. We varied the real part of the refractive index from $n = 1.33$ (water) to $n = 1.8$ (melanin) and varied the imaginary part from $k = 0.0$ (no absorption) to $k = 0.20$ (Fig. 5). With no absorption, the reflectance from two scales overlaying a white background approaches 100%, but this decreases to 1% with $k = 0.06$ (the imaginary part of the refractive index of a black *Morpho didius* ground scale) (Vukusic et al. 1999). The effect of the real refractive index is dominated by that of the imaginary refractive index until $k > 0.06$. For a scale with a high imaginary part ($k > 0.10$) the pattern reverses, and a high real part is primarily responsible for increases in reflectance. For example, when $k = 0.15$, the reflectance when $n = 1.33$ is 88% lower than when $n = 1.8$. When $0.06 < k < 0.10$, the reflectance depends on both components of the refractive index. This suggests that melanin's particular optical properties (high real and imaginary components of the refractive index) are not necessary to make ultra-black butterfly scales, only a strongly absorbing material – ideally one with a real part of the refractive index lower than that of melanin.

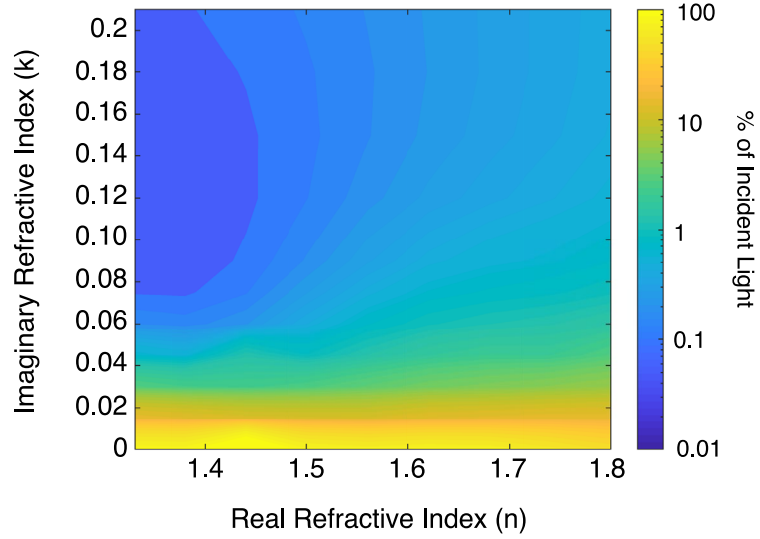


Figure 5: Reflectance is primarily driven by the imaginary part of the refractive index. Contour plot of the simulated reflectance at 500nm from scales with 99 unique combinations of the real and imaginary parts of the refractive index. Reflectance is considered to be the reflectance from two overlapping scales backed by a 100% reflective white surface. Real part of the refractive index varies from water ($n=1.33$) to melanin ($n=1.8$), and the imaginary part varies from $k=0.0$ (no absorption) to $k=0.20$. Color indicates reflectance.

2.4 Discussion

Our results demonstrate that butterflies have convergently evolved nanostructures that reflect as little as 0.06% of incident light at 90° incidence. Consistently, ultra-black butterflies have substantially larger trabeculae between the upper and lower scale lamina that increase the surface area for absorption by cuticular melanin. Both the ridges and trabeculae increase the absorption of the entire scale with

their structure alone, even excluding the absorption of the individual component. This is consistent with a growing body of literature supporting sparse packing, high surface area, and strong absorption as the general design principles of natural ultra-black materials like bird of paradise feathers (McCoy et al. 2018) or synthetic ones such as carbon nanotube arrays (Brown et al. 2002; Mizuno et al. 2009). Interestingly, in the butterflies, these principles are being applied in a layer that is only $1/5^{\text{th}}$ the thickness of synthetic or other natural materials.

Similar to other work, we find that the nano-holes are crucial for reducing reflection by absorbing light that is channeled into the holes (Zhao et al. 2011; Han et al. 2015; Siddique et al. 2017). However, previous modeling of ultra-black butterfly scales has only included the ridges, holes, and upper and lower lamina of the scale, neglecting the trabeculae (Zhao et al. 2011). The trabeculae were found here to be the major structural difference between regular and ultra-black butterfly scales, and they contribute to much of the increase in absorption in our model. In addition, unlike prior work that found the ridges have an insignificant effect on broadband absorption (Siddique et al. 2017), we found support for a substantial role of the periodic ridges in reducing reflection that is on par with that of the trabeculae. These differences in the role of the ridges, however, may be the result of differences in scale geometry. Papilionid butterflies have two rows of quasi-periodic holes between ridges that increases the spacing between ridges to greater than $1\text{ }\mu\text{m}$ which may reduce the contribution of the

ridges to absorption. Nymphalid butterflies, by contrast, typically have a ridge spacing within the wavelength range of visible light. Additionally, the diversity of hole shapes (chevrons, rectangles, and quasi-honeycombs) and sizes (ranging from 350 nm – 750 nm) suggest that enhanced absorption from resonance effects when the hole radius (r) \approx wavelength (λ) may be either less important or a more flexible criterion than previously hypothesized (Zhao et al. 2011).

It is uncertain what evolutionary pressures have led to ultra-black coloration in butterflies. However, many of the species here display in open, sunny locations where a more reflective black material would produce significant specular reflections that would decrease the contrast of colored patches used in inter- and intraspecific signaling (Kemp and Rutowski 2011). Indeed, black color is sexually dimorphic in *Trogonoptera* and *Catonephele* with males displaying ultra-black patches and females displaying a black with a higher reflectance (Parsons 1996; Muyschondt 1973). Ultra-black wing patches frequently border brightly colored areas, as is found in in other ultra-black animals (McCoy et al. 2018; McCoy et al. 2019), and our findings are consistent with the hypothesis that butterflies use these ultra-black patches to enhance the contrast of those colors in a signaling context (Vukusic et al. 2004).

Further research is needed to understand the biological function of ultra-black scales in inter- and intraspecific interactions as well as evaluate the suitability of butterfly scales for replication as a synthetic ultra-black material. Despite having a

slightly higher reflectance than carbon nanotube alternatives, butterfly scales offer two key advantages for replication: they are thinner than known alternatives and they can be fabricated at lower temperatures via plasma-enhanced chemical vapor deposition (Siddique et al. 2017) instead of being grown from carbon nanotubes. These findings have important implications for the design of optical instrumentation, photovoltaic cells, and, if scaled up in size, radar absorbing materials.

3. Ultra-black camouflage in deep-sea fishes

This chapter has been adapted from:

AL Davis, KN Thomas, FE Goetz, BH Robison, S Johnsen, KJ Osborn (2020).

Ultra-black camouflage in deep-sea fishes. *Current Biology*, 30(17), 3470-3476

3.1 Introduction

Open-ocean animals exhibit several strategies for hiding from visual predators: among them are mirrored surfaces, transparency, counterillumination, and pigmentation (Johnsen 2014). Transparency and mirror-based camouflage are most effective under diffuse ambient lighting and are thus more common in near-surface waters (McFall-Ngai 1990; Johnsen 2005). Counterillumination operates by replacing the downwelling light blocked by the body from viewers below with light emitted by banks of ventral photophores (Herring 1977; Young et al. 1980; Widder 1999; Haddock et al. 2010) but does not protect organisms from predators viewing laterally or from above. Pigmentation is common in pelagic animals at all depths, however, in the mesopelagic and bathypelagic realms, where there is little solar illumination and organisms must contend with light from bioluminescent sources, pigmentation may be a particularly effective camouflage strategy (Young 1983; Johnsen 2005; Haddock et al. 2010; Widder 2010; Martini and Haddock 2017). In the darkness of the lower mesopelagic and bathypelagic zones, reflecting even a small percentage of bioluminescence may reveal an animal to visual predators or potential prey. Mirrored surfaces and white animals reflect

> 50% of light, while transparent animals reflect > 0.4%, potentially enough to allow detection where vision is often tuned to detect just a few photons (Johnsen 2001; Johnsen 2003; Zylinski and Johnsen 2011). Because of the predicted ineffectiveness of these other camouflage methods against bioluminescence, we hypothesized that selective pressure to limit reflected light would lead to the evolution of pigmented body surfaces with near-zero reflectance in deep-sea animals. Here, we focus on deep-sea fishes, which are often black, instead of deep-sea invertebrates which are typically red but appear black due to the lack of red light in the deep-sea (Johnsen 2005), because black surfaces have the potential to inspire the design of synthetic ultra-black materials.

3.2 Methods

3.2.1 Sample collection

We focused our sampling efforts on mesopelagic and bathypelagic fishes that typically occupy depths where ambient sunlight levels are below the thresholds of vision. Specimens for histology were collected on multiple R/V *Western Flyer* research cruises from April 2014 to June 2018 and one research cruise on the R/V *Point Sur* in the Gulf of Mexico in June 2019. In total, we measured reflectance of 39 meso- and bathypelagic fish specimens from 18 species on two research cruises, the first in the Monterey Bay, CA (R/V *Western Flyer*) and the second in the Gulf of Mexico (R/V *Point Sur*) (Gulf of Mexico: 8-22 June 2019, Lat: ~27.5°N Long: ~87°W; Monterey Bay: 21-26 June 2018, Lat: ~36.7°N Long: ~122°W; Appendix B - Table 3). Specimens were collected

via Tucker trawl between 0m and 2000m (Childress et al. 1978) or with the remotely operated vehicle *Doc Ricketts*. Most specimens were dead or moribund, but, immediately after collection, specimens were placed in chilled seawater (4-6°C) to minimize tissue degradation until reflectance measurements. Measurements were taken within one hour of specimen recovery. Tissue samples were taken following reflectance measurements.

3.2.2 Reflectance measurements

Many deep-sea, pelagic fishes have delicate skin, which makes damage from the trawl net common. We chose specimens for our reflectance measurements that had either fully intact skin or large areas of intact skin with minimal visible damage. It is possible that there was damage to the epidermis of our specimens from the net, however, given how thin the epidermis is and that it is generally transparent in fishes, it is likely that any error caused by this damage would act to increase our measured reflectance (therefore providing an underestimate of how black these fishes are). This damage to the epidermis may also have prevented us from evaluating the presence of other modifications to tissue ultrastructure that could minimize surface reflection (i.e., antireflection coatings that have been found in some deep-sea amphipods (Bagge et al. 2016)). Spectral reflectance was measured from freshly caught fish in seawater using a multi-channel spectroradiometer (USB2000 Ocean Optics Inc., Dunedin, FL, USA) coupled with a Xenon UV-VIS light source (PX-2 Ocean Optics) and fiber-optic back-reflectance probe (R400-7 Ocean Optics) run through OceanView acquisition software

(v.1.6.7). We took measurements at 90° relative to the plane of the skin. The skin reflectance was measured from 3-6 locations per specimen depending on the amount of undamaged skin and the size of the fish (the number of measurements per species can be found in Appendix B - Table 3). Following Davis et al. (2020), all measurements were calibrated to a Spectralon™ block with 2% diffuse reflectance (Labsphere, North Sutton, NH, USA) and then divided by 50 to get the reflectance relative to a 100% white standard. We report the median reflectance across all measurements for a species, as opposed to average reflectance from these measurements, because the reflectance values are so small that just a single relatively high reflectance measurement (from a slightly damaged area of skin, for example) can skew the average reflectance (for individual reflectance spectra see Appendix B – Figure 19).

3.2.3 Histological analysis

We performed histology on samples of skin from 15 species of fishes from eight distantly related orders (Appendix B – Table 3). Specimens were prepared in two labs with similar but varying protocols. Differences in specimen preparation are not likely to substantially affect the results because melanosomes are structurally robust. Below are the methods pertaining to each species. *Oneirodes* sp. (Figure 7A, Appendix B – Figure 20E), *Photostomias guernei* (Appendix B - Figure 20M), *Bassozetus compressus*, *Echiostoma barbatum* (juvenile, Appendix B - Figure 20K-L), *Eurypharynx pelecanoides* (Appendix B - Figure 20A), *Eustomias schmidtii*, *Lampadena luminosa*, and *Pseudoscopelus* sp. were

prepared as follows. Small sections of skin were placed in 2.5% glutaraldehyde buffered with seawater for light microscopy and scanning and transmission electron microscopy (SEM and TEM, respectively). For TEM, small pieces of skin were cut using a razor blade, washed with 1x phosphate-buffered saline (PBS), post-fixed with 1% osmium tetroxide (OsO_4), then stained with 0.5% uranyl acetate. Following staining, the samples were placed in 30% ethanol and dehydrated to 100% ethanol in a stepwise fashion. Once the samples were fully dehydrated, they were embedded in Spurr's resin (Spurr 1969), sectioned using a diamond knife on a Leica Ultracut microtome (Leica, Wetzlar, Germany), and collected on copper TEM grids. The grids were then imaged at the Duke Shared Materials and Instrumentation Facility on an FEI Tecnai G² Twin transmission electron microscope (ThermoFisher Scientific, Waltham, MA, USA) at magnifications between 1700x – 19000x. Samples for SEM were dehydrated in the same process as TEM samples, then dried using a LADD CPD3 critical point dryer (Ladd Research Industries, Williston, VT, USA) to preserve tissue ultrastructure. Specimens were then mounted on aluminum SEM stubs using copper tape and sputter coated with ~7nm of gold (Denton Desk V; Denton Vacuum LLC, Moorestown, NJ, USA). The samples were imaged using an Apreo S scanning electron microscope (ThermoFisher Scientific, Waltham, MA, USA) at the Duke Shared Materials and Instrumentation Facility with an acceleration voltage of 1kV and magnifications between 1200x – 6500x. Finally, slides for light-level histology were generated by taking thin sections in the same manner as TEM and staining them

with Toluidine blue, mounting them with coverslips, and imaging them on a Zeiss Axiocam HRc digital camera on a Zeiss Axiophot microscope (Zeiss, Oberkochen, Germany).

Anoplogaster cornuta, *Cetominus* sp., *Cyclothone* sp. (Appendix B - Figure 20I-J), *Idiacanthus antrostomus* (Figure 7B-F, Appendix B – Figure 20N-Q), *Lampanyctus* sp. (Appendix B - Figure 20F-G), *Poromitra crassiceps* (Appendix B - Figure 20B-D), *Sagamichthyes abei* (Appendix B - Figure 20H), and *Stomias* sp. were prepared using the following methods. Intact skin, typically the ventral surface or behind the pectoral fins, was excised from specimens then fixed in either 2% cacodylate buffered glutaraldehyde or 4% formaldehyde in seawater. Tissues for SEM were transferred to hexamethyldisilazane through a dehydration series and dried overnight in a fume hood before mounting and coating with gold-palladium for examination with a Zeiss EVO MA 15 scanning electron microscope at the Smithsonian National Museum of Natural History (NMNH) Scientific Imaging Lab. Tissues for light microscopy and TEM were embedded Spurr's Low-Viscosity resin (Spurr 1969) from Polysciences, Hardness A prior to sectioning and staining. Thick sections for light microscopy and ultra-thin sections for TEM were sectioned with the RMC MT6000 ultramicrotome, thick (1 µm) with the Histo Jumbo diamond knife (Diatome, US) and ultra-thin (70 and 100 nm) with a 45° diamond knife (DuPont Instruments). Thick sections were mounted either unstained or stained with Richardson's blue (Richardson et al. 1960) prior to imaging

with an Olympus BX63F Compound Fluorescent Microscope (Olympus Corporation, Tokyo, Japan) at the NMNH Scientific Imaging Lab. Ultrathin sections were collected on copper grids and stained for TEM with 2 % uranyl acetate in 50 % ethanol and 0.4 % lead citrate in basic water (1 sodium hydroxide pellet per 50 ml water). Grids were imaged with the FEI Talos F200X TEM at George Washington University Nanofabrication and Imaging Center.

We used SEM to analyze melanosome geometry. We were able to visualize the melanosomes by imaging the side of the skin that was cut by the razor blade or in areas where we had disrupted the epidermal basement membrane. We then used Fiji (Schindelin et al. 2012) to measure the short and long axes of 40-100 individual melanosomes per species to calculate the aspect ratio and sphere equivalent diameter (SED). We also used Fiji for analysis of light microscopy images to measure the thickness of the melanosome layer at 30 evenly spaced locations along one section of skin per species. All calculations were done using R [version 3.6.2] via RStudio [version 1.2.5033] (R Core Team 2014; RStudio Team 2015).

3.2.4 Comparing melanosome geometry to published values

In order to assess the possibility that melanosomes in deep-sea fishes are specialized to produce low reflectance, we compared the geometric parameters calculated here (SED and AR) to previously published data on melanosome geometry from the skin of ectothermic vertebrates. We limited our comparison to ectothermic

vertebrates because mammals and birds have changes in melanosome morphology associated with metabolism (Li et al. 2014). Additionally, we only considered melanosomes in the skin because melanosome geometry is known to vary by tissue type (Rossi et al. 2019). In total, we assessed melanosome geometry in 50 species across reptiles, amphibians, and fishes. Thirty-six species were drawn from Li et al. (2014), six from Rossi et al. (2019), and the remaining eight were measured from published TEM images of fish melanophores (Nakamura 1987; Obika and Meyer-Rochov 1990; Park 2002; Guo et al. 2007; Beeching et al. 2013; Failde et al. 2014; Djurdjevic et al. 2015). Melanosome measurements were taken from TEM images using Fiji (Schindilen et l. 2012). Because measurements from TEM images are biased towards small sizes, as the plane through which the melanosome was cut is not known, we report the maximum measured SED from available images and the corresponding aspect ratio, in Figure 8.

3.2.5 Optical Modeling

To assess the effect of melanosome geometry on reflectance, we performed three-dimensional finite-difference time-domain (FDTD) simulations of random closed-packed ellipsoids using the Lumerical FDTD solver version 2019b (Lumerical Inc., Vancouver, BC, Canada)). In FDTD simulations, Maxwell's equations are solved across a three-dimensional grid with a user-specified resolution, and the electromagnetic waves evolving iteratively through time. Random close-packed aggregations of ellipsoids mimicking the arrangement seen in the dermis of deep-sea fishes were generated by

modifying the Uniform Random Particle Distribution (URPD) structure in Lumerical to include a term for the aspect ratio of the melanosome and specify random angles of orientation in the x, y, and z-plane. Generally, the URPD structure generates an array of non-overlapping objects until either the domain has been filled or the desired maximum number of objects have been added. Then, the function repeats this process a specified number of times to maximize the number of objects. In our case, the object was an ellipsoid made of melanin and we set the number of iterations of the function to 2000. The desired number of ellipsoids was set to be greater than the maximum number that would fit in the domain to ensure close packing.

After modifying the URPD structure to generate ellipsoids of different aspect ratios, we simulated 169 combinations of melanosome aspect ratio and sphere equivalent diameter (SED) by varying the aspect ratio from 1.0 to 4.0 in increments of 0.25 and SED from 100nm to 3000nm (100nm intervals for $SED \leq 1000\text{nm}$ and 500nm intervals for $SED > 1000$). For these simulations, we used a minimum mesh step of 0.25nm, a $5\mu\text{m} \times 5\mu\text{m} \times 5\mu\text{m}$ domain (except for $SED = 100\text{nm}$ and 200nm which had the same thickness as the other simulations but due to computational constraints had cross sections of $1\mu\text{m} \times 1\mu\text{m}$ and $2\mu\text{m} \times 2\mu\text{m}$, respectively). All simulations had periodic boundary conditions in the x and y directions, a plane wave source (400nm – 700nm) propagating in the z direction, and a reflecting boundary condition backing the melanosome layer to approximate reflective collagen and muscle tissue underneath the

melanosomes. The real part of the refractive index of the melanosomes was set by the Cauchy equation:

$$n(\lambda) = A + B/\lambda^2$$

We set $A = 1.648$ and $B = 2.37 \times 10^4 \text{ nm}^2$, and the imaginary part of the refractive index was fitted with the exponential:

$$k(\lambda) = 0.56e^{-\lambda/270\text{nm}} \text{ [Stavenga et al. 2015; Figure 8]}$$

The melanosomes were assumed to be embedded in a medium with a uniform refractive index of $n = 1.33$, closely approximating those of seawater and cytoplasm (Johnsen and Widder 1999).

To determine the effect of melanosome layer thickness on reflectance, we performed 10 additional simulations varying the thickness of the domain from $1\mu\text{m}$ to $10\mu\text{m}$ in $1\mu\text{m}$ intervals. All 10 simulations were performed with 800nm melanosomes that had an aspect ratio of 2.0 (approximately the combination that produced the lowest reflectance in our model).

3.2.6 Sighting distance calculation

To calculate the benefit of reduced skin reflectance, we used the computational sighting distance model from Ruxton and Johnsen (2016) to calculate relative sighting distances of fishes with skin reflectance ranging from 0% to 2%. In this model the sighting distance is proportional to the LambertW function of the square root of the number of photons leaving the target (where the LambertW function is the inverse of $y =$

$x e^x$). Because the fish is reflecting <2% of the photons from an already dim source (a bioluminescent searchlight, flash, or glow), the LambertW is roughly linear, and the relative sighting distance depends on the square root of the number of photons being reflected back by the fish. Normalized values were used because the beam shape emitted from the bioluminescence of deep-sea animals is unknown and it undoubtedly varies from species to species. Without knowing the beam shape, it is not possible to determine what percentage of emitted photons hit the prey fish and any absolute sighting distance values are likely to be incorrect. We took the relative sighting distance to be 1.0 at a reflectance of 2%, then fit a square root function that travels through the origin and 1.0 at 2% to calculate relative sighting distance for reflectances between 0% and 2% yielding the following function:

$$(r = \frac{\sqrt{\text{Reflectance}}}{\sqrt{2}})$$

3.2.7 Quantification and statistical analysis

3.2.7.1 Reflectance spectra

All reflectance spectra were imported into RStudio (RStudio Team 2015) and then normalized to a calibration standard with 100% reflectance (all values were initially recorded relative to a 2% reflectance standard). The reflectance at 480nm reported in Figure 6 was calculated as the median reflectance at 480nm across all measurements for

a given species. We then fit a LOESS regression for each species in RStudio to the median reflectance at every wavelength (Appendix B - Figure 19). The average reflectance from 350-700nm for each species is reported as the area under the LOESS curve divided by the wavelength range (350nm).

3.2.7.2 Melanosome geometry

We calculated the mean and median melanosome aspect ratio from between 40 and 100 individual melanosomes per species in RStudio (exact number of melanosomes for each species can be found in Figure 8). All melanosome sizes are reported as the melanosome sphere equivalent diameter (SED). For the purposes of calculating SED melanosomes were treated as prolate ellipsoids and SED is given by the expression:

$$\frac{d_l}{r^{2/3}}$$

Where d_l is the length of the long axis of the melanosome and r is the ratio of the long axis to the short axis (Jennings and Parslow 1988).

3.2.7.3 FDTD simulations

FDTD simulations of reflectance from close-packed melanosomes yielded reflectance values for wavelengths between 400-700nm. We then calculated the mean reflectance from 400-700nm for every combination of melanosome aspect ratio and sphere equivalent diameter ($n = 169$ simulations). After calculating the average reflectance for each simulation, we used LOESS regression to interpolate reflectance for combinations of aspect ratio and SED within our simulated range (Figure 8A).

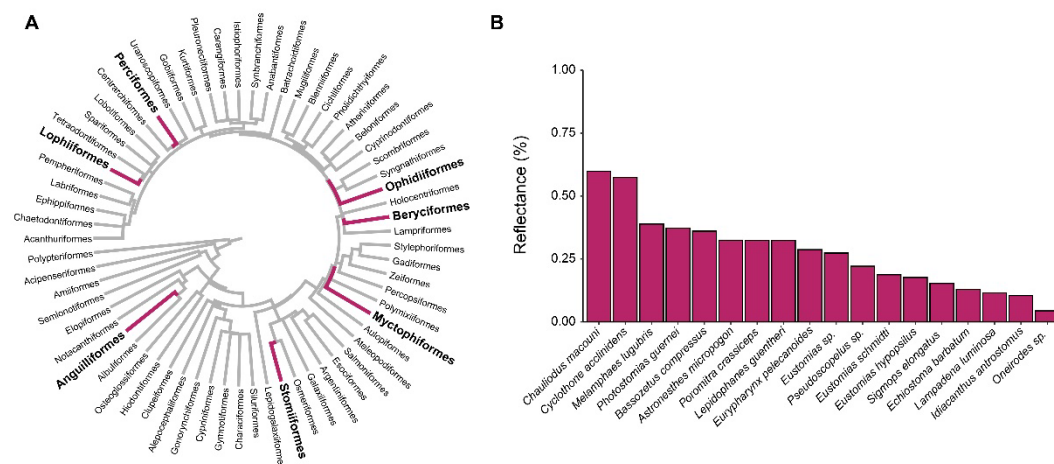
3.3 Results

3.3.1 Reflectance of ultra-black fishes

To test for ultra-black coloration (average reflectance $< 0.5\%$ across the visible spectrum) as opposed to black coloration (reflectance $> 0.5\%$) in deep-sea fishes, we collected specimens via Tucker trawl (Childress et al. 1978) on two research cruises, one in the Gulf of Mexico and the other in Monterey Bay, CA. Fishes were kept in chilled seawater ($4-6^{\circ}\text{C}$) between capture and reflectance measurement. We used a back-reflectance probe calibrated to a 2% diffuse reflectance standard to measure the reflectance at perpendicular incidence from the blackest undamaged patches of skin. In total, we measured the skin reflectance from 18 species of black fish representing seven taxonomic orders ($n = 39$ specimens total, Appendix B - 3, Appendix B - Figure 19). Of these, 16 species exhibited reflectances less than 0.5% at 480nm (approximately the peak wavelength of deep-sea ambient sunlight and most oceanic bioluminescence (Widder et al. 1983)), and the remaining two species (*Chauliodus macouni* and *Cyclothone acclinidens*) reflected less than 0.6% at 480nm (Figure 6). The mean reflectance across the visible spectrum for each species ranged from 0.051% to 1.04% , with 14 species exhibiting broadband reflectance $< 0.5\%$. This low reflectance puts deep-sea fishes on par with the blackest known animals, with the species exhibiting the lowest reflectance measured here (*Oneirodes* sp., 0.044% at 480nm , 0.051% average reflectance from $350-700\text{nm}$) surpassing the darkness of ultra-black butterflies ($0.06\% - 0.5\%$ reflectance) and equaling

the blackest birds of paradise (0.05% - 0.31% reflectance) (McCoy et al. 2018; McCoy et al. 2019; Davis et al. 2020). By comparison, man-made materials such as black paper reflect ~10% of incident light and the blackest synthetic materials, manufactured from vertically aligned carbon nanotubes, reflects 0.045% of light (Mizuno et al. 2009).

Except for *Cyclothone acclinidens*, *Chauliodus macouni*, and *Sigmops elongatus*, we found ultra-black skin covering most of the body, suggesting that it functions to reduce reflection from bioluminescence (including the searchlights of predators and defensive reactions of prey (Young 1983). Generally, the fishes studied here are intermediate in size, therefore pressure to hide from both potential predators and prey could be important forces driving the evolution of ultra-black skin. We also hypothesize that ultra-black skin in ambush predators that use lures such as *Oneirodes* sp., *Eustomias* spp., and *Astronesthes micropogon*, serves to reduce reflection from their own bioluminescent lures. In species such as *S. elongatum* and *C. macouni*, ultra-black skin is found above and below a mirrored stripe running the length of the body, suggesting that for areas of the body with high curvature where mirror-based camouflage may be less effective, ultra-black may provide a substitute. Finally, ultra-black skin is found only around the gut in species like *C. acclinidens* and may be used to conceal light emitted from recently consumed bioluminescent prey (Robison et al. 1977; Ruby and Morin 1979; Haddock et al. 2010).



3.3.2 Close-packed melanosome layers mediate extremely low reflectance

species, we found a layer of close-packed melanosomes (organelles that contain melanin) that extends continuously with few, if any, unpigmented gaps and no clear separation into individual melanophores (pigment cells containing melanosomes) (Figures 7, Appendix B – Figure 20). Such continuity in the melanosome layer contrasts with many darkly pigmented (but not ultra-black) fishes where melanophores in the skin are separated by unpigmented gaps occupied by collagen and other cells (Burton 1978; Goda and Fujii 2001; Beeching et al. 2013; Failde et al. 2014; Djurdjevic et al. 2015). The average thickness of the melanosome layer in the ultra-black species for which we could acquire light microscopy data was $7.9\mu\text{m}$ ($n = 6$ species) with a range of $2.8\mu\text{m} \pm 1.2\mu\text{m}$ (*Eustomias schmidtii*) to $14.3\mu\text{m} \pm 8.7\mu\text{m}$ (*Oneirodes* sp.) (simulated below). We found a similar layer in the six species (Appendix B - Figure 20, Appendix B - Table 3) for which we did not have the opportunity to measure reflectance, suggesting that this skin morphology may be important for reducing reflectance in other orders.

Melanophores are found in various fishes within various dermal strata (Hawkes 1974a; Hawkes 1974b; Goda and Fujii 2001; Guo et al. 2007; Kalogianni et al. 2011; Beeching et al. 2013; Djurdjevic et al. 2015), and occasionally in the epidermis (Roberts et al. 1972; Burton 1978). The melanosome layers observed here were consistently located immediately between the epidermal basement membrane and the stratum spongiosum (Figures 7, Appendix B – Figure 20), a loosely organized collagenous layer of the dermis (Hawkes 1974b). Species exhibited various amounts of randomly oriented collagen fibers

typical of the stratum spongiosum around and between melanosomes (Figure 7B, Appendix B – Figure 20A, B,E,H,K), but none exhibited the expected layer of collagen typically surrounding and supporting pigment cells in fishes (Roberts et al. 1972; Hawkes 1974a; Guo et al. 2007; Kalogianni et al. 2011). Several species had a thick stratum compactum internal to the melanosome layer (Figure 7C, E,F, Appendix B - 20N,O), as well as various other layers of continuous and discontinuous melanophores below the stratum compactum (Figure 7A,C,E, Appendix B – Figure 20L,M,O).

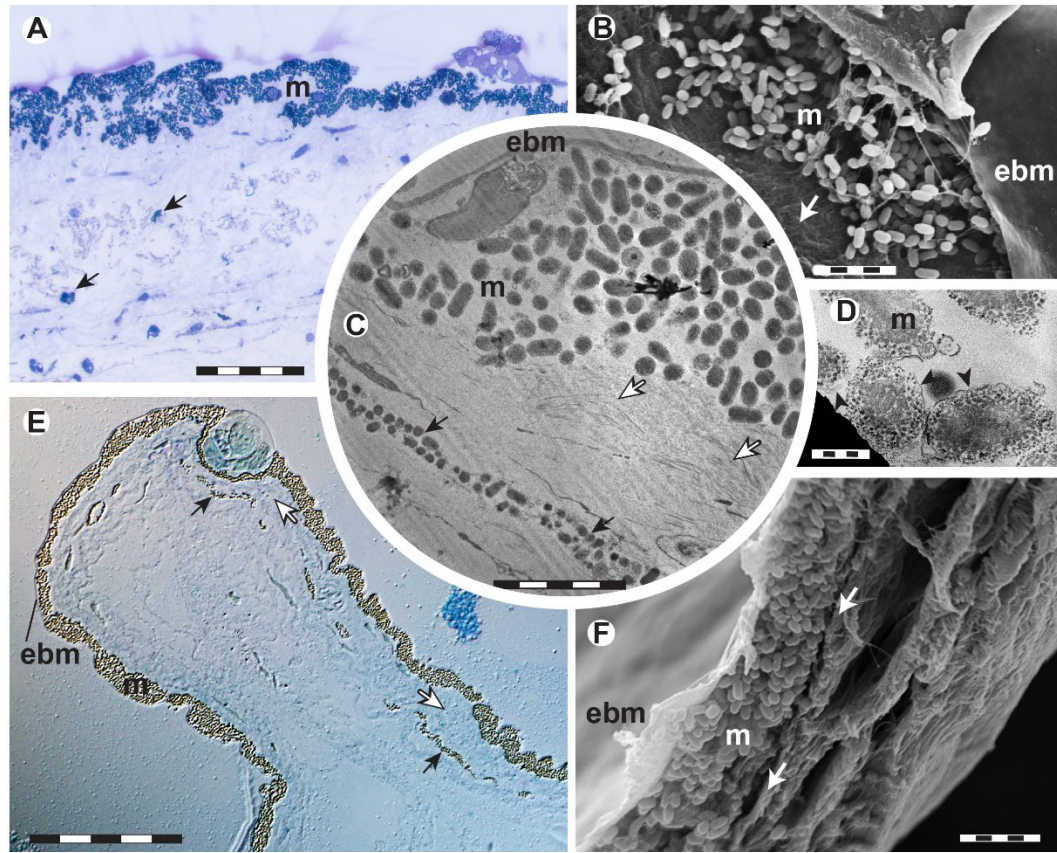


Figure 7: Skin ultrastructure and melanosome geometry. Histology and TEM of the skin of *Oneiroides* sp. (A) and *Idiacanthus antrostomas* (B-F) reveal a continuous layer of melanosomes (m) immediately beneath the epidermal basement membrane (ebm). Melanosomes are membrane bound organelles (black arrowheads). Melanophores (black arrows) are seen beneath the stratum compactum (white arrows). Scale bars A, E 50 μm , B,C,F 5 μm , D 0.5 μm . See also Appendix B - Figure 20.

We used SEM images to measure melanosome length and width to calculate individual melanosome size (as sphere equivalent diameter – the diameter of a sphere with a volume equivalent to the melanosome - hereafter SED) and aspect ratio (the ratio of the length to width) in seven species (*Bassozetus compressus*, *Echiostoma barbatum*, *Eurypharynx pelecانoides*, *Idiacanthus antrostomus*, *Lampadena luminosa*, *Oneiroides* sp., and

Pseudoscopelus sp.; Appendix B - Table 3). We chose these parameters because both the size and aspect ratio of an ellipsoid change the amount and direction of scattering and thus have the potential to affect the reflectance of melanosome layers. Melanosome sphere equivalent diameter (SED) ranged from 440nm \pm 50nm (*E. pelecanoioides*) to 785nm \pm 120nm (*E. barbatum*) with a mean across all species of 612nm (n = 7) (Figure 8). The mean melanosome aspect ratio was 2.1 and species averages ranged from 1.5 \pm 0.3 (*E. pelecanoioides*) to 2.9 \pm 0.6 (*Oneirodes* sp.) (Figure 8). Compared to other ectothermic vertebrates, ultra-black fish had larger (higher SED) melanosomes, particularly for a given aspect ratio (Nakamura et al. 1987; Obika and Meyer-Rochow 1990; Hirose and Matsumoto 1993; Park 2002; Skold et al. 2002; Hirata et al. 2005; Guo et al. 2007; Li et al. 2014; Djurdjevic et al. 2015; Rossi et al. 2019). We restricted our comparison to ectothermic vertebrates because birds and mammals have convergently evolved changes in the melanocortin system related to metabolism that affect melanosome geometry (Li et al. 2014). The large melanosome size in ultra-black deep-sea fishes compared to other vertebrates may affect the absorption of light in the melanosome layer.

3.3.3 Size and aspect ratio of melanosomes combine to produce low reflectance

After identifying the skin ultrastructure responsible for producing ultra-black coloration in these deep-sea fishes, we used mathematical models to determine the mechanism by which the melanosome layer produced low reflectance. To do this we used 3-dimensional finite-difference time-domain (FDTD) optical simulations of random

close-packed aggregations of melanosomes. Given the substantial interspecific variation in aspect ratio and SED observed with SEM, we chose to simulate layers of melanosomes with 169 different combinations of SED and aspect ratio (13×13). Thus, in our models, aspect ratio varied from 1.0 to 4.0 in increments of 0.25, and SED varied from 100nm to 3000nm in increments of 100nm for $SED \leq 1000\text{nm}$, and 500nm for $SED > 1000\text{nm}$. Simulations of $5\mu\text{m} \times 5\mu\text{m} \times 5\mu\text{m}$ skin sections backed by a 100% broadband reflector, mimicking the white muscle and collagen beneath the melanosomes, revealed that both size and aspect ratio had significant impacts on reflectance (Figure 8A). Layers containing melanosomes with an aspect ratio near 2.0 and SED of 600 – 800nm have the lowest reflectance. As SED increases above 1000nm, modeled reflectance of the melanosome layer increases sharply from $<1.5\%$ at $SED = 600\text{nm}$ to $>10\%$ at $SED = 2000\text{nm}$. Similarly, reflectance increases in layers with small melanosomes ($SED < 400\text{nm}$), particularly when the melanosomes have low aspect ratios. Based on these models we hypothesize that the melanosome layer produces low reflectance by scattering light sideways within the layer, thus increasing the pathlength for light absorption.

Comparing the measured melanosome geometry to the model results reveals that the melanosomes in ultra-black fish are well optimized for producing low reflectance, suggesting both the relative accuracy of the model and possible selection for the melanosome geometry observed (Figure 8A). This contrasts with the melanosome

geometry in the skin of 50 other species of ectothermic vertebrates, which produce black and brown coloration and have SEDs between 270nm and 550nm and aspect ratios between 1.26 and 2.24 (Nakamura et al. 1987; Obika and Meyer-Rochow 1990; Hirose and Matsumoto 1993; Park 2002; Skold et al. 2002; Hirata et al. 2005; Guo et al. 2007; Li et al. 2014; Djurdjevic et al. 2015; Rossi et al. 2019). Our modeling indicates that, due to differences in melanosome geometry, even if other ectothermic vertebrates had continuous melanosome layers, those layers would produce higher reflectances than the fishes studied here. These differences between ultra-black fishes and other ectothermic vertebrates suggest that that melanosome geometry observed in deep-sea fishes is not typical of ectothermic vertebrates and may have evolved to minimize reflectance. Additionally, the relationship between melanosome geometry and reflectance may be important in generating variation in melanin-based coloration in other vertebrate taxa.

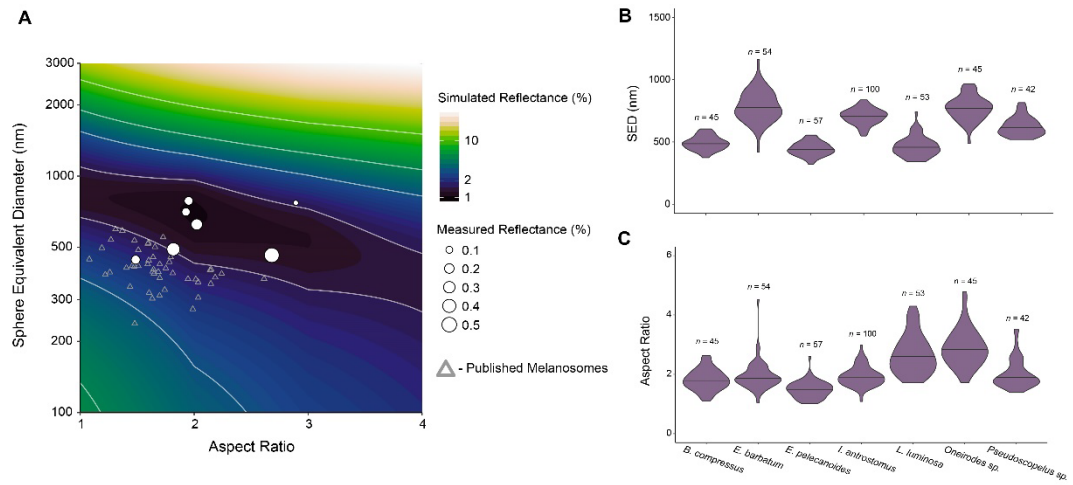


Figure 8: Finite-difference time-domain modeling of close-packed melanosomes. (A) FDTD simulations of the reflectance from 350 – 700nm of close-packed melanosomes with 169 unique combinations of aspect ratio and size reveal that the melanosome geometries of ultra-black deep-sea fishes (shown by white circles) are well optimized to produce the lowest reflectances. Melanosomes from the skin of other ectothermic vertebrates ($n = 50$ species; grey triangles) are smaller for their aspect ratio than those of deep-sea fish and according to our model would produce higher reflectances (Burton 1978; Nakamura et al. 1987; Hirose and Matsumoto 1993; Park 2002; Le Guellee et al. 2004; Hirata et al. 2005; Guo et al. 2007; Failde et al. 2014; Li et al. 2014; Djurdjevic et al. 2015). Melanosome sizes between 600nm and 800nm and aspect ratios between 1.5 and 3.0 produce the lowest reflectance, and all but two species of ultra-black deep-sea fish fall within this range. Grey contours represent reflectance values of 1.5%, 3%, 5%, and 10%. Point sizes are scaled so the area of the point is proportional to the median measured reflectance of that species. (B) Melanosome size (as sphere equivalent diameter) for seven species of ultra-black fishes. (C) Melanosome aspect ratio for the same seven species.

3.3.4 Effect of melanosome layer thickness

While most of the ultra-black species we examined via SEM had melanosomes with geometries that predict low reflectance in our models, the blackest species measured (*Oneirodes* sp.) is predicted to have a higher reflectance than other species

analyzed here. This poor agreement between the modeled and measured reflectance of *Oneiroides* sp. may be a result of modeling melanosome layers with the same thickness for all combinations of melanosome SED and aspect ratio. *Oneiroides* sp. has the thickest layer of melanosomes, indicating that the thickness of the melanosome layer may influence reflectance. To investigate the effect of layer thickness on reflectance, we performed 10 additional simulations in which we varied the thickness of the melanosome layer between 1 μ m and 10 μ m with the same 5 μ m x 5 μ m cross section as the previous simulations, using melanosomes with SED = 800nm and an aspect ratio of 2.0 (the combination of SED and aspect ratio with the lowest modeled reflectance). Reflectance decreased from 9.1% with a 1 μ m thick layer to 3.6% reflectance with a 2 μ m layer to 2.0% reflectance for a 3 μ m layer (Figure 9A, blue dots). The predicted reflectance averaged across 400nm – 700nm was roughly constant once the layer was thicker than 7 μ m. Typically, when a material is neither optically thick (i.e., changing the thickness of the material does not change its reflectance), nor strongly reflective at its surface, a doubling of the thickness results in reflectance that is the square of the original reflectance (when reflectance is treated as a fraction). In our simulations varying melanosome layer thickness, we find that the reflectance does not decrease with increasing thickness as quickly as that relationship would predict (Figure 9A, black curve). Therefore, reflectance from the skin of black fishes is likely to be significantly affected by surface reflection from the top of the layer.

3.3.5 Effect of reflectance on underwater sighting distance

We have demonstrated that at least 16 species of deep-sea fish reflect less than 0.5% of perpendicularly incident light at 480nm, making them some of the blackest known animals. Ultra-black coloration is achieved with a continuous, thin layer of melanosomes that are optimized in size and aspect ratio to produce the lowest reflectance. It is unclear, however, the magnitude of camouflage benefits conferred by being ultra-black as opposed to just black. To determine the camouflage benefits of ultra-black skin we used a computational model developed by Ruxton and Johnsen (2016) to calculate the relative sighting distances by predators of fishes with skin reflectance ranging from 2% to 0% (where the sighting distance would equal zero on perfectly black background). We calculate relative sighting distances (as opposed to absolute distances) because without knowing the intensity of a light source or the shape of the beam, absolute values are unlikely to be accurate. At low light levels, as is the case with a fish reflecting < 2% of an already dim source (*i.e.*, a bioluminescent flash, lure, glow, or searchlight), against the black deep-sea background, the model predicts that the sighting distance is proportional to the square root of the number of photons being reflected back to the viewer. Using this relationship, we find that reducing skin reflectance from 2% to 1% reduces sighting distance by 29% and that decreasing further to 0.5% or 0.05% reflectance reduces sighting distance by 50% and 84%, respectively (Figure 9). Because visual predators typically search a volume of space, and this

reduction in sighting distance is linear, the camouflage benefits of ultra-black skin may be even greater than the reduction in sighting distance calculated here. Given the small size of the fishes studied here it is likely that predator-prey interactions occur over short distances where even small differences in sighting distance can have meaningful effects on interaction outcomes.

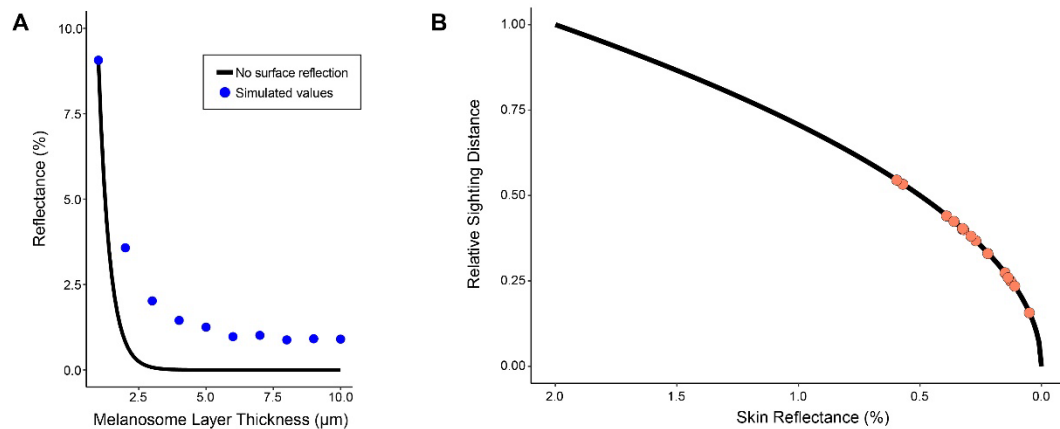


Figure 9: Effect of layer thickness and camouflage benefit of ultra-black skin. (A) Comparison of predicted reflectance for a material that is not optically thick or limited by surface reflection and simulated reflectance from melanosome aggregations varying in thickness from 1μm to 10μm. This suggests that the reflectance from melanosome layers is significantly limited by reflection from the surface, not by the absorption of the layer. The melanosomes in these simulations had an aspect ratio of 2.0 and SED - 800 (approximately the combination producing the lowest reflectance). (B) Reducing skin reflectance from the maximum to the minimum measured here – 2% to 0.05%, that of *Oneirodes* sp. – decreases the relative sighting distance of the fish by six-fold. Points along the line represent individual species. For computational model of sighting distance, see Methods.

3.3 Discussion

We have demonstrated that at least 16 species of deep-sea fishes from multiple distantly related orders have evolved ultra-black skin covering all or parts of the body. In all of these species, we found a continuous layer of ellipsoidal melanosomes that, according to our optical modeling, are the optimal size and shape to produce the lowest reflectance. Furthermore, the melanosomes in deep-sea fishes occupy an area of the melanosome geometry morphospace that is not common among other ectothermic vertebrates, suggesting that melanosome geometry may have specifically evolved in this manner to decrease reflectance. We also found that this reduction in reflectance created by the melanosome layer results in significant reductions in sighting distance, offering a powerful form of camouflage in the deep sea.

In most described ultra-black taxa (*e.g.*, birds, butterflies, and jumping spiders), black patches are bordered by brightly colored patches, and adjacent areas of bright coloration and very low reflectance are thought to increase the contrast of color signals (McCoy et al. 2018; McCoy et al. 2019; Davis et al. 2020). Here, we propose a different function of ultra-black coloration – camouflage (as has been proposed for the structurally-enhanced black coloration in vipers (Spinner et al. 2013) and stick insects (Maurer et al. 2017)). The mechanism we describe here that underlies extremely low reflectance in deep-sea fishes - absorption by melanin in a highly scattering architecture - is similar to those found in birds, butterflies, and jumping spiders (McCoy et al. 2018;

McCoy et al. 2019; Davis et al. 2020). However, in fishes, the light scattering is caused by the melanosomes themselves without the need for the chitin or keratin matrices present in other taxa (McCoy et al. 2018; McCoy et al. 2019; Davis et al. 2020; Wong and Marek 2020). This simple arrangement of close-packed, small particles with a size and shape optimized to produce the lowest reflectance has the potential to inspire the development of new synthetic ultra-black materials.

4. Nanosphere layers increase visual signal conspicuousness in the cleaner shrimps *Ancylomenes pedersoni* and *Lysmata amboinensis*

This work was done in collaboration with Dr. Eleanor Caves and Dr. Sönke Johnsen.

4.1 Introduction

Organisms use visual signals for many functions, including, but not limited to, attracting mates, warding off predators, and communicating with mutualistic partners (Hill 1991; Searcy and Nowicki 2005; Cheney et al. 2009; Maan and Cummings 2012; Price 2017; Caro and Ruxton 2019; Koski 2020). Often these signals are colorful and created using pigments (e.g., the purportedly honest carotenoid signals found in various taxa (Kodric-Brown 1989; Weaver et al. 2018)) or structural colors, such as the brilliant colors of butterflies or birds of paradise (Silberglied and Taylor 1978; Kemp and Rutowski 2007; Wilts et al. 2014). Other signals are achromatic (e.g., white or black), and much of the work on achromatic signals focuses on the role of melanin pigments in dark brown or black coloration (Hill 2006; Da Silva et al. 2013; Roulin 2016; Galvan and Alonso-Alvarez 2017). White coloration as a signal, however, is also found across taxa, although less attention has been given to its structural and chemical basis (but see Stavenga et al. (2004) and Wilts et al. (2017)).

Cleaner shrimp are tropical marine decapod crustaceans that engage in a mutualism with client fish in which the shrimp remove and eat ectoparasites and dead skin (Becker and Grutter 2004). Several species of cleaner shrimp use white body parts to

signal their intent to clean to client fish (Chapuis and Bschary 2010; Caves et al. 2018; Caves et al. 2019). One species, *Anyclomenes pedersoni*, initiates cleaning interactions by whipping its long white antennae back and forth (Caves et al. 2018). A second species, *Lysmata amboinensis*, performs a “leg rocking” behavior with its white legs to advertise cleaning services to potentially predatory fish, a display that can also be accompanied by whipping of the white antennae (Wicksten 2009; Caves et al. 2019). White signals can be particularly effective when animals are signaling to multiple different species, as cleaner shrimp are to multiple species of fish, because they should appear conspicuous regardless of the receiver’s visual system (Wilkins and Osorio 2019). Furthermore, white signals, unlike colored signals, should be effective across different depths and water types. One limitation of the cleaner shrimp signaling system, however, is that the antennae are very thin ($\sim 150\mu\text{m}$ in diameter), potentially limiting their detectability from a distance. One way to mitigate the effects of small size could be to evolve micro- or nanostructures that maximize reflectance from the antennae, similar to the pterin nanoparticles found on the wings of white pierid butterflies (Stavenga et al. 2004).

Here, we use spectroradiometry to measure the spectral reflectance of cleaner shrimp antennae from two species, *Anyclomenes pedersoni* and *Lysmata amboinensis*. Then, we use electron microscopy and optical modeling techniques to describe and model the ultrastructure of the antennae to determine whether cleaner shrimp have evolved

structures that increase reflectance and assess whether those structures are optimal to produce maximal reflectance.

4.2 Methods

4.2.1 Specimen acquisition

The two species used in this study were selected to represent taxa from different locations and genera that both use white antennae to signal to client fish. *Ancylomenes pedersoni* (Chace 1958) is found throughout the Caribbean and has been shown to use antennae whipping to signal intent to clean (Caves et al. 2018). *Lysmata amboinensis* (De Man 1888) is found throughout the tropical Indo-Pacific and Red Sea, and signals to client fish by rocking its white front legs back and forth while simultaneously waving its antennae and using them to tap the client (Caves et al. 2019). Two specimens of *Ancylomenes pedersoni* were purchased from Dynasty Marine Associates (Marathon, FL, USA), and two specimens of *Lysmata amboinensis* were purchased from LiveAquaria (Rhineland, WI, USA). Prior to spectroradiometry, animals were housed in two 2.5-gallon tanks (one per species) filled with artificial seawater made from InstantOcean (United Pet Group, Blacksburg, VA, USA) and individuals were separated by a plastic divider. All individuals were kept on a 16:8 light dark cycle.

4.2.2 Spectroradiometry

Spectral reflectance of the antennae (at 400-700nm) was measured under a stereo microscope (SMZ1500 Nikon, Tokyo, Japan). We used a custom replacement for one of

the two oculars that allows light to be collected by a 400-micron diameter fiber optic cable (R400-7 Ocean Optics Inc., Dunedin, FL, USA) and then sent to a multi-channel spectroradiometer (USB2000 Ocean Optics Inc.). Fiber optic light sources (ACE I, Schott Corporation, Mainz, Germany) were placed at 45° angles on both sides of the scope to provide light. Three-millimeter-long sections of antenna were excised from all four specimens and placed on a platform covered with black electrical tape. Measurements were calibrated using a piece of Spectralon™ with 99% diffuse reflectance (Labsphere, North Sutton, NH, USA) that was shaped to the same size and dimensions as the antenna sections. Each section of antenna was measured five times to account for variations in the position or angle of the light sources.

4.2.3 Morphological analysis

To identify any underlying structural features that may enhance reflectance from the antennae of *A. pedersoni* and *L. amboinensis*, we used scanning electron microscopy. Two 3mm long sections of antenna per animal were excised from two specimens per species and fixed for 12 hours in 2.5% glutaraldehyde buffered with seawater. After fixation, each sample went through a dehydration series of 30%, 50%, 50%, 70%, 70%, 90%, 90%, 100%, 100% EtOH (15 minutes per step). Samples were then dried using a LADD CPD3 critical point dryer (Ladd Research Industries, Williston, VT, USA) to preserve tissue ultrastructure. Once dried, samples were freeze-fractured to expose the cross-section of the antenna, mounted on aluminum SEM stubs with copper tape, and

sputter-coated with an ~8nm thick layer of gold (Denton Desk V; Denton Vacuum LLC, Moorestown, NJ, USA). The samples were imaged using an Apreo S scanning electron microscope (ThermoFisher Scientific, Waltham, MA, USA) at the Duke Shared Materials and Instrumentation Facility with an acceleration voltage of 1kV and magnifications of 2500x – 15000x. We used the image analysis software Fiji (Schindelin et al. 2012) for morphometric analyses of the nanosphere layer found using SEM.

4.2.4 Optical modeling

We performed finite-difference time-domain simulations (FDTD) using the Lumerical solver version 2020b (Ansys, Canonsburg, PA, USA) to assess how the morphology and optical properties of the nanosphere layer found using SEM affected reflectance. Specifically, we focused on the effects of layer thickness, nanosphere diameter, and nanosphere refractive index. In FDTD simulations, Maxwell's equations are solved across a three-dimensional grid with a user-specified spatial resolution, and the electromagnetic waves evolving through time in a stepwise manner. Random close-packed aggregations of nanospheres mimicking the arrangement observed in the antennae were generated using the Uniform Random Particle Distribution (URPD) structure in Lumerical. The URPD structure generates an array of non-overlapping objects until either the domain has been filled or the user-specified maximum number of objects have been added. The function then repeats this process to maximize the number

of objects. In our case, the object was a non-absorbing sphere, and we repeated the process 10000 times to maximize the number of spheres.

In total, we performed three different sets of simulations to determine the effects of sphere refractive index, sphere diameter, and sphere layer thickness on reflectance. The refractive index of the spheres is not known, but similar pteridine or protein spheres have been found in other invertebrates and shown to have refractive indices ranging from ~1.55 to ~2 (Stavenga et al. 2004; Mathger et al. 2013; Wilts et al. 2017; Palmer et al. 2018; Palmer et al. 2020). For our first set of simulations to determine the effect of sphere refractive index on reflectance we simulated a 2 μ m thick layer of non-absorbing spheres underneath a 5 μ m layer of chitin, varying sphere refractive index from 1.57 (approximately that of chitin) to 2.00 (a conservative lower estimate of the index of the pteridine granules found in white Pierid butterflies (Wilts et al. 2017)) in increments of 0.01. Our second set of simulations assessed the effects of sphere diameter on the reflectance of the entire layer. We simulated a 2 μ m thick layer composed of nanospheres ranging between 100nm and 1000nm in diameter, in 30nm intervals. Finally, for our third set of simulations, we simulated layers of nanospheres (300-400nm diameter) between 1 μ m and 10 μ m thick in 300nm intervals to determine how reflectance changes with layer thickness. For both the investigation into the effects of layer thickness and sphere diameter, we simulated the entire range using three different sphere refractive

indices, 1.57 (chitin), 1.78 (isoxanthopterin found in other crustacean reflecting layers), and 2.0 (Pierid butterfly pteridines).

All simulations were performed in a $4\mu\text{m} \times 4\mu\text{m} \times 12\mu\text{m}$ domain with periodic boundary conditions in the x and y directions, broadband (400nm – 700nm) plane wave source propagating in the z direction, and perfectly-matched layer boundary conditions in the z direction (a computational representation of open boundaries that does not reflect any light at the edges of the computational domain). Because we simulated one nanosphere layer and antennae have a layer that wraps all the way around (making it effectively two layers thick to normally incident light), we report reflectance as: $R + RT^2$, where R is the reflectance of one layer and T is the transmission.

4.3 Methods

4.3.1 Spectroradiometry

In *A. pedersoni*, antennal reflectance increased approximately linearly from 20% at 400nm to 40% at 470nm and remained between 40% and 48% at wavelengths longer than 470nm (Figure 10). Antennal reflectance was higher in *L. amboinensis*, ranging between 50% and 63% across the entire range considered here (400nm – 700nm). Interestingly, the shapes of the reflectance curves were nearly identical in *L. amboinensis* and to *A. pedersoni*, except for a steeper decline in reflectance at short wavelengths in *A. pedersoni*. In both animals, reflectance increased from 400nm to 500nm, peaked at ~500nm, and slowly declined as wavelength increased. Variation between samples at a given

wavelength was generally low in *A. pedersoni* (< 1.5% at all wavelengths) and slightly higher in *L. amboinensis* (3-4%). The reflectance measured here was lower than other bright white color patches in animals such as *Pieris rapae* wings (60-80% - Stavenga et al. (2004)) or the white stripes of *Sepia officinalis* (60-70% - Mathger et al. (2013)), however some of this difference may be due to the geometry of the tissue. Cleaner shrimp antennae are cylindrical rather than flat, causing light to scatter in directions that are not captured by the fiber optic, likely leading to an underestimate of the reflectance under more realistic viewing conditions.

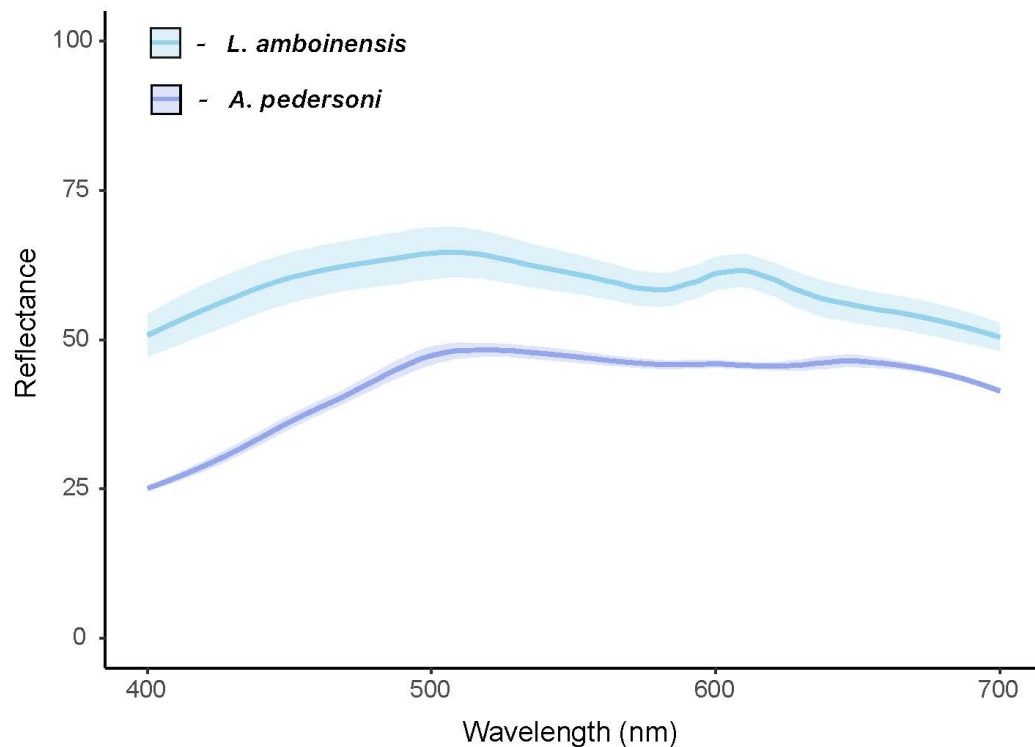


Figure 10: Reflectance from cleaner shrimp antennae. Both *L. amboinensis* and *A. pedersoni* antennae reflect 40-60% of light across much of the visible range. *L. amboinensis* antennae generally reflect more light than *A. pedersoni* antennae, but both of the curves exhibit a similar shape. Both curves increase from 400nm to 500nm, then slowly decline as wavelength increases. Colored ribbons represent +/- 1SE.

4.3.2 Are there structures in the antennae that may increase reflectance?

We found that both *A. pedersoni* and *L. amboinensis* antennae contained a layer of nanospheres (Figure 11). The sphere layer in *A. pedersoni* was located just inside the outer chitin cuticle of the antenna and appeared to be backed by a thin membrane. In contrast, the sphere layer in *L. amboinensis* was located between the outer chitin cuticle and another chitin layer. We also found a partial layer of nanospheres on the interior

surface of the antenna in *L. amboinensis*; however, we could not determine whether this was a second layer that was washed away during the sample preparation process or nanospheres from the primary layer that were washed out into the interior of the antenna. Nanospheres in *A. pedersoni* had an average diameter of $395 \pm 40\text{nm}$ (mean \pm sd), while *L. amboinensis* had slightly smaller nanospheres ($362 \pm 42\text{nm}$; $p < 0.001$; Figure 12). It was difficult to measure the exact thickness of the nanosphere layer due to distortions from the freeze fracturing process, but it appeared to be between $1\mu\text{m}$ and $3\mu\text{m}$ in both species.

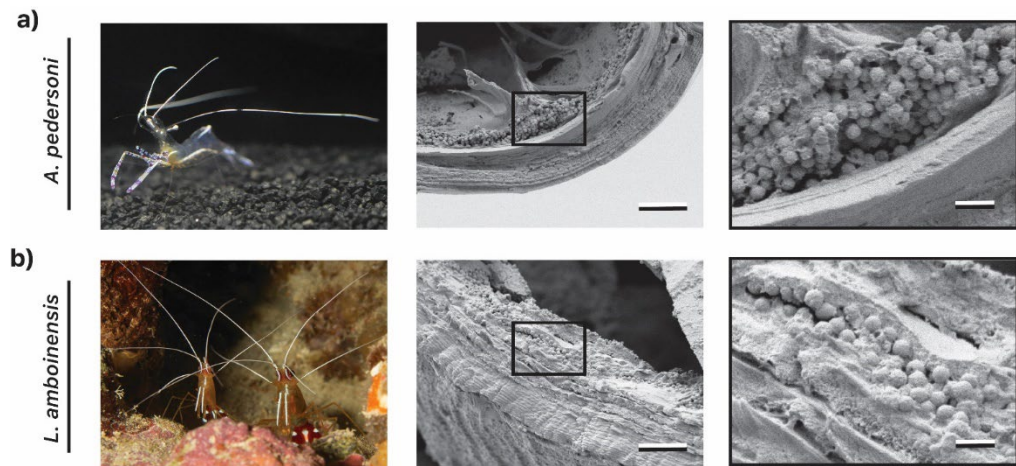


Figure 11: Cross section of cleaner shrimp antennae.(A) (Left) Image of *Ancylomenes pedersoni* highlighting the white antennae. Photo: Sarah Solie. (Middle) SEM image of the cross section of an *A. pedersoni* antenna showing a similar chitin outer wall to the one seen in *L. amboinensis*, the nanosphere layer, and a thin membrane inside of the sphere layer. Scale bar 5μm. (Right) Higher magnification image of just the nanosphere layer. Scale bar 1μm. (B) (Left) Image of two *Lysmata amboinensis* highlighting the white antennae. Photo: Frank Gradyan. (Middle) SEM image of the cross section of a *L. amboinensis* antenna showing the chitin outer wall, nanosphere layer, and what appears to be a second chitin layer. Scale bar 5μm. (Right) Higher magnification image of the same location highlighting the nanosphere layer. Scale bar 1μm.

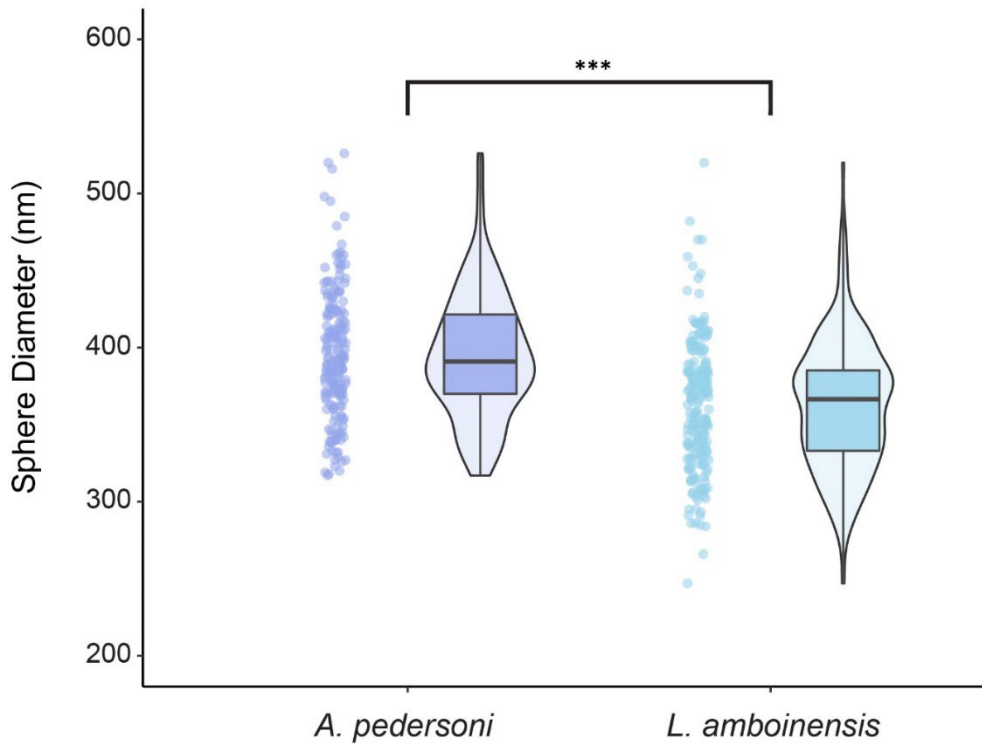


Figure 12: Nanosphere diameter in cleaner shrimp antennae. Measurements of the nanospheres found in the antennae in both species show that both species generally have nanospheres between 300-450nm. The distribution of sizes, however, skews larger in *A. pedersoni* ($p < 0.001$; students t-test).

4.3.3 Are the nanosphere layers optimized to maximize reflectance?

After identifying nanosphere layers in the antennae of *A. pedersoni* and *L. amboinensis*, we used finite-difference time-domain modeling to assess the influence of the sphere layers on overall reflectance and whether the sphere layers are optimal to increase reflectance. Specifically, we analyzed refractive index, sphere diameter, and layer thickness.

First, we examined the effect of nanosphere diameter. Our modeling shows a sharp increase in reflectance at all three refractive indices used as sphere diameter increased from 100nm to 400nm (Figure 13c). At diameters greater than 400nm the effect of sphere diameter on reflectance was refractive index dependent. When $n = 2.0$, reflectance decreased from approximately 60% for 400nm spheres to 39% for 1000nm spheres. For both $n = 1.78$ and $n = 1.57$, reflectance plateaued at 38% and 10%, respectively, once sphere diameters reached 400nm. Regardless of the refractive index of the nanospheres found in shrimp antennae, they are optimally sized to produce the maximum reflectance.

We found a strong linear effect of refractive index on reflectance with the reflectance from a 2 μ m layer increasing from 8.7% at $n = 1.57$ to 57% at $n = 2.0$ (Figure 13a). Even the addition of relatively low refractive index nanospheres ($n = 1.57$) underneath a 5 μ m thick layer of chitin increases reflectance ~4.6x compared to the chitin layer alone (1.9% compared to 8.7%). Although we cannot be certain of the chemical makeup of the nanospheres, if they have a refractive index of ~1.78, similar to pteridines found in other decapod reflecting layers (Palmer et al. 2018; Palmer et al. 2020), they could increase reflectance over 19-fold (1.9% reflectance for a 5 μ m chitin layer compared to 36.9% reflectance for a chitin layer backed by spheres with $n = 1.78$). Lastly, the third parameter we varied in our simulations was nanosphere layer thickness. We simulated 30 layers from 1 μ m to 10 μ m thick and found that increasing the

thickness of the layer caused reflectance to increase asymptotically (Figure 13b). There was a strong linear relationship between thickness and reflectance for very thin layers, with a decreasing slope as thickness approached $10\mu\text{m}$. The shape of the relationship between layer thickness and reflectance depended on the refractive index of the nanospheres. In this case, the lower the refractive index, the thicker a layer must be to reach its asymptotic reflectance. It should be noted that while the $1\text{-}3\mu\text{m}$ thick layers of nanospheres found in cleaner shrimp do not reflect as much light as thicker layers in our simulations, there are other factors that may constrain layer thickness such as small amounts of absorption from the spheres that are not captured in our model. Adding a small amount of absorption to a highly scattering structure may cause thicker layers to be less effective than thinner layers at reflecting light.

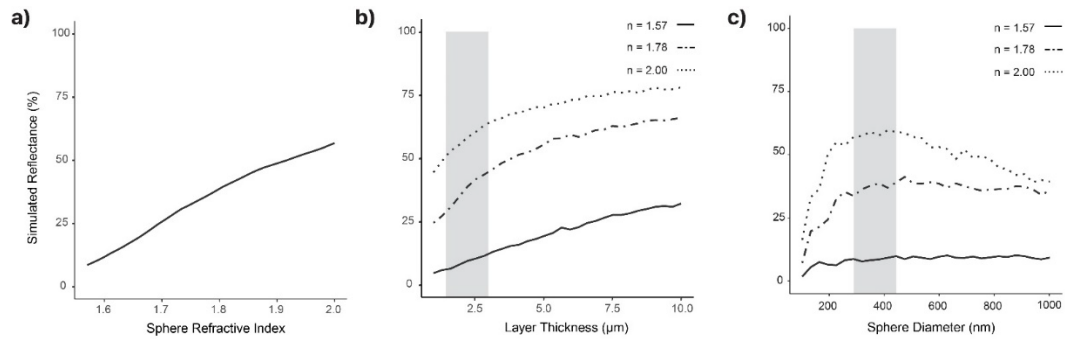


Figure 13: Finite-difference time-domain modeling of nanosphere layers.

(A) Simulated reflectance from a 2 μm thick layer of nanospheres underneath a 5 μm chitin layer demonstrating the roughly linear relationship between nanosphere refractive index and reflectance. Our control simulation, a 5 μm chitin layer with no sphere layer underneath had a simulated reflectance of 1.9%. (B) FDTD simulations of nanosphere layers of varying thicknesses for three different refractive indices (1.57, 1.78, and 2.00) showing that reflectance increases quickly with thickness for thin layers and begins to plateau as one approaches 10 μm thick layers. For high refractive indices, reflectance plateaus for a thinner layer. The grey box highlights the observed range of layer thickness in cleaner shrimp. (C) Simulated reflectance from 2 μm thick layers of nanospheres with diameters ranging from 100 nm to 1000 nm at three refractive indices. For higher refractive indices ($n = 1.78$ and $n = 2.0$), reflectance increases sharply as sphere diameter increases from 100 nm to 400 nm before slightly decreasing or leveling off at diameters greater than 400 nm. At low refractive indices, reflectance reaches a plateau at diameters ~ 300 nm and remains constant with size. The grey box indicates the range of sphere diameters found in both species and highlights that cleaner shrimp nanospheres are optimal in diameter to produce maximum reflectance regardless of refractive index.

4.4 Discussion

Here we show that two species of cleaner shrimp that use their white antennae to signal to client fish, *A. pedersoni* and *L. amboinensis*, have evolved 1-3 μm thick layers of nanospheres inside their antennae, and modeling suggests that this nanosphere layer increases reflectance by 4.6x to 19x compared to a 5 μm chitin layer with no nanospheres

underneath. Furthermore, by exploring the effects of changing the morphology of the nanosphere layer, we show that the nanospheres found here are the optimal diameter to maximize reflectance. Although we do not know the composition of the nanospheres, they are similar in size and appearance to granules found in reflective layers in other decapod crustaceans, including isoxanthopterin granules forming the retinal reflectors of *Cherax quadricarinatus* (Palmer et al. 2018), *Homarus americanus* (Kleinholtz 1959), *Litopenaeus vannamei* (Palmer et al. 2020), *Machrobrachium rosenbergii* (Palmer et al. 2018), *Penaeus setiferus* (Zyznar and Nicol 1971). Similar granules are also found in the reflecting layers of the photophores of the deep-sea shrimp *Oplophorus spinosus* and *Systellaspis debilis* (Nowell et al. 1988), suggesting that cleaner shrimp may be using a widespread structural toolkit in a novel way to increase reflectance from the antennae.

Cleaner shrimp all face a similar challenge: they are small animals that live at set locations and must both attract clients to those locations and advertise their cleaning services to clients upon their arrival. Signal theory predicts that if signals communicate similar messages to similar receivers, they should be under selection to be similar across species (as in, e.g., convergent floral syndromes (Schiestl and Johnson 2013)). One reason species might display signals of a certain form is if that form is particularly conspicuous to the intended receiver in the signaling environment (e.g. Marler 1957). Cleaner shrimp face a particular challenge in being conspicuous to their intended receiver, in that dozens of species of fish, with diverse visual capabilities (see, e.g., Marshall et al. 2019)

can all serve as clients, and the visual environment can be highly heterogeneous, varying in both depth (and thus light level and spectral composition) and visual background.

White signals are particularly useful compared to colorful signals in these situations because their apparent color is generally unaffected by spectral composition, light level, and the visual background. The data presented here are consistent with the hypothesis that cleaners are under selection to increase the visibility of their signaling traits in a way that is effective for a range of visual systems and diverse visual environments.

5. Conclusions and Future Directions

This dissertation has three primary conclusions. First, ultra-black coloration can serve multiple functions in animals. Butterflies from four subfamilies within the Nymphalidae and Papilionidae have evolved ultra-black scales that reflect as little as 0.05% of light (Chapter 2). Ultra-black coloration in these species is found adjacent to bright color patches and it is frequently sexually dimorphic (Appendix A – Table 1). This suggests that ultra-black scales may serve to increase the apparent brightness of sexual signals in butterflies, despite potentially reducing the apparent saturation (Pitt and Winter 1974). I also found that deep-sea fishes from seven distantly related orders are equally as black as the butterflies from Chapter 2, but for a different function – camouflage (Chapter 3). Deep-sea fishes, however, exist in a world where the only way to be well-camouflaged is to absorb or transmit almost all of the light that hits them. Indeed, I found that at least 16 species of deep-sea fishes have evolved a continuous melanosome layer in the skin that allows them to reflect $< 0.5\%$ of light.

The second primary conclusion is that pigments can produce ultra-black coloration without being embedded in a chitin or keratin structure. Previously, every described ultra-black animal, including birds (McCoy et al. 2018; McCoy et al. 2019), peacock spiders (McCoy et al. 2019), and butterflies (Davis et al. 2020), has achieved low reflectance by embedding melanin in a highly scattering keratin or chitin structure. Ultra-black deep-sea fishes, however, reflect $< 0.5\%$ of light using melanin as both the

absorber and the structural element. All the deep-sea fishes studied here have a continuous layer of ellipsoidal melanosomes in the skin. These melanosomes are the optimal size and shape to minimize the reflectance of the melanosome layer. I hypothesize that this minimization in reflectance is the result of the melanosomes in deep-sea fish skin being the optimal size to maximize scattering within the melanosome layer, thus increasing the number of chances for absorption. Similar to what has been found in other ultra-black taxa, multiple scattering and absorption by melanin are the underlying principles of ultra-black coloration in fishes. What separates deep-sea fishes, though, is that the melanosomes provide all the scattering without the need for an additional structure. This dual role of the melanosomes, providing both scattering and absorption, is possible because melanin has a very high real part of the refractive index relative to most other biological materials (Stavenga et al. 2015).

Finally, the third conclusion of this dissertation is that variations of the simple, scattering nanoparticle layer found in ultra-black deep-sea fishes can also be used to produce coloration with exceptionally high reflectance. I found that two species of cleaner shrimp, *Ancylomenes pedersoni* and *Lysmata amboinensis*, have a layer of spherical nanoparticles in their antennae that optical modeling suggests can increase reflectance by up to 19-fold (Chapter 4). The nanoparticles in cleaner shrimp antennae are the optimal size to maximize reflectance, similar to how deep-sea fish melanosomes are the optimal size and shape to minimize it. The primary difference between nanoparticle

layers that produce ultra-black and bright white coloration is the composition of the nanoparticles. Highly absorbing nanoparticles, such as melanin, produce low reflectance. Conversely, non-absorbing nanoparticles produce high reflectance. This simplified system may be used to produce other colors, as well, and it offers a potentially interesting example of a simple, color production mechanism that could inspire new man-made materials.

5.1 Future Directions

5.1.1 Empirical Tests of the Effects of Increasing Contrast on Signal Effectiveness

An important extension of the work presented in Chapter 2, as well as previous studies of ultra-black animals with bright color patches (McCoy et al. 2018; McCoy et al. 2019a, b), is empirically testing the effects of decreasing reflectance to $< 0.5\%$ on signal effectiveness. Contrast has been shown to be important for animals that use color signals and, all else being equal, signals are predicted to maximize color or brightness contrast with the background to improve either the probability of detection (Endler 1992) or the distance at which those signals can be detected in attenuating media such as water (Johnsen 2002). Indeed, we see that dark patches bordering colorful signals create high brightness contrast between the signal and the background in birds (Doucet et al. 2007; Doucet and Meadows 2009), fishes (Marshall 2000; Losey 2003), lizards (McClean et al. 2014), and butterflies (Stavenga et al. 2004). Furthermore, some animals go to great

lengths behaviorally to increase contrast, for example by clearing lighter color debris from display courts to present a darker, more uniform background (Uy and Endler 2004; Chiver and Schlinger 2017). Despite substantial evidence that high contrast is important for animal color signals, there are no empirical tests of how decreasing reflectance to extreme levels ($< 0.5\%$) impacts the effectiveness or perceived attractiveness of color signals.

The most definitive test of the effects on low reflectance on signal effectiveness involves assessing receiver responses to signals with varying levels of contrast. One way this could be done is by manipulating the reflectance of ultra-black patches in a smaller animal, such as a peacock spider or butterfly, and assessing effectiveness using two-choice tests. Two-choice tests have often been used to study the relative attractiveness of signals to potential mates (Griggio et al. 2007; Griggio et al. 2010; Taylor et al. 2011; Stange et al. 2017; Dyson et al. 2020). By performing two-choice tests with animals that have varying levels of reflectance on the black patches and controlling for contrast between the color patch and ultra-black patches, one can determine whether the relationship between contrast and preference is linear, or some other shape. The shape of this relationship can help distinguish between three competing hypotheses about the importance of ultra-black coloration. The first hypothesis is that there is a linear relationship between contrast and preference, meaning ultra-black coloration is just an extreme form of features that matter in other signaling systems. The second hypothesis

is that there are diminishing returns with increasing contrast. If this is correct, it prompts other questions about whether sexual selection is particularly strong in ultra-black species, or whether there are environmental factors that make ultra-black coloration advantageous. Finally, there may be a distinct benefit of ultra-black coloration that is not seen with more typical high contrast patterns. It has been hypothesized that surrounding a bright, colorful signal with ultra-black coloration may make the color appear self-luminous (Kreezer 1930; Speigle and Brainerd 1996; McCoy et al. 2018). If this is the case, one would expect to find a threshold of contrast, above which preference for a signal is significantly stronger due to this optical illusion. Behavioral tests are paramount to disentangle these hypotheses and better understand the forces driving the evolution of ultra-black coloration in animals.

5.1.2 Effects of pigment granule geometry on chromatophore reflectance

Chapters 3 and 4 revealed that the size and shape of pigment granules have a substantial impact on the reflectance and absorption of aggregations of these granules. Although these are specific examples where particularly high or low reflectance was needed, countless animals have chromatophores containing aggregations of pigment granules (Bagnara et al. 1968; Schliwa 1986; Henze et al. 2019). Chromatophores containing the same pigments are often treated equally, but as I have demonstrated in this dissertation, pigment granule geometry offers a hidden source of diversity that may affect the color of animal chromatophores. For example, a chromatophore containing red

pteridine pigment could have granules of a size that maximize scattering of short and middle wavelength light, shifting the reflectance of the entire chromatophore towards longer wavelengths. One way to study the potential for pigment granule geometry to affect the color of chromatophores is by using optical modeling techniques, such as FDTD modeling. For a given pigment, one could simulate aggregations of nanoparticles with various combinations of size and shape and compare the simulated hue and brightness of the reflected light in each simulation. This modeling approach, if done for multiple pigments that have different absorption profiles, would allow us to draw generalized conclusions about the effects of pigment granule size and shape on reflectance. An alternative approach to modeling the effects of pigment granule geometry would be to pair FDTD modeling with a comparative survey, similar to what I presented in Chapter 3. For example, looking at reflectance and pigment granule geometry across a group of fishes or lizards that all contain the same pterin pigment could be used to identify a parameter space for optical modeling of those chromatophores. From there, modeling could be used to validate or explain any observed differences in coloration within that group. Regardless of the approach, exploring the diversity of pigment granule geometry and its effects on color will further our understanding of color production mechanisms in animals and potentially reveal previously unrecognized specializations in color production. Furthermore, a more

sophisticated understanding of the effects of pigment granule geometry on color has the potential to inform the production of artificial pigments.

5.1.3 Comparative studies of optical adaptations in cleaning and non-cleaning shrimps

In Chapter 4, I demonstrated that two species of cleaner shrimp, *Ancylomenes pedersoni* and *Lysmata amboinensis*, have a layer of non-absorbing nanospheres in their white antennae that increase reflectance. Although this finding suggests that the nanosphere layer is meant to make the antennae more conspicuous to client fish, we do not know whether this layer is found in related non-cleaners. It has been suggested that cleaners often have conspicuous white body parts that closely related cleaners do not (Walls 1983; Ellis 1985; Caves 2018), however some facultative cleaners have white antennae that may or may not serve a signaling function (Titus et al. 2017). An interesting extension of the work presented here would be a comparative survey of white body parts and nanostructures from obligate cleaners, facultative cleaners, and non-cleaners. If obligate and facultative cleaners possess reflectance-increasing nanostructures that are not found in non-cleaners, this would further strengthen the hypothesis that the nanosphere layers found in *A. pedersoni* and *L. amboinensis* evolved to make their antennae more conspicuous to client fishes. If, however, both cleaners and non-cleaners have a nanosphere layer in the antennae, nanospheres may represent a more widely used structural tool for creating white color in decapod shrimp.

In conclusion, the work presented in this dissertation prompts many exciting questions and provides a foundation for future research investigating the functions of ultra-black coloration, pigment-structure interactions, and signal design. Our understanding of the production of ultra-black and bright white coloration in butterflies, fishes, cleaner shrimp, and other taxa is rapidly expanding (McCoy et al. 2018; McCoy et al. 2019a; McCoy et al. 2019b). Despite this expansion, we have no empirical tests of the functions of extreme coloration. Furthermore, the breadth of taxa that have been systematically studied with respect to extreme coloration is limited. By focusing on behavioral tests of the function of extreme coloration and systematic studies of the distribution of these traits within phylogenetic groups, we can begin to understand the evolutionary forces driving the production of this trait in animals.

Appendix A. Supplemental information for Chapter 2

Table 1: Black butterfly specimen list for reflectance measurements.

Family	Subfamily	Species	Color	Shape
Nymphalidae	Biblidinae	<i>C. antinoe</i>	Ultra-black	Rectangular
		<i>C. numilia (f)</i>	Black	Rectangular
		<i>C. numilia (m)</i>	Ultra-black	Rectangular
		<i>E. chlorocroa</i>	Ultra-black	Chevron
	Danainae	<i>E. dufresne</i>	Ultra-black	Rectangular
		<i>E. klugi</i>	Ultra-black	Rectangular
		<i>E. midamus</i>	Matte brown	Crescent
	Heliconinae	<i>H. doris</i>	Ultra-black	Rectangular
		<i>H. ismensius</i>	Black	Rectangular
		<i>H. wallacei</i>	Ultra-black	
Papilionidae	Papilioninae	<i>T. brookiana (f)</i>	Brown	Honeycomb
		<i>T. brookiana (m)</i>	Ultra-black	Honeycomb
		<i>T. helena</i>	Ultra-black	Honeycomb
		<i>P. bangui</i>	Ultra-black	
		<i>P. iphidamus</i>	Ultra-black	
		<i>P. oribaeus</i>	Ultra-black	

Table 2: Butterfly scale simulation model parameters. Size parameters used for FDTD simulations of ultra-black butterfly scales. Parameters were taken from our blackest species, *C. antinoe*.

Model Parameter	Size (nm)
Hole width (long axis)	500
Hole width (short axis)	330
Inter-lamina distance	1200
Ridge height	600
Upper lamina thickness	200
Crossrib thickness	80

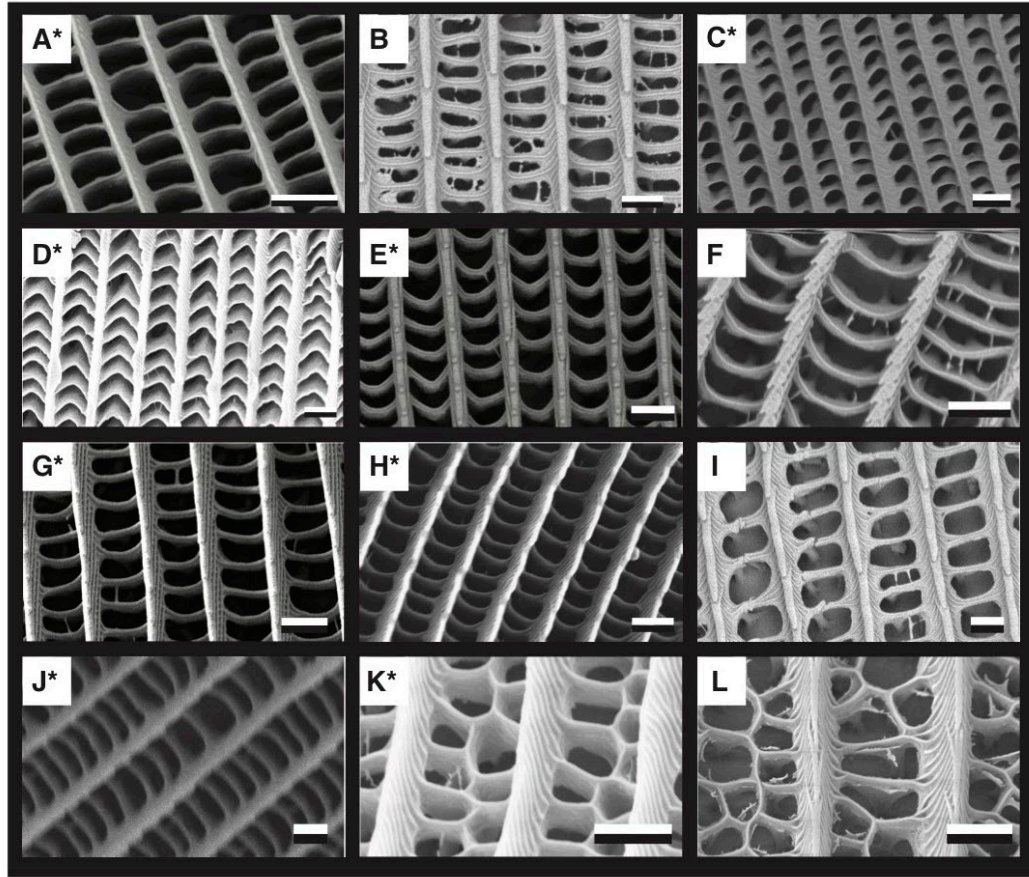


Figure 14: Diversity of butterfly scale hole shapes and sizes.(A) *Catonephele antinoe* (B) *Catonephele numilia* female (C) *Catonephele numilia* male (D) *Eunica chlorocroa* (E) *Euploea dufresne* (F) *Euploea midamus* (G) *Euploea klugi* (H) *Heliconius doris* (I) *Heliconius ismenius* (J) *Napeocles jucunda* (K) *Trogonoptera brookiana* male (L) *Trogonoptera brookiana* female; All species possess periodic holes bordered by long ridges, but the holes are smaller in ultra-black species compared to closely related black or brown species. All scale bars are 1 μ m. *denotes ultra-black species.

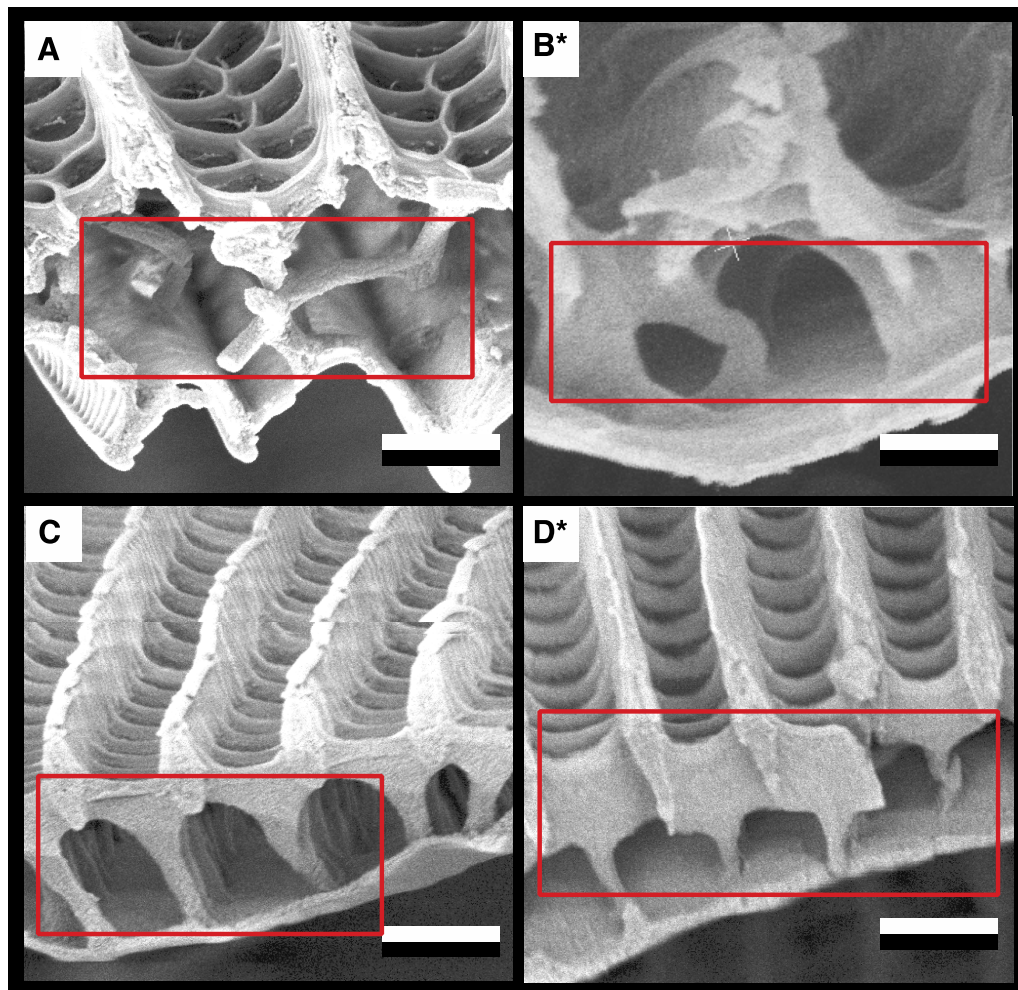


Figure 15: Scale trabeculae from ultra-black male and dark brown female butterflies. (A) *Trogonoptera brookiana* female (B) *Trogonoptera brookiana* male (C) *Catonephele numilia* female (D) *Catonephele numilia* male. The trabeculae (outlined in the red box) are larger in ultra-black male butterflies than in regular dark brown/black females of the same species

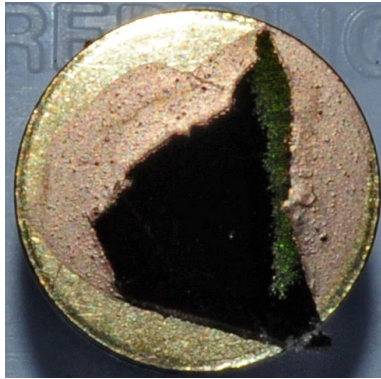


Figure 16: Section of ultra-black butterfly wing sputter coated with gold. Ultra-black wings are still black when coated with gold, indicating that there is a structural component to absorption.

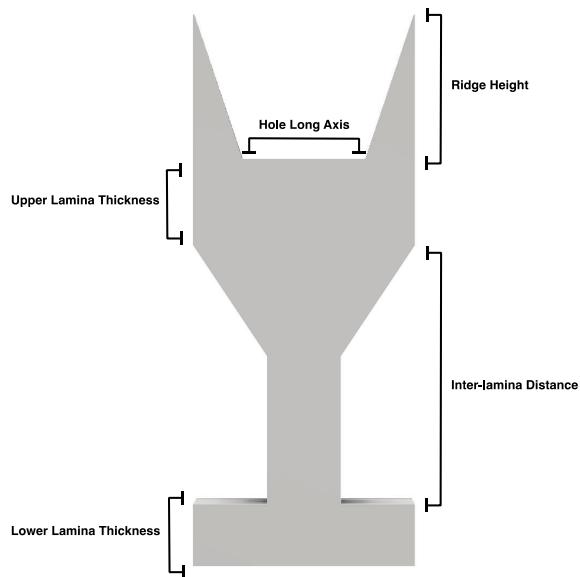


Figure 17: Butterfly scale unit cell diagram. Schematic diagram of unit cell used for FDTD simulations. The unit cell was simulated with periodic boundaries to form a semi-infinite sheet of repeating cells.

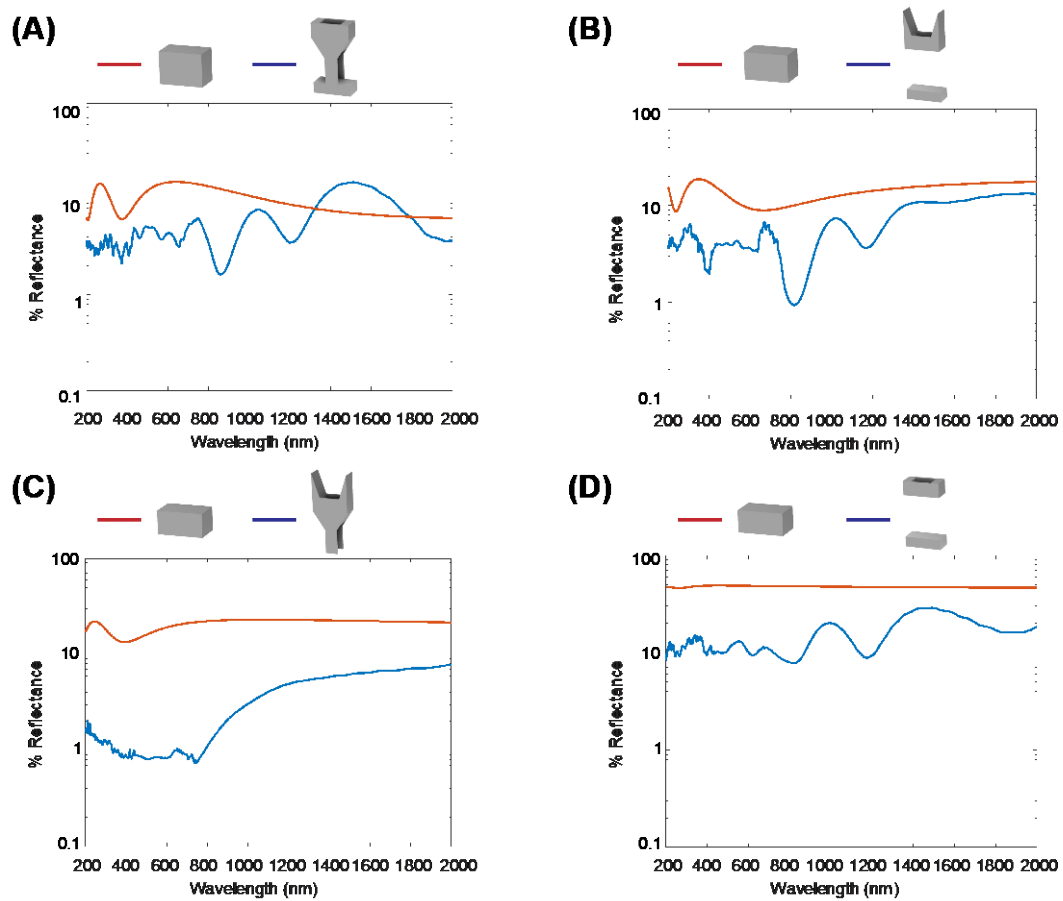


Figure 18: Simulated reflectance of butterfly scales and blocks consisting of an equal volume of absorbing material.

Appendix B. Supplemental information for Chapter 3

Table 3: Species list for spectral measurements and histology. List of deep-sea fish species with the number of specimens, reflectance measurements per species, and the type(s) of microscopy performed. Grey rows are species for which we have reflectance measurements.

Order	Family	Species	# Specimens	# Spectral Measurements	SEM	TEM	LM
Anguilliformes	Eurypharyngidae	<i>Eurypharynx pelecanoioides</i>	1	16	X		
Beryciformes	Melamphaidae	<i>Melamphaes lugubris</i>	1	3			
		<i>Poromitra crassiceps</i>	7	24	X	X	X
		<i>Cetomimus</i> sp.	1		X		X
		<i>Anoplogaster cornuta</i>	1		X		X
Lophiiformes	Oneirodidae	<i>Oneirodes</i> sp.	1	3	X		X
Myctophiformes	Myctophidae	<i>Lampadena luminosa</i>	1	5	X		
		<i>Lepidophanes guentheri</i>	1	4			
		<i>Lampanyctus</i> sp.	1			X	X
Ophidiiformes	Ophidiidae	<i>Bassozetus compressus</i>	1	10	X		
Perciformes	Chiasmodontiae	<i>Pseudoscopelus</i> sp.	1	7	X		X
Stomiiformes	Gonostomatidae	<i>Cyclothone acclinidens</i>	7	22			
		<i>Cyclothone</i> sp.	1		X		X
	Stomiidae	<i>Sigmops elongatus</i>	3	13			
		<i>Astronesthes micropogon</i>	1	4			
		<i>Chauliodus macouni</i>	1	3			
		<i>Echiostoma barbatum</i>	1	5	X	X	X
		<i>Eustomias hypopsilus</i>	1	7			
		<i>Eustomias schmidtii</i>	1	6			X
		<i>Eustomias</i> sp.	1	5			
		<i>Idiacanthus antrostomus</i>	3	21	X	X	X
		<i>Photostomias guernei</i>	4	19		X	X
		<i>Stomias</i> sp.	1		X		X
Alepocephaliformes	Platytrochidae	<i>Sagamichthys abei</i>	1		X		X

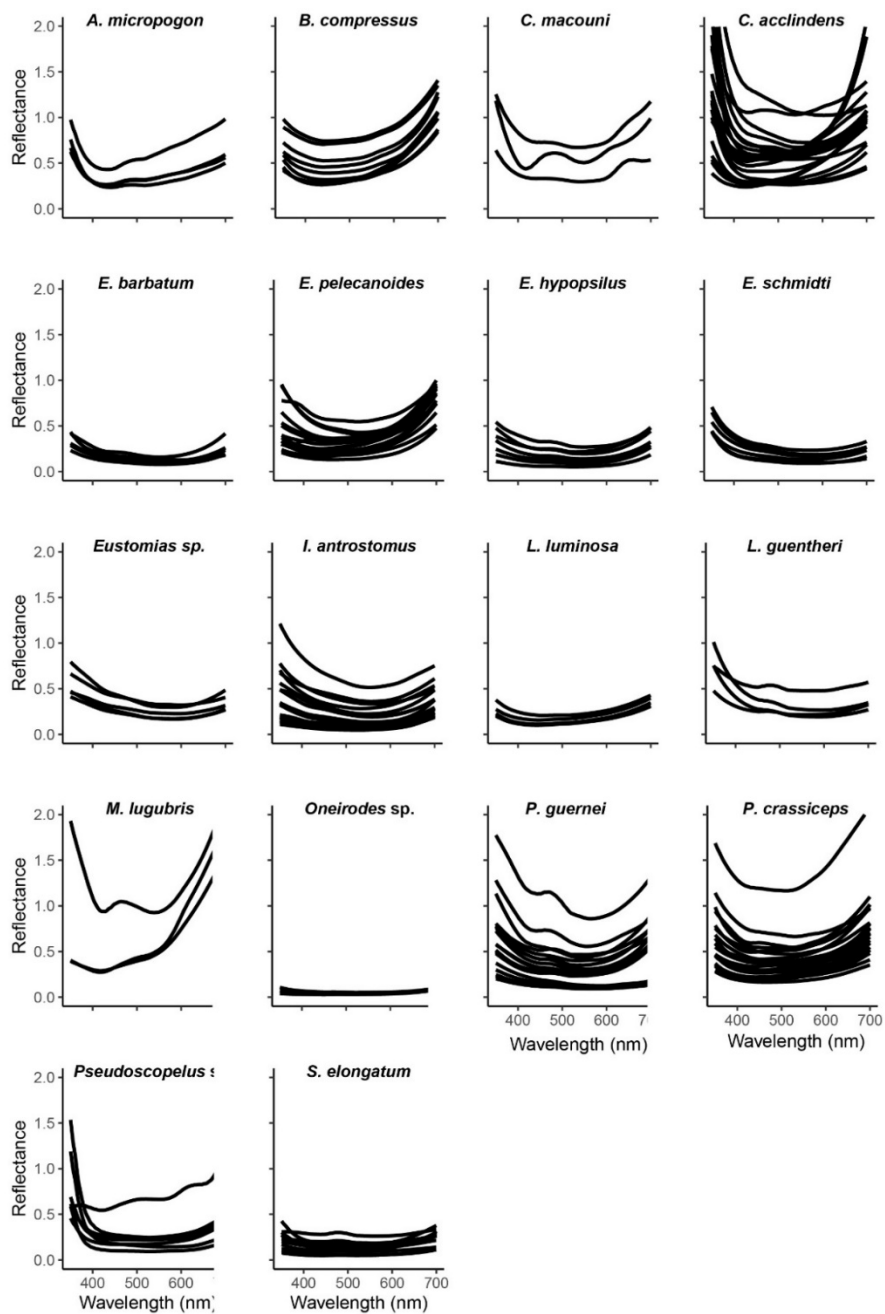


Figure 19: Deep-sea fish reflectance spectra. Individual reflectance measurements for each species (fit with LOESS curve).

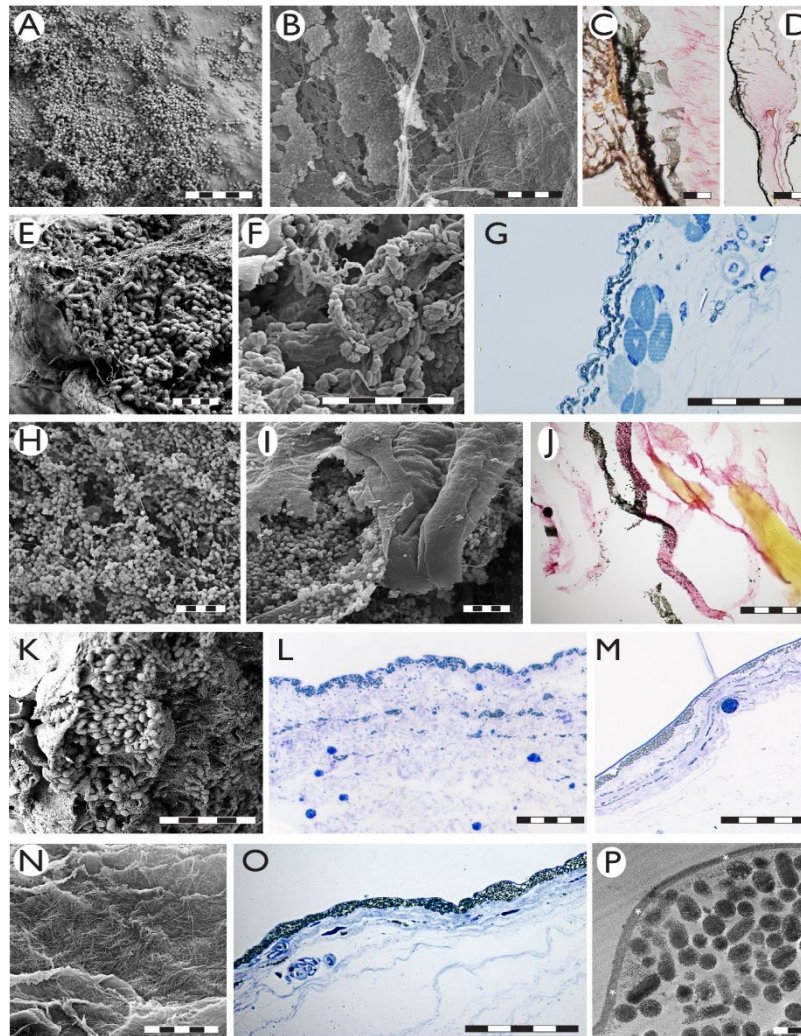


Figure 20: Histology of ultra-black fishes. (A) *E. pelecyanoides*, SEM showing melanosome layer and stratum compactum. B–D. *P. crassiceps*, SEM and light images showing melanosome layers with collagen fibers. A melanosome layer is seen below the basement membrane as well as a melanosome layer below the stratum compactum. E. *Oneirodes* sp., SEM. F–G. *Lampanyctus* sp. SEM and light images showing melanosomes and underlying dermis/muscles. H. *Pseudoscopelus* sp. showing the melanosome layer. I–J. *Cyclothone* sp. SEM and light images of melanosomes below the basement membrane. K–L. *E. barbatum* SEM and light images showing surface layer of melanosomes, and deeper dermal layer. M. *P. guernei* light images showing melanosome layer. N–Q. *I. antrostomus* SEM, light images, and TEM showing lamellae of the stratum compactum, melanosome layer, and scattered deeper dermal melanophores. Scale bars A, H, K, N 10 μm ; B, E, F, I 5 μm ; J, G, L, O 50 μm ; P 1 μm ; M 100 μm ; C 20 μm ; D 200 μm .

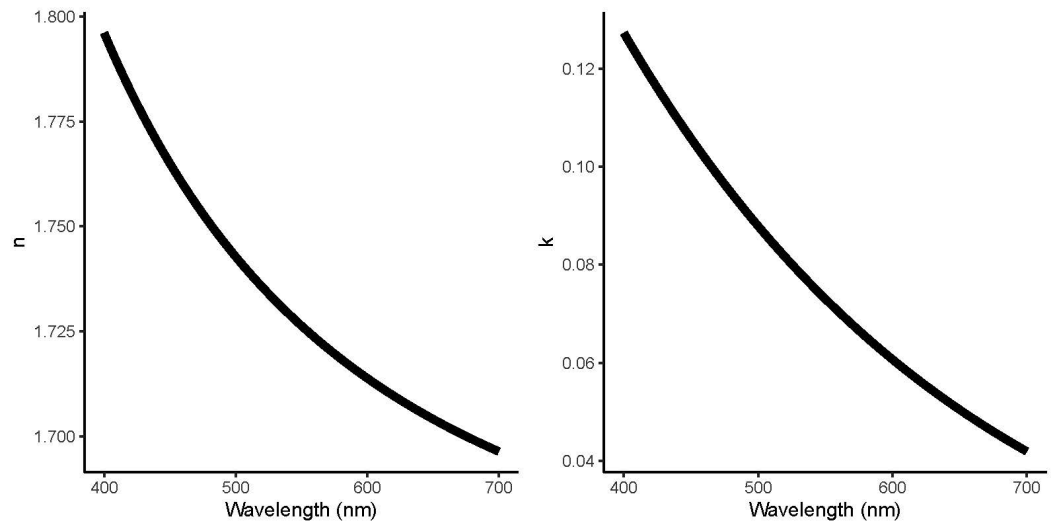


Figure 21: Simulated melanosome refractive index profile. Plot of the real (left) and imaginary (right) components of the refractive index used in all melanosome simulations.

References

- Allen, J.J., Mäthger, L.M., Barbosa, A., Buresch, K.C., Sogin, E., Schwartz, J., Chubb, C. and Hanlon, R.T. (2010). Cuttlefish dynamic camouflage: responses to substrate choice and integration of multiple visual cues. *Proc. Roy. Soc. B* 277, 1031-1039.
- Andrade, P. and Carneiro, M. (2021). Pterin-based pigmentation in animals. *Bio. Lett.* 17, 20210221.
- Arenas, L.M., Troscianko, J. and Stevens, M. (2014). Color contrast and stability as key elements for effective warning signals. *Front. Eco. Evo.* 2, 25.
- Bagge, L.E., Osborn, K.J. and Johnsen, S. (2016). Nanostructures and monolayers of spheres reduce surface reflections in hyperiid amphipods. *Curr. Bio.* 26, 3071-3076.
- Bagnara, J.T., Taylor, J.D. and Hadley, M.E. (1968). The dermal chromatophore unit. *J. Cell Bio.* 38, 67-79.
- Bagnara, J.T. (2003). Enigmas of pterorhodin, a red melanosomal pigment of tree frogs. *Pig. Cell Res.* 16, 510-516.
- Barnett, J.B., Michalis, C., Scott-Samuel, N.E. and Cuthill, I.C. (2021). Color pattern variation forms local background matching camouflage in a leaf-mimicking toad. *J. Evo. Bio.* 34, 1531-1540.
- Beck, M.L., Davies, S. and Sewall, K.B. (2018). Urbanization alters the relationship between coloration and territorial aggression, but not hormones, in song sparrows. *Anim. Behav.* 142, 119-128.
- Becker, J.H. and Grutter, A.S. (2004). Cleaner shrimp do clean. *Coral reefs* 23, 515-520.
- Beeching, S.C., Glass, B.A. and Rehorek, S.J. (2013). Histology of melanic flank and opercular color pattern elements in the Firemouth Cichlid, *Thorichthys meeki*. *J. Morph.* 274, 743-749.
- Bell, R.C. and Zamudio, K.R. (2012). Sexual dichromatism in frogs: natural selection, sexual selection and unexpected diversity. *Proc. Roy. Soc. B.* 279, 4687-4693.

- Bhosale, P. and Bernstein, P.S. (2007). Vertebrate and invertebrate carotenoid-binding proteins. *Arch. Biochem. Biophys.* 458, 121-127.
- Bonser, R.H. (1995). Melanin and the abrasion resistance of feathers. *Condor*. 97, 590-591.
- Brown, R.J., Brewer, P.J. and Milton, M.J. (2002). The physical and chemical properties of electroless nickel–phosphorus alloys and low reflectance nickel–phosphorus black surfaces. *J. Mat. Chem.* 12, 2749-2754.
- Burley, N. and Coopersmith, C.B. (1987). Bill color preferences of zebra finches. *Ethology*. 76, 133-151.
- Burton, D. (1978). Melanophore distribution within the integumentary tissues of two teleost species, *Pseudopleuronectes americanus* and *Gasterosteus aculeatus* form leiurus. *Can. J. Zoo.* 56, 526-535.
- Burt Jr, E.H. and Ichida, J.M. (2004). Gloger's rule, feather-degrading bacteria, and color variation among song sparrows. *Condor*. 106, 681-686.
- Candolin, U. (2000). Changes in expression and honesty of sexual signaling over the reproductive lifetime of sticklebacks. *Proc. Roy. Soc. B.* 267, 2425-2430.
- Cao, W., Zhou, X., McCallum, N.C., Hu, Z., Ni, Q.Z., Kapoor, U., Heil, C.M., Cay, K.S., Zand, T., Mantanona, A.J. and Jayaraman, A. (2021). Unraveling the structure and function of melanin through synthesis. *J. Am. Chem. Soc.* 143, 2622-2637.
- Caro, T. and Mallarino, R. (2020). Coloration in mammals. *Trends Eco. Evo.* 35, 357-366.
- Caro, T. and Ruxton, G. (2019). Aposematism: unpacking the defences. *Trends Eco. Evo.* 34, 595-604.
- Caves, E.M. (2018). *The Visual Ecology of the Cleaner Shrimp-Client Fish Mutualism* (Doctoral dissertation, Duke University).
- Caves, E.M., Chen, C. and Johnsen, S. (2019). The cleaner shrimp *Lysemata amboinensis* adjusts its behavior towards predatory versus non-predatory clients. *Bio. Lett.* 15, 20190534.

- Caves, E.M., Green, P.A. and Johnsen, S. (2018). Mutual visual signaling between the cleaner shrimp *Ancylomenes pedersoni* and its client fish. *Proc. Roy. Soc. B.* 285, 20180800.
- Chapuis, L. and Bshary, R. (2010). Signaling by the cleaner shrimp *Periclimenes longicarpus*. *Anim. Behav.* 79, 645-647.
- Chatelain, M., Gasparini, J., Jacquin, L. and Frantz, A. (2014). The adaptive function of melanin-based plumage coloration to trace metals. *Bio. Lett.* 10, 20140164.
- Cheney, K.L., Grutter, A.S., Blomberg, S.P. and Marshall, N.J. (2009). Blue and yellow signal cleaning behavior in coral reef fishes. *Curr. Bio.* 19, 1283-1287.
- Childress, J.J., Barnes, A.T., Quetin, L.B. and Robison, B.H. (1978). Thermally protecting cod ends for the recovery of living deep-sea animals. *Deep Sea Res.* 25, 419-422.
- Chiver, I. and Schlinger, B.A. (2017). Clearing up the court: sex and the endocrine basis of display-court manipulation. *Anim. Behav.* 131, 115-121.
- Cott, H.B. (1940). *Adaptive coloration in animals*. Oxford University Press.
- Cronin, T.W., Johnsen, S., Marshall, N.J. and Warrant, E.J. (2014). *Visual ecology*. Princeton University Press.
- Cuthill, I.C., Allen, W.L., Arbuckle, K., Caspers, B., Chaplin, G., Hauber, M.E., Hill, G.E., Jablonski, N.G., Jiggins, C.D., Kelber, A. and Mappes, J. (2017). The biology of color. *Science*. 357.
- Cuthill, I.C., Matchette, S.R. and Scott-Samuel, N.E. (2019). Camouflage in a dynamic world. *Curr. Op. Behav. Sci.* 30, 109-115.
- Da Silva, A., van den Brink, V., Emaresi, G., Luzio, E., Bize, P., Dreiss, A.N. and Roulin, A. (2013). Melanin-based color polymorphism signals aggressive personality in nest and territory defence in the tawny owl (*Strix aluco*). *Behav. Eco. Sociobio.* 67, 1041-1052.
- Davis, A.L., Nijhout, H.F. and Johnsen, S. (2020). Diverse nanostructures underlie thin ultra-black scales in butterflies. *Nat. Comm.* 11, 1-7.

- De Ibarra, N.H. and Vorobyev, M. (2009). Flower patterns are adapted for detection by bees. *J. Comp. Phys. A*. 195, 319-323.
- Delhey, K. (2017). Gloger's rule. *Curr. Bio.* 27, R689-R691.
- Delhey, K. (2019). A review of Gloger's rule, an ecogeographical rule of color: Definitions, interpretations and evidence. *Bio. Rev.* 94, 1294-1316.
- Denton, E.J. and Nicol, J.A.C. (1966). A survey of reflectivity in silvery teleosts. *J. Mar. Bio. Assoc. UK*. 46, 685-722.
- Denton, E.J. and Land, M.F. (1971). Mechanism of reflexion in silvery layers of fish and cephalopods. *Proc. Roy. Soc. B*. 178, 43-61.
- Detto, T. and Backwell, P.R. (2009). The fiddler crab *Uca mjoebergi* uses ultraviolet cues in mate choice but not aggressive interactions. *Anim. Behav.* 78, 407-411.
- Djurdjević, I., Kreft, M. E., & Sušnik Bajec, S. (2015). Comparison of pigment cell ultrastructure and organisation in the dermis of marble trout and brown trout, and first description of erythrophore ultrastructure in salmonids. *J. Anat.* 227, 583-595.
- Doucet, S.M., Mennill, D.J., Hill, G.E. (2007). The evolution of signal design in manakin plumage ornaments. *Am. Nat.* 169, 62-80.
- Doucet, S.M., Meadows, M.G. (2009). Iridescence: a functional perspective. *J. Roy. Soc. Int.* 6, 115-132.
- Dyson, M.L., Perez, D.M., Curran, T., McCullough, E.L. and Backwell, P.Y. (2020). The role of claw color in species recognition and mate choice in a fiddler crab. *Behav. Eco. Sociobio.* 74, 1-11.
- Eliason, C.M. and Clarke, J.A. (2018). Metabolic physiology explains macroevolutionary trends in the melanistic color system across amniotes. *Proc. Roy. Soc. B*. 285, 20182014.
- Ellis, G. R. (1985). Cleaner Shrimp. *Freshw. Mar. Aquar.* 83-86.

- Endler, J.A. (1984). Progressive background in moths, and a quantitative measure of crypsis. *Bio. J. Linn. Soc.* 22, 187-231.
- Endler, J.A. (1992). Signals, signal conditions, and the direction of evolution. *Am. Nat.* 139, 125-153.
- Endler, J.A. and Thery, M. (1996). Interacting effects of lek placement, display behavior, ambient light, and color patterns in three neotropical forest-dwelling birds. *Am. Nat.* 148, 421-452.
- Endler, J.A. and Day, L.B. (2006). Ornament color selection, visual contrast and the shape of color preference functions in great bowerbirds, *Chlamydera nuchalis*. *Anim. Behav.* 72, 1405-1416.
- Espeland, M., Breinholt, J., Willmott, K.R., Warren, A.D., Vila, R., Toussaint, E.F., Maunsell, S.C., Aduse-Poku, K., Talavera, G., Eastwood, R. and Jarzyna, M.A. (2018). A comprehensive and dated phylogenomic analysis of butterflies. *Curr. Bio.* 28, 770-778.
- Exnerová, A., Svádová, K., Štys, P., Barcalová, S., Landová, E.V.A., Prokopova, M., Fuchs, R. and Socha, R. (2006). Importance of color in the reaction of passerine predators to aposematic prey: experiments with mutants of *Pyrrhocoris apterus* (Heteroptera). *Bio. J. Linn. Soc.* 88, 143-153.
- Fabricant, S.A., Exnerová, A., Ježová, D. and Štys, P. (2014). Scared by shiny? The value of iridescence in aposematic signaling of the hibiscus harlequin bug. *Anim. Behav.* 90, 315-325.
- Faílde, L.D., Bermúdez, R., Vigliano, F., Coscelli, G.A. and Quiroga, M.I. (2014). Morphological, immunohistochemical and ultrastructural characterization of the skin of turbot (*Psetta maxima* L.). *Tiss. Cell.* 46, 334-342.
- Fukuda, S. and Konuma, J. (2019). Using three-dimensional printed models to test for aposematism in a carabid beetle. *Bio. J. Linn. Soc.* 128, 735-741.
- Galvan, I. (2010). Plumage coloration can be perceived as a multiple condition-dependent signal by Great Tits *Parus major*. *Ibis.* 152, 359-367.

- Galván, I. and Alonso-Alvarez, C. (2017). Individual quality via sensitivity to cysteine availability in a melanin-based honest signaling system. *J. Exp. Bio.* 220, 2825-2833.
- Galván, I. and Solano, F. (2016). Bird integumentary melanins: biosynthesis, forms, function and evolution. *Int. J. Mol. Sci.* 17, 520.
- Garrouste, R., Hugel, S., Jacquelin, L., Rostan, P., Steyer, J.S., Desutter-Grandcolas, L. and Nel, A. (2016). Insect mimicry of plants dates back to the Permian. *Nat. Comm.* 7, 1-6
- Girard, M.B. and Endler, J.A. (2014). Peacock spiders. *Curr. Bio.* 24, R588-R590.
- Goda, M. and Fujii, R. (2001). Coloration and chromatophores of the domino damselfly, *Dasyllus trimaculatus*. *Zoo. Sci.* 18, 165-174.
- Goldstein, G., Flory, K.R., Browne, B.A., Majid, S., Ichida, J.M. and Burt Jr, E.H. (2004). Bacterial degradation of black and white feathers. *The Auk.* 121, 656-659.
- Goris, R.C. (2011). Infrared organs of snakes: an integral part of vision. *J. Herp.* 45, 2-14.
- Grafen, A. and Johnstone, R.A. (1993). Why we need ESS signaling theory. *Phil. Trans. Roy. Soc. B.* 340, 245-250.
- Griggio, M., Serra, L., Licheri, D., Monti, A. and Pilastro, A. (2007). Armaments and ornaments in the rock sparrow: a possible dual utility of a carotenoid-based feather signal. *Behav. Eco. Sociobio.* 61, 423-433.
- Griggio, M., Hoi, H. and Pilastro, A. (2010). Plumage maintenance affects ultraviolet color and female preference in the budgerigar. *Behav. Process.* 84, 739-744.
- Griggio, M., Zanollo, V. and Hoi, H. (2010). UV plumage color is an honest signal of quality in male budgerigars. *Eco. Res.* 25, 77-82.
- Gunderson, A.R. (2008). Feather-degrading bacteria: a new frontier in avian and host-parasite research?. *The Auk.* 125, 972-979.
- Guo, H., Huang, B., Qi, F. and Zhang, S. (2007). Distribution and ultrastructure of pigment cells in the skins of normal and albino adult turbot, *Scophthalmus maximus*. *Chin. J. Ocean. Limn.* 25, 199-208.

- Haddock, S.H., Moline, M.A. and Case, J.F. (2010). Bioluminescence in the sea. *An. Rev. Mar. Sci.* 2, 443-493.
- Han, Z., Li, B., Mu, Z., Yang, M., Niu, S., Zhang, J. and Ren, L. (2015). An ingenious super light trapping surface templated from butterfly wing scales. *Nano. Res. Lett.* 10, 1-8.
- Hansen, D.M., Van der Niet, T. and Johnson, S.D. (2012). Floral signposts: testing the significance of visual 'nectar guides' for pollinator behavior and plant fitness. *Proc. Roy. Soc. B.* 279, 634-639.
- Hart, N.S. (2001). The visual ecology of avian photoreceptors. *Prog Ret. Eye Res.* 20, 675-703.
- Hashimoto, H., Goda, M., Futahashi, R., Kelsh, R. and Akiyama, T. (2021). *Pigments, pigment cells and pigment patterns*. Springer Nature.
- Hawkes, J.W. (1974). The structure of fish skin. *Cell Tiss. Res.* 149, 147-158.
- Hawkes, J.W. (1974). The structure of fish skin. II. The chromatophore unit. *Cell Tiss. Res.* 149, 159-172.
- Henze, M.J., Lind, O., Wilts, B.D. and Kelber, A. (2019). Pterin-pigmented nanospheres create the colors of the polymorphic damselfly *Ischnura elegans*. *J. Roy. Soc. Int.* 16, 20180785.
- Herring, P.J. (1977). Bioluminescence of marine organisms. *Nature.* 267, 788-793.
- Hill, G.E. (1991). Plumage coloration is a sexually selected indicator of male quality. *Nature.* 350, 337-339.
- Hill, G.E. (2006). Female mate choice for ornamental coloration. In '*Bird Coloration. Vol. 2. Function and Evolution.*' (Eds GE Hill and KJ McGraw.) 137-200.
- Hill, G.E. and Farmer, K.L. (2005). Carotenoid-based plumage coloration predicts resistance to a novel parasite in the house finch. *Naturwissenschaften*, 92, 30-34.

- Hirata, M., Nakamura, K.I. and Kondo, S. (2005). Pigment cell distributions in different tissues of the zebrafish, with special reference to the striped pigment pattern. *Dev. Dyn.* 234, 293-300.
- Hirose, E. and Matsumoto, J. (1993). Deficiency of the gene B impairs differentiation of melanophores in the medaka fish, *Oryzias latipes*: fine structure studies. *Pig. Cell Res.* 6, 45-51.
- Hofreiter, M. and Schöneberg, T. (2010). The genetic and evolutionary basis of color variation in vertebrates. *Cell. Mol. Life Sci.* 67, 2591-2603.
- Hutton, P. and McGraw, K.J. (2016). Urban impacts on oxidative balance and animal signals. *Front. Eco. Evo.* 4, 54.
- Ingram, A.L. and Parker, A.R. (2008). A review of the diversity and evolution of photonic structures in butterflies, incorporating the work of John Huxley (The Natural History Museum, London from 1961 to 1990). *Phil. Trans. Roy. Soc. B.* 363, 2465-2480.
- Insausti, T.C. and Casas, J. (2008). The functional morphology of color changing in a spider: development of ommochrome pigment granules. *J. Exp. Bio.* 211, 780-789.
- Irestedt, M., Jönsson, K.A., Fjeldså, J., Christidis, L. and Ericson, P.G. (2009). An unexpectedly long history of sexual selection in birds-of-paradise. *BMC Evo. Bio.* 9, 1-11.
- Jacquín, L., Lenouvel, P., Haussy, C., Ducatez, S. and Gasparini, J. (2011). Melanin-based coloration is related to parasite intensity and cellular immune response in an urban free living bird: The feral pigeon *Columba livia*. *J. Avi. Bio.* 42, 11-15.
- Jennings, B.R. and Parslow, K. (1988). Particle size measurement: the equivalent spherical diameter. *Proc. Roy. Soc. A.* 419, 137-149.
- Jiang, W., Yan, L., Ma, H., Fan, Y., Wang, J., Feng, M. and Qu, S. (2018). Electromagnetic wave absorption and compressive behavior of a three-dimensional metamaterial absorber based on 3D printed honeycomb. *Sci. Rep.* 8, 1-7.
- Johnsen, S. (2001). Hidden in plain sight: the ecology and physiology of organismal transparency. *Bio. Bull.* 201, 301-318.

- Johnsen, S. (2002). Cryptic and conspicuous coloration in the pelagic environment. *Proc. Roy. Soc. B.* 269, 243-256.
- Johnsen, S. (2003). Lifting the cloak of invisibility: The effects of changing optical conditions on pelagic crypsis. *Integr. Comp. Bio.* 43, 580-590.
- Johnsen, S. (2005). The red and the black: bioluminescence and the color of animals in the deep sea. *Integr. Comp. Bio.* 45, 234-246.
- Johnsen, S. (2012). *The Optics of Life*. Princeton University Press.
- Johnsen, S. (2014). Hide and seek in the open sea: pelagic camouflage and visual countermeasures. *Ann. Rev. Mar. Sci.* 6, 369-392.
- Johnsen, S. and Widder, E.A. (1999). The physical basis of transparency in biological tissue: ultrastructure and the minimization of light scattering. *J. Theor. Bio.* 199, 181-198.
- Kalogianni, E., Alexis, M., Tsangaris, C., Abraham, M., Wendelaar Bonga, S.E., Iger, Y., Van Ham, E.H. and Stoumboudi, M.T. (2011). Cellular responses in the skin of the gilthead sea bream *Sparus aurata* L. and the sea bass *Dicentrarchus labrax* (L.) exposed to high ammonia. *J. Fish Bio.* 78, 1152-1169.
- Kelber, A., Vorobyev, M. and Osorio, D. (2003). Animal color vision—behavioral tests and physiological concepts. *Bio. Rev.* 78, 81-118.
- Kemp, D.J. (2007). Female butterflies prefer males bearing bright iridescent ornamentation. *Proc. Roy. Soc. B.* 274, 1043-1047.
- Kemp, D.J. and Rutowski, R.L. (2007). Condition dependence, quantitative genetics, and the potential signal content of iridescent ultraviolet butterfly coloration. *Evolution.* 61, 168-183.
- Kemp, D.J. and Rutowski, R.L. (2011). The role of coloration in mate choice and sexual interactions in butterflies. *Adv. Study Behav.* 43, 55-92.
- Keyser, A.J. and Hill, G.E. (1999). Condition-dependent variation in the blue-ultraviolet coloration of a structurally based plumage ornament. *Proc. Roy. Soc. of London. B.* 266, 771-777.

- Kikuchi, D.W., Seymoure, B.M. and Pfennig, D.W. (2014). Mimicry's palette: widespread use of conserved pigments in the aposematic signals of snakes. *Evo. & Dev.* 16, 61-67.
- Kinoshita, S. (2008). *Structural colors in the realm of nature*. World Scientific.
- Kleinholz, L.H. (1959). Purines and pteridines from the reflecting pigment of the arthropod retina. *Bio. Bull.* 116, 125-135.
- Kodric-Brown, A. (1989). Dietary carotenoids and male mating success in the guppy: an environmental component to female choice. *Behav. Eco. Sociobio.* 25, 393-401.
- Koski, M.H. (2020). The role of sensory drive in floral evolution. *New Phyt.* 227, 1012-1024.
- Kreezer, G. (1930). Luminous appearances. *J. Gen. Psych.* 4, 247-281.
- Kumar, S., Stecher, G., Suleski, M. and Hedges, S.B. (2017). TimeTree: a resource for timelines, timetrees, and divergence times. *Mol. Bio. Evo.* 34, 1812-1819.
- Le Guellec, D., Morvan-Dubois, G., and Sire, J. Y. (2003). Skin development in bony fish with particular emphasis on collagen deposition in the dermis of the zebrafish (*Danio rerio*). *Int. J. Dev. Bio.* 48, 217-231.
- Leonard, A.S. and Papaj, D.R. (2011). 'X' marks the spot: The possible benefits of nectar guides to bees and plants. *Func. Eco.* 25, 1293-1301.
- Li, Q., Clarke, J.A., Gao, K.Q., Zhou, C.F., Meng, Q., Li, D., D'Alba, L. and Shawkey, M.D. (2014). Melanosome evolution indicates a key physiological shift within feathered dinosaurs. *Nature.* 507, 350-353.
- Liu, X., Coxon, P.R., Peters, M., Hoex, B., Cole, J.M. and Fray, D.J. (2014). Black silicon: fabrication methods, properties and solar energy applications. *En. Envir. Sci.* 7, 3223-3263.
- Luo, H., Chen, F., Wang, F., Wang, X., Dai, W., Hu, S. and Gong, R. (2018). Preparation and microwave absorption properties of honeycomb core structures coated with composite absorber. *AIP Adv.* 8, 056635.

- Maan, M.E. and Cummings, M.E. (2012). Poison frog colors are honest signals of toxicity, particularly for bird predators. *Am. Nat.* 179, E1-E14.
- Mallet, J. (1993). Speciation, raiation, and color pattern evolution in Heliconius butterflies: evidence from hybrid zones. *Hybr. Zones Evo. Proc.*, 226-260.
- Mappes, J., Marples, N. and Endler, J.A. (2005). The complex business of survival by aposematism. *Trends Eco. Evo.* 20, 598-603.
- Marler, P. (1957). Specific distinctiveness in the communication signals of birds. *Behavior*, 13-39.
- Marshall NJ. (2000). Communication and camouflage with the same 'bright' colors in reef fishes. *Phil. Trans. Roy. Soc. B.* 355, 1243-1248.
- Marshall, N.J., Cortesi, F., de Busserolles, F., Siebeck, U.E. and Cheney, K.L. (2019). Colors and color vision in reef fishes: Past, present and future research directions. *J. Fish Bio.* 95, 5-38.
- Martini, S. and Haddock, S.H. (2017). Quantification of bioluminescence from the surface to the deep sea demonstrates its predominance as an ecological trait. *Sci. Rep.* 7, 1-11.
- Mäthger, L.M., Senft, S.L., Gao, M., Karaveli, S., Bell, G.R., Zia, R., Kuzirian, A.M., Dennis, P.B., Crookes-Goodson, W.J., Naik, R.R. and Kattawar, G.W. (2013). Bright white scattering from protein spheres in color changing, flexible cuttlefish skin. *Adv. Func. Mat.* 23, 3980-3989.
- Maurer, D.L., Kohl, T. and Gebhardt, M.J., 2017. Cuticular microstructures turn specular black into matt black in a stick insect. *Arthropod structure & development*, 46(2), pp.147-155.
- McLean CA., Moussalli A., Stuart-Fox D. 2014. Local adaptation and divergence in color signal conspicuousness between monomorphic and polymorphic lineages in a lizard. *J. Evol. Biol.* 27, 2654-2664.
- McCoy, D.E., Feo, T., Harvey, T.A. and Prum, R.O. (2018). Structural absorption by barbule microstructures of super black bird of paradise feathers. *Nat. Comm.* 9, 1-8.

- McCoy, D.E. and Prum, R.O. (2019). Convergent evolution of super black plumage near bright color in 15 bird families. *J. Exp. Bio.* 222, 208140.
- McCoy, D.E., McCoy, V.E., Mandsberg, N.K., Shneidman, A.V., Aizenberg, J., Prum, R.O. and Haig, D. (2019). Structurally assisted super black in colorful peacock spiders. *Proc. Roy. Soc. B.* 286, 20190589.
- McElroy, M.T. (2016). Teasing apart crypsis and aposematism—evidence that disruptive coloration reduces predation on a noxious toad. *Bio. J. Linn. Soc.* 117, 285-294.
- McFall-Ngai, M.J. (1990). Crypsis in the pelagic environment. *Am. Zoo.* 30, 175-188.
- McGraw, K.J. and Ardia, D.R. (2003). Carotenoids, immunocompetence, and the information content of sexual colors: an experimental test. *Am. Nat.* 162, 704-712.
- Medina, I., Vega-Trejo, R., Wallenius, T., Symonds, M.R. and Stuart-Fox, D. (2020). From cryptic to colorful: Evolutionary decoupling of larval and adult color in butterflies. *Evo. Lett.* 4, 34-43.
- Merilaita, S. (1998). Crypsis through disruptive coloration in an isopod. *Proc. Roy. Soc. B.* 265, 1059-1064.
- Micillo, R., Panzella, L., Iacomino, M., Prampolini, G., Cacelli, I., Ferretti, A., Crescenzi, O., Koike, K., Napolitano, A. and d'Ischia, M. (2017). Eumelanin broadband absorption develops from aggregation-modulated chromophore interactions under structural and redox control. *Sci. Rep.* 7, 1-12.
- Mizuno, K., Ishii, J., Kishida, H., Hayamizu, Y., Yasuda, S., Futaba, D.N., Yumura, M. and Hata, K. (2009). A black body absorber from vertically aligned single-walled carbon nanotubes. *PNAS.* 106, 6044-6047.
- Moses, D.N., Mattoni, M.A., Slack, N.L., Waite, J.H. and Zok, F.W. (2006). Role of melanin in mechanical properties of *Glycera* jaws. *Acta Biomater.* 2, 521-530.
- Muchhala, N., Johnsen, S. and Smith, S.D. (2014). Competition for hummingbird pollination shapes flower color variation in Andean Solanaceae. *Evo.* 68, 2275-2286.

- Muysshondt, A. (1973). Notes on the life cycle and natural history of butterflies of El Salvador I A. *Catonephele numilia esite* (Nymphalidae-Catonephelinae). *J. New York Ento. Soc.* 81, 164-174.
- Nakamura, N., Ikeda, Y. and Obika, M. (1987). Video and electron microscopic studies on pigment transport in *Gambusia melanophores*. *Japan. J. Ichth.* 34, 351-360.
- Nokelainen, O., Brito, J.C., Scott-Samuel, N.E., Valkonen, J.K. and Boratyński, Z. (2020). Camouflage accuracy in Sahara–Sahel desert rodents. *J. Anim. Eco.* 89, 1658-1669.
- Nowel, M.S., Shelton, P.M.J. and Herring, P.J. (1998). Cuticular photophores of two decapod crustaceans, *Oplophorus spinosus* and *Systellaspis debilis*. *Bio. Bull.* 195, 290-307.
- Obika, M. and Meyer-Rochow, V.B. (1990). Dermal and epidermal chromatophores of the Antarctic teleost *Trematomus bernacchii*. *Pig. Cell Res.* 3, 33-37.
- Olson, V.A. and Owens, I.P. (1998). Costly sexual signals: are carotenoids rare, risky or required?. *Trends Eco. Evo.* 13, 510-514.
- Ortiz, E., Bächli, E., Price, D. and Williams-Ashman, H.G. (1963). Red pteridine pigments in the dewlaps of some anoles. *Physio. Zoo.* 36, 97-103.
- Oskooi, A.F., Roundy, D., Ibanescu, M., Bermel, P., Joannopoulos, J.D. and Johnson, S.G. (2010). MEEP: A flexible free-software package for electromagnetic simulations by the FDTD method. *Comp. Phys. Comm.* 181, 687-702.
- Ozeki, H., Ito, S., Wakamatsu, K. and Thody, A.J. (1996). Spectrophotometric characterization of eumelanin and pheomelanin in hair. *Pig. Cell Res.* 9, 265-270.
- Palmer, B.A., Hirsch, A., Brumfeld, V., Aflalo, E.D., Pinkas, I., Sagi, A., Rosenne, S., Oron, D., Leiserowitz, L., Kronik, L. and Weiner, S. (2018). Optically functional isoxanthopterin crystals in the mirrored eyes of decapod crustaceans. *PNAS.* 115, 2299-2304.
- Palmer, B.A., Yallapragada, V.J., Schiffmann, N., Wormser, E.M., Elad, N., Aflalo, E.D., Sagi, A., Weiner, S., Addadi, L. and Oron, D. (2020). A highly reflective biogenic photonic material from core–shell birefringent nanoparticles. *Nat. Nanotech.* 15, 138-144.

- Park, J.Y. (2002). Structure of the skin of an air-breathing mudskipper, *Periophthalmus magnuspinnatus*. *J. Fish Bio.* 60, 1543-1550.
- Parsons, M.J. (1996). A phylogenetic reappraisal of the birdwing genus *Ornithoptera* (Lepidoptera: Papilionidae: Troidini) and a new theory of its evolution in relation to Gondwanan vicariance biogeography. *J. Nat. Hist.* 30, 1707-1736.
- Pearn, S.M., Bennett, A.T. and Cuthill, I.C. (2001). Ultraviolet vision, fluorescence and mate choice in a parrot, the budgerigar *Melopsittacus undulatus*. *Proc. Roy. Soc. B.* 268, 2273-2279.
- Peichl, L. (2005). Diversity of mammalian photoreceptor properties: adaptations to habitat and lifestyle?. *Anat. Rec. A.* 287, 1001-1012.
- Pirih, P., Wilts, B.D. and Stavenga, D.G. (2011). Spatial reflection patterns of iridescent wings of male pierid butterflies: curved scales reflect at a wider angle than flat scales. *J. Comp. Phys. A.* 197, 987-997.
- Pitt, I.T. and Winter, L.M. (1974). Effect of surround on perceived saturation. *JOSA.* 64, 1328-1331.
- Plotkin, M., Volynchik, S., Ermakov, N.Y., Benyamini, A., Boiko, Y., Bergman, D.J. and Ishay, J.S. (2009). Xanthopterin in the oriental hornet (*Vespa orientalis*): light absorbance is increased with maturation of yellow pigment granules. *Photochem. Photobio.* 85, 955-961.
- Price, T.D. (2017). Sensory drive, color, and color vision. *Am. Nat.* 190, 157-170.
- Pryke, S.R. (2007). *Reproductive Biology and Phylogeny of Birds, Part B: Sexual Selection, Behavior, Conservation, Embryology and Genetics.*
- R Core Team (2014). R: A language and environment for statistical computing. R Foundation for Statistical Computing, Vienna, Austria. URL <http://www.R-project.org/>.
- RStudio Team (2015). RStudio: Integrated Development for R. RStudio, Inc., Boston, MA URL <http://www.rstudio.com/>

- Ramachandran, V.S., Tyler, C.W., Gregory, R.L., Rogers-Ramachandran, D., Duensing, S., Pillsbury, C. and Ramachandran, C. (1996). Rapid adaptive camouflage in tropical flounders. *Nature*. 379, 815-818.
- Richardson, K.C., Jarett, L. and Finke, E.H. (1960). Embedding in epoxy resins for ultrathin sectioning in electron microscopy. *Stain Tech.* 35, 313-323.
- Roberts, R.J., Young, H. and Milne, J. (1972). Studies on the skin of plaice (*Pleuronectes platessa* L.) 1. The structure and ultrastructure of normal plaice skin. *J. Fish Bio.* 4, 87-98.
- Robison, B.H., Ruby, E.G. and Morin, J.G. (1977). Luminous bacteria associated with the gut contents of midwater fishes. *West. Soc. Nat.* 58, 23.
- Rosenthal, E.I., Holt, A.L. and Sweeney, A.M. (2017). Three-dimensional midwater camouflage from a novel two-component photonic structure in hatchetfish skin. *J. Roy. Soc. Int.* 14, 20161034.
- Rossi, V., McNamara, M.E., Webb, S.M., Ito, S. and Wakamatsu, K. (2019). Tissue-specific geometry and chemistry of modern and fossilized melanosomes reveal internal anatomy of extinct vertebrates. *PNAS*. 116, 17880-17889.
- Roulin, A. (2016). Condition-dependence, pleiotropy and the handicap principle of sexual selection in melanin-based coloration. *Bio. Rev.* 91, 328-348.
- Roux, K.E. and Marra, P.P. (2007). The presence and impact of environmental lead in passerine birds along an urban to rural land use gradient. *Arch. Environ. Cont. Toxic.* 53, 261-268.
- Ruby, E.G. and Morin, J.G. (1979). Luminous enteric bacteria of marine fishes: a study of their distribution, densities, and dispersion. *Appl. Environ. Microbio.* 38, 406-411.
- Rutowski, R.L., Macedonia, J.M., Morehouse, N. and Taylor-Taft, L. (2005). Pterin pigments amplify iridescent ultraviolet signal in males of the orange sulphur butterfly, *Colias eurytheme*. *Proc. Roy. Soc. B.* 272, 2329-2335.
- Ruxton, G.D. and Johnsen, S. (2016). The effect of aggregation on visibility in open water. *Proc. Roy. Soc. B.* 283, 20161463.

- Sarna, T. and Plonka, P.M. (2005). Biophysical studies of melanin. In *Biomedical EPR, Part A: Free Radicals, Metals, Medicine, and Physiology* (pp. 125-146). Springer, Boston, MA.
- Schaefer, H.M. and Stobbe, N. (2006). Disruptive coloration provides camouflage independent of background matching. *Proc. Roy. Soc. B.* 273, 2427-2432.
- Scheifler, R., Coeurdassier, M., Morilhat, C., Bernard, N., Faivre, B., Flicoteaux, P., Giraudoux, P., Noël, M., Piotte, P., Rieffel, D. and De Vauflery, A. (2006). Lead concentrations in feathers and blood of common blackbirds (*Turdus merula*) and in earthworms inhabiting unpolluted and moderately polluted urban areas. *Sci. Tot. Environ.* 371, 197-205.
- Schiestl, F.P. and Johnson, S.D. (2013). Pollinator-mediated evolution of floral signals. *Trends Eco Evo.* 28, 307-315.
- Schindelin, J., Arganda-Carreras, I., Frise, E., Kaynig, V., Longair, M., Pietzsch, T., Preibisch, S., Rueden, C., Saalfeld, S., Schmid, B. and Tinevez, J.Y. (2012). Fiji: an open-source platform for biological-image analysis. *Nat. Meth.* 9, 676-682.
- Schliwa, M. (1986). Pigment cells. In *Biology of the Integument* (pp. 65-77). Springer, Berlin, Heidelberg.
- Schwalm, P.A., Starrett, P.H. and McDiarmid, R.W. (1977). Infrared reflectance in leaf-sitting neotropical frogs. *Science.* 196, 1225-1226.
- Schweikert, L.E., Fitak, R.R., Caves, E.M., Sutton, T.T. and Johnsen, S. (2018). Spectral sensitivity in ray-finned fishes: diversity, ecology and shared descent. *J. Exp. Bio.* 221, 189761.
- Schweikert, L.E., Fitak, R.R. and Johnsen, S. (2018). De novo transcriptomics reveal distinct phototransduction signaling components in the retina and skin of a color-changing vertebrate, the hogfish (*Lachnolaimus maximus*). *J. Comp. Phys. A.* 204, 475-485.
- Searcy, W.A. and Nowicki, S. (2010). *The evolution of animal communication*. Princeton University Press.

- Sefc, K.M., Brown, A.C. and Clotfelter, E.D. (2014). Carotenoid-based coloration in cichlid fishes. *Comparative Biochemistry and Physiology Part A: Molecular & Integrative Physiology*, 173, pp.42-51.
- Shawkey, M.D., Pillai, S.R., Hill, G.E., Siefferman, L.M. and Roberts, S.R. (2007). Bacteria as an agent for change in structural plumage color: correlational and experimental evidence. *Am. Nat.* 169, S112-S121.
- Siddique, R.H., Donie, Y.J., Gomard, G., Yalamanchili, S., Merdzhanova, T., Lemmer, U. and Hölscher, H. (2017). Bioinspired phase-separated disordered nanostructures for thin photovoltaic absorbers. *Science Adv.* 3, 1700232.
- Silberglied, R.E. and Taylor, O.R. (1978). Ultraviolet reflection and its behavioral role in the courtship of the sulfur butterflies *Colias eurytheme* and *C. philodice* (Lepidoptera, Pieridae). *Behav. Eco. Sociobio.* 3, 203-243.
- Simons, M.J., Briga, M., Koetsier, E., Folkertsma, R., Wubs, M.D., Dijkstra, C. and Verhulst, S. (2012). Bill redness is positively associated with reproduction and survival in male and female zebra finches. *PLoS One*, 7, 40721.
- Sköld, H.N., Aspöngren, S. and Wallin, M. (2002). The cytoskeleton in fish melanophore melanosome positioning. *Micro. Res. Tech.* 58, 464-469.
- Smith, J.M. and Harper, D. (2003). *Animal signals*. Oxford University Press.
- Smith, S.H., Hessong-Brown, J., Lipshutz, S.E., Phillips, J.N., Rochefort, C., Derryberry, E.P. and Luther, D.A. (2021). Long-term changes of plumage between urban and rural populations of white-crowned sparrows (*Zonotrichia leucophrys*). *J. Urban Eco.* 7, 038.
- Snoeijs, T., Dauwe, T., Pinxten, R., Vandesande, F. and Eens, M. (2004). Heavy metal exposure affects the humoral immune response in a free-living small songbird, the great tit (*Parus major*). *Arch. Environ. Cont. Toxic.* 46, 399-404.
- Spaethe, J.A.A.L.J., Schmidt, A., Hickelsberger, A. and Chittka, L. (2001). Adaptation, constraint, and chance in the evolution of flower color and pollinator color vision. In *Cognitive ecology of pollination: animal behavior and floral evolution*. Cambridge University Press.

- Speigle, J.M. and Brainard, D.H. (1996). Luminosity thresholds: effects of test chromaticity and ambient illumination. *JOSA A*. 13, 436-451.
- Spinner, M., Kovalev, A., Gorb, S.N. and Westhoff, G. (2013). Snake velvet black: hierarchical micro-and nanostructure enhances dark coloration in *Bitis rhinoceros*. *Sci. Rep.* 3, 1-8.
- Spurr, A.R. (1969). A low-viscosity epoxy resin embedding medium for electron microscopy. *J. Ultrastruc. Res.* 26, 31-43.
- Stange, N., Page, R.A., Ryan, M.J. and Taylor, R.C. (2017). Interactions between complex multisensory signal components result in unexpected mate choice responses. *Anim. Behav.* 134, 239-247.
- Stavenga, D.G. (1989). Pigments in compound eyes. In *Facets of vision* (pp. 152-172). Springer, Berlin, Heidelberg.
- Stavenga, D.G., Leertouwer, H.L., Osorio, D.C. and Wilts, B.D. (2015). High refractive index of melanin in shiny occipital feathers of a bird of paradise. *Light: Sci. & Appl.* 4, 243-243.
- Stavenga, D.G., Stowe, S., Siebke, K., Zeil, J. and Arikawa, K. (2004). Butterfly wing colors: scale beads make white pierid wings brighter. *Proc. Roy. Soc. B*. 271, 1577-1584.
- Stavenga, D.G. and Arikawa, K. (2006). Evolution of color and vision of butterflies. *Arthr. Struc. & Dev.* 35, 307-318.
- Stevens, M. and Merilaita, S. (2009). Defining disruptive coloration and distinguishing its functions. *Phil. Trans. Roy. Soc. B*. 364, 481-488.
- Stevens, M. and Merilaita, S. eds. (2011). *Animal camouflage: mechanisms and function*. Cambridge University Press.
- Svensson, P.A. and Wong, B.B.M. (2011). Carotenoid-based signals in behavioral ecology: a review. *Behavior*. 148, 131-189.
- Taylor, R.C., Klein, B.A. and Ryan, M.J. (2011). Inter-signal interaction and uncertain information in anuran multimodal signals. *Curr. Zoo.* 57, 153-161.

- Titus, B.M., Vondriska, C. and Daly, M. (2017). Comparative behavioral observations demonstrate the 'cleaner' shrimp *Periclimenes yucatanicus* engages in true symbiotic cleaning interactions. *Roy. Soc. Open Sci.* 4, 170078.
- Uy, J.A.C., Endler, J.A. (2004). Modification of the visual background increases the conspicuousness of golden-collared manakin displays. *Behav. Ecol.* 15, 1003-1010.
- Velando, A., Beamonte-Barrientos, R. and Torres, R. (2006). Pigment-based skin color in the blue-footed booby: an honest signal of current condition used by females to adjust reproductive investment. *Oecologia*. 149, 535-542.
- Vukusic, P., Sambles, J.R., Lawrence, C.R. and Wootton, R.J. (1999). Quantified interference and diffraction in single *Morpho* butterfly scales. *Proc. Roy. Soc. B.* 266, 1403-1411.
- Vukusic, P., Sambles, J.R. and Lawrence, C.R. (2004). Structurally assisted blackness in butterfly scales. *Proc. Roy. Soc. B.* 271, 237-239.
- Walls, J. G. (1983). Two colorful cleaner shrimp of the genus *Lysmata*. *Trop. Fish Hobbyist* 54-56.
- Wang, W., Zhang, W., Fang, X., Huang, Y., Liu, Q., Bai, M. and Zhang, D. (2014). Omnidirectional light absorption of disordered nano-hole structure inspired from *Papilio ulysses*. *Optics Lett.* 39, 4208-4211.
- Weaver, R.J., Santos, E.S., Tucker, A.M., Wilson, A.E. and Hill, G.E., 2018. Carotenoid metabolism strengthens the link between feather coloration and individual quality. *Nat. Comm.* 9, 1-9.
- Wicksten, M.K. (2009). Interactions with fishes of five species of *Lysmata* (Decapoda, Caridea, Lysmatidae). *Crustaceana*, 82, 1213-1223.
- Widder, E.A. (1999). Bioluminescence. In *Adaptive mechanisms in the ecology of vision* (pp. 555-581). Springer, Dordrecht.
- Widder, E.A. (2010). Bioluminescence in the ocean: origins of biological, chemical, and ecological diversity. *Science*. 328, 704-708.
- Widder, E.A., Latz, M.I. and Case, J.F. (1983). Marine bioluminescence spectra measured with an optical multichannel detection system. *Bio. Bull.* 165, 791-810.

- Wilkins, L. and Osorio, D. (2019). Object colors, material properties and animal signals. *J. Exp. Bio.* 222, 204487.
- Wilts, B.D., Michielsen, K., De Raedt, H. and Stavenga, D.G. (2014). Sparkling feather reflections of a bird-of-paradise explained by finite-difference time-domain modeling. *PNAS*. 111, 4363-4368.
- Wilts, B.D., Wijnen, B., Leertouwer, H.L., Steiner, U. and Stavenga, D.G. (2017). Extreme refractive index wing scale beads containing dense pterin pigments cause the bright colors of pierid butterflies. *Adv. Opt. Mat.* 5, 1600879.
- Wong, V.L. and Marek, P.E. (2020). Structure and pigment make the *Eyed elater's* eyespots black. *PeerJ*. 8, 8161.
- Xiao, F., Yang, C., Shi, H., Wang, J., Sun, L. and Lin, L. (2016). Background matching and camouflage efficiency predict population density in four-eyed turtle (*Sacalia quadriocellata*). *Behav. Proc.* 131, 40-46.
- Yan, R., Chen, M., Zhou, H., Liu, T., Tang, X., Zhang, K., Zhu, H., Ye, J., Zhang, D. and Fan, T. (2016). Bio-inspired plasmonic nanoarchitected hybrid system towards enhanced far red-to-near infrared solar photocatalysis. *Sci. Rep.* 6, 1-11.
- Young, R.E. (1983). Oceanic bioluminescence: an overview of general functions. *Bull. Mar. Sci.* 33, 829-845.
- Young, R.E., Kampa, E.M., Maynard, S.D., Mencher, F.M. and Roper, C.F. (1980). Counterillumination and the upper depth limits of midwater animals. *Deep Sea Res. A*. 27, 671-691.
- Zhao, Q., Fan, T., Ding, J., Zhang, D., Guo, Q. and Kamada, M. (2011). Super black and ultrathin amorphous carbon film inspired by anti-reflection architecture in butterfly wing. *Carbon*. 49, 877-883.
- Zhao, Q., Guo, X., Fan, T., Ding, J., Zhang, D. and Guo, Q. (2011). Art of blackness in butterfly wings as natural solar collector. *Soft Matter*. 7, 11433-11439.
- Zhou, M., Johnson, A.M. and Fuller, R.C. (2014). Patterns of male breeding color variation differ across species, populations, and body size in rainbow and orangethroat darters. *Copeia*. 2014, 297-308.

- Zylinski, S. and Johnsen, S. (2011). Mesopelagic cephalopods switch between transparency and pigmentation to optimize camouflage in the deep. *Curr. Bio.* 21, 1937-1941.
- Zyznar, E.S. and Nicol, J.C. (1971). Ocular reflecting pigments of some malacostraca. *J. Exp. Mar. Bio. Eco.* 6, 235-248.

Biography

Alexander Davis was born in Annapolis, MD and raised in Arnold, Maryland. He attended the University of North Carolina – Chapel Hill, during which time he received UNC's Taylor Fellowship to fund his research. He graduated with highest honors for a B.S. in Biology (May 2018) and received UNC's Coker Award for excellence in organismal biology. He has published two first-author publications from his undergraduate work. He entered the Doctoral program at Duke in August 2018, supported by a Department of Defense National Defense Science and Engineering Graduate Fellowship and the James B Duke Fellowship. He has since published three first-author papers related to his dissertation work, as well as three middle-author papers related to sensory biology and computational modeling of biophotonic structures. He has furthered his professional development while at UNC and Duke by teaching a seminar on the intersection of physics and biology and participating in the Triangle chapter of the Scientific Research and Education Network. He has also received numerous awards and distinctions during his time at Duke, including: Deep-sea Biology Society's Paper of the Year (2021), the Duke-Exeter Collaboration Fund Fellowship (2019), the American Microscopical Society's Best Student Presentation Award, and numerous grants in aid.